Institut für Biochemie, Campus Mitte der Medizinischen Fakultät
Charité – Universitätsmedizin Berlin

DISSERTATION

Genom und Metabolismus stabilisierende Antitumor-Therapie (GMSAT) in den humanen Kolon- und Brustkrebszelllinien HT-29 und MDA-MB-231

Zur Erlangung des akademischen Grades
Doctor medicinae (Dr. med.)

vorgelegt der Medizinischen Fakultät
Charité – Universitätsmedizin Berlin

von

Jérôme Ruhnau
aus Krefeld

Datum der Promotion: 26.06.2022

Inhalt

Abkürzungsverzeichnis

GMSAT	Genom und Metabolismus stabilisierende Antitumor Therapie genome and metabolism stabilizing antitumor-therapy
MDIS	minimalistisches Synergie Screening minimalistic drug interaction screening
CSP	vermutete synergistische Potenz conjectured synergistic potency
BPR	Bruchpunktregion breakpoint region
DCA	Dichloroacetat dichloroacetate
CNV	Kopienzahlvariationen copy number variations
segCNV	segmentale Kopienzahlvariationen segmental copy number variations
SNP	Einzelnukleotid-Polymorphismus single nucleotide polymorphism
HPLC	Hochleistungsflüssigkeitschromatographie high performance liquid chromatography
ROS	reaktive Sauerstoffspezies reactive oxygen species
MTT	3-(4,5-Dimethylthiazol-2-yl)-2,5-diphenyltetrazoliumbromid 3-(4,5-dimethylthiazol-2-yl)-2,5-diphenyltetrazolium bromide
SRB	Sulforhodamin B Sulforhodamine B

Zusammenfassung

Einleitung: Die tumorale Mikroevolution führt regelhaft zu Rezidiven, Therapieresistenz und Progress einer Tumorerkrankung. Wichtige Voraussetzungen für die Mikroevolution ist die genomische Instabilität und ein Tumorstoffwechsel, der die Metabolite für eine hohe Zellteilungsrate bereitstellt. In dieser Arbeit wurde deshalb neben der Analyse der genomischen Instabilität ein Therapiekonzept entwickelt, das auf synergistisch interagierenden Pharmaka beruht, deren Hauptansatzpunkte die Stabilisierung des Genoms und die Modulierung des Tumorstoffwechsels darstellen.

Methoden: Einzelnukleotid-Polymorphismus (SNP)-Daten von 111 Tumorproben und 917 Tumorzelllinen wurden verwendet, um das Genom verschiedener Tumorentitäten nach segmentalen Kopienzahlvariationen (segCNV) und damit zusammenhängenden Bruchpunktregionen (BPR) zu untersuchen. Mittels 3-(4,5-Dimethylthiazol-2-yl)-2,5-diphenyltetrazoliumbromid (MTT)- und Sulforhodamin B (SRB)-Assays wurden Dosis-Wirkungskurven von 14 Pharmaka in Brust- und Kolonzelllinien erstellt. Die Pharmaka wurden im Rahmen des dafür entwickelten minimalistischen Synergie Screenings (MDIS) auf Synergien überprüft. Gefundene Synergien wurden mit der Methode von Chou und Talalay verifiziert. Für die Kombination aus PX-478 und Dichloroacetat (DCA) wurde zur weiteren Analyse die Produktion reaktiver Sauerstoffspezies (ROS) mittels Hochleistungsflüssigkeits-chromatographie (HPLC) ermittelt.

Ergebnisse: Die Analysen von SNP-Array-Daten zeigten, dass genomische Reorganisation in Tumoren im Gegensatz zu gesunden Zellen häufig vorkommt. Einige BPR sind in allen untersuchten Krebsarten zu finden, während andere ausschließlich in bestimmten Tumorentitäten auftreten. Im MDIS konnten von 91 möglichen Kombinationen 18 für HT-29 als potenziell synergistisch identifiziert werden. Die Kombination zwischen PX-478 und DCA zeigte eine 62,4% stärkere antitumorale Wirkung als die Summe der Einzeleffekte. Fünf der gefundenen Synergien wurden mit der Methode von Chou und Talalay überprüft und vier konnten bestätigt werden. Die Synergien aus DCA und PX-478, DCA und NHI-2 sowie Nutlin-3 und PX-478 konnten sowohl in HT-29 als auch MDA-MB-231 bestätigt werden. HPLC-Analysen zeigten für die Kombination aus DCA und PX-478 eine signifikant erhöhte ROS-Bildung.

Schlussfolgerung: BPR stellen ein wichtiges Korrelat der genomischen Instabilität in Tumoren dar. Am Beispiel der Genom und Metabolismus stabilisierenden Antitumor-Therapie (GMSAT) zeigte sich das MDIS als effektives Werkzeug in der Detektion vielversprechender Synergien. Die Kombination aus PX-478 und DCA zeigte sich synergistisch und effektiv in allen untersuchten Tumorentitäten.

Abstract

Introduction: Tumoral microevolution frequently leads to recurrent disease, progression and therapy resistance in cancer. Important driving factors of the microevolution are the genomic instability and the tumor metabolism which converge on an accelerated proliferation rate combined with a high mutagenicity. The aim of this work is to better understand the mechanisms of genomic instability in tumors as well as alterations in metabolism and to develop a therapy concept which focusses on synergistic interactions of genome and metabolism targeting compounds.

Methods: Single-nucleotide polymorphism (SNP) array data of 111 tumor samples and 917 cancer cell lines were analysed to determine the occurrence of segmental copy number alterations (segCNV) and the respective breakpoint regions (BPR). Dose response curves of 14 selected compounds were created with 3-(4,5-dimethylthiazol-2-yl)-2,5-diphenyltetrazolium bromide (MTT) and Sulforhodamine B (SRB) assays. All possible pairwise combinations were tested by a minimalistic drug interaction screening (MDIS), a method designed to cost efficiently screen for synergistic interactions. Detected synergisms were further verified by the method of Chou and Talalay. The combination of PX-478 and Dichloroacetate (DCA) was further analysed by high performance liquid chromatography (HPLC) determine reactive oxygen species (ROS) production.

Results: Analysis of SNP array data suggested that breakpoint regions regularly occur in tumors in general, whereas some BPR are characteristic for specific tumor entities. Out of 91 possible pairwise combinations, MDIS detected 18 HT-29 cells. Five synergies were further analysed by the method of Chou and Talalay of which four could be confirmed. PX-478 in combination with DCA exhibited a 62.4% stronger antitumoral effect than the sum of the single drug effects in MDIS. Three of the combinations DCA + PX-478, DCA + NHI-2 and Nutlin-3 + PX-478 could be confirmed in HT-29 and MDA-MB-231 cells. HPLC analyses showed that the combination led to a significant increase in ROS production.

Conclusion: Breakpoint regions are an important correlate of genomic instability in tumors. MDIS proved to be an effective screening tool in the detection of potential synergistic interactions at the example of genome and metabolism stabilizing antitumor therapy (GMSAT). The combination of PX-478 and DCA was found to exert synergistic effects in all investigated tumor entities.

1 Einleitung

1.1 Die tumorale Mikroevolution

In den meisten Tumorentitäten verbleiben nach primärer Therapie Tumorzellen im Körper erhalten, die im Verlauf zu Rezidiven oder Metastasierung führen können [73]. Die tumorale Mikroevolution ermöglicht es den Tumorzellen, Eigenschaften zu entwickeln, die zu Immunevasion, erneuter Proliferation, Metastasierung [24] und der Entwicklung therapieresistenter Subpopulationen [9] führen. Voraussetzung für die Mikroevolution ist die genetische Instabilität [3], die zu einer erhöhten Mutationsrate führt. Ein zweiter Faktor ist eine beschleunigte Zellteilungsrate, die durch eine Dysregulation im Zellzyklus begünstigt wird [17]. Zudem sind große Menge an energieliefernden Metaboliten für die Synthese von DNA und Zellbestandteilen notwendig, die durch einen dysregulierten Tumorstoffwechsel geliefert werden [78].

1.2 Genomische Reorganisation

Während der Tumorigenese finden meist diverse genetische und epigenetische Veränderungen statt [20,24,30,38,54,78]. Molekulare Mechanismen wie Störungen an der Replikationsgabel (fork stalling) oder nichtallelische homologe Rekombination [41,59,83] können zu Veränderungen des Genoms wie Kopienzahlvariationen (CNV) und segmentale Kopienzahlvariationen (segCNV) führen, die im Verlauf der Tumorigenese zunehmen [5,65,70]. Unterschiede in segCNV können aus SNP-Array-Datenbanken erhoben werden und Hinweis auf Bruchpunktregionen (BPR) im Genom sein, die anfällig für genomische Reorganisation sind.

Eine bekannte Theorie ist das zufällige Bruchpunkt-Modell (random breakage model), das davon ausgeht, dass chromosomale Veränderungen sich zufällig über das Genom verteilen [49]. Allerdings deuten andere Untersuchungen darauf hin, dass es spezielle Regionen gibt, sogenannte “fragile sites” [16,23,40], die besonders anfällig für Brüche im Genom sind [49,58,62,85]. Um diese Prozesse besser zu verstehen, wurden in der ersten Studie SNP-Array-Daten von 111 Krebsgewebeproben, 20 Proben einer gesunden Kontrollkohorte und 917 Krebszelllinien ausgewertet [71].

1.3 Genom und Metabolismus stabilisierende Anti-Tumor Therapie (GMSAT)

Um die tumorale Mikroevolution einzudämmen, wurde ein Konzept entwickelt, das als zentrale Ansatzpunkte das Genom, den Tumorstoffwechsel und Zellüberleben/Wachstum definiert [62]. Eine andere komplexe Erkrankung, die ebenfalls eine Mikroevolution durchläuft, ist die Infektion mit dem humanen Immundefizienz-Virus (HIV). Bedingt durch die hohe Mutationsrate der viralen reversen Transkriptase [60] kommt es noch heute zur Entwicklung von Therapieresistenzen, insbesondere bei den nukleotidischen Reverse-Transkriptase-Inhibitoren (NRTI) [44]. Glücklicherweise kann eine HIV-Infektion heutzutage mit einer Kombinationstherapie (combined antiretroviral therapy, *“cART”*) [46] effektiv in Remission gehalten werden. Für die Therapie einer so komplexen Erkrankung wie Krebs ist vermutlich eine komplexere Kombinationstherapie von Nöten, die den Tumor auf mehreren Ebenen angreift. Ein Beispiel für einen solchen Ansatz ist das CUSP9-Konzept. Hier wurden mehrere Pharmaka, die bereits für andere Erkrankungen zugelassen sind, als Therapieansatz für das rezidivierende Glioblastom vorgeschlagen [22,29,66]. Die Kombination mehrerer Präparate hat das Potenzial, einen breiteren Effekt auf die verschiedenen Subpopulationen eines Tumors zu haben und damit die Progressionsfreiheit zu erhöhen [2]. Mit dem Ziel einer antitumoralen Kombinationstherapie wurde der Fokus auf möglichst oral verfügbare “small molecules” gelegt [17,33,87], deren Ansatzpunkte zum GMSAT-Konzept passen [62].

1.4 Die Suche nach synergistischen Interaktionen ausgewählter Pharmaka

Bei einer Vielzahl von potenziellen Substanzen ist ein industrielles, High-Throughput-Konzept sinnvoll, um die effektivsten Kombinationen zu ermitteln. Industrielle Finanzierung spielt in der Forschung eine immer größere Rolle [69]. Dabei liegt der Fokus vermehrt auf neu entwickelten und patentierbaren Medikamenten [47], während bereits patentierte Medikamente oder Generika, für die bereits klinische Zulassungen und Langzeit-Daten bestehen, vernachlässigt werden. Besonders interessant sind Medikamente, die in Kombination eine synergistische antitumorale Wirkung haben. Für die Suche nach Synergien wurden bereits Methoden publiziert [64,82], von denen viele auf High-Throughput-Untersuchungen basieren [6,44].
Diese sind jedoch oft mangels Infrastruktur und Finanzierung schwer umsetzbar. Deshalb wurde durch Jonas Parczyk, Andreas Klein und mich im Rahmen dieser Arbeit ein minimalistisches Synergie Screening (MDIS) entwickelt, dessen Ziel es ist, Synergien verlässlich und kosteneffizient in einer verhältnismäßig großen Anzahl an Medikamenten vorherzusagen [62].
In der Literatur existieren mehr als 10 verschiedene Definitionen von synergistischer Interaktion [20]. Bereits Mitte des 20. Jahrhundert wurde mit der Loewe-Synergie [38] eine Methode zur Quantifizierung von Synergien beschrieben, die auf einem sogenannten combination index (CI) basiert. Im Verlauf wurde die “median effect method” von Chou und Talalay entwickelt, die auf dem Massenwirkungsgesetz [10,37] beruht. Die Quantifizierung synergistischer Interaktionen mehrerer Konzentrationen über die gesamte Dosis-Wirkungs-Kurve mit der Compu-Syn-Software [42] ist heutzutage eine weit verbreitete und etablierte Methode [86]. Da diese strenge Definition den Rahmen eines MDIS sprengt, müssen die vielversprechendsten Vorhersagen des MDIS im Anschluss als Synergie bestätigt werden.

1.5 Medikamente

Medikamente wurden nach dem GMSAT-Konzept den Ansatzpunkten Genom, Tumorstoffwechsel und Zellüberleben/Wachstum zugeordnet.
Im Bereich Genom ist das small molecule PRIMA-1met interessant, welches die Wildtyp-Konformation und -Funktionen von mutiertem p53 (‘Wächter des Genoms‘ [34,74]) wieder herstellen kann [7,57]. Nutlin-3 dagegen verhindert die p53-MDM2-Interaktion und hemmt damit den p53-Abbau [79]. SJ172550, ein weiteres small molecule, setzt ganz ähnlich an der p53-MDM4-Interaktion an und führt so zu einer erhöhten p53 Konzentration [35].
Für den Ansatzpunkt Metabolismus wurde unter anderem DCA ausgewählt, ein bereits lange bekanntes Medikament, welches bereits bei hereditärer Laktatazidose eingesetzt wurde [68]. Über die Hemmung der Pyruvatdehydrogenase-Kinase und somit Aktivierung der Pyruvatdehydrogenase (PDH), sorgt es für eine vermehrte Einschleusung von Pyruvat in den Zitratzyklus und kehrt den Warburg-Effekt damit partiell um [8]. Andere wichtige Medikamente sind der HIF-1a-Inhibitor PX-478, Metformin, welches den Komplex 1 der Atmungskette hemmt [82], der Laktat Dehydrogenase A (LDH-A)-Inhibitor NHI-2 sowie der Hexokinase 2 (HK2)-Inhibitor 3-Bromopyruvat (3-BP) [30]. Ein wichtiger tumoraler Stoffwechselweg ist zudem der Abbau von Glutamin [13]. Dieser wird durch den Glutaminase-Inhibitor CB-839 adressiert [21].
In der Kategorie Zellüberleben/Wachstum wurde neben dem Survivin-Inhibitor YM155 [50] und dem (PI3K)-Inhibitor Pictilisib/GDC-0941 [77] auch InoC2PAF [19,56] und das Ingwerderivat 6-Shogaol ausgewählt, welches den AKT/mTOR Pathway hemmt. [26].

2 Material und Methodik

2.1 Zellkultur

Bei HT-29 handelt es sich um eine primäre Kolonkarzinom Zelllinie mit p53 Mutation (R273H), die 1964 von Fogh und Trempe insoliert wurde. Zudem ist eine Dysregulation von c-MYC [4] beschrieben. HT-29 wurde freundlicherweise von Karsten Parczyk (Bayer AG) zur Verfügung gestellt und ursprünglich über ATCC (Katalog-Nummer: HTB-38) bezogen.
In allen Versuchen wurde sie mit Penicillin/Streptomycin (100 U ml^{-1})-haltigem DMEM mit L-Glutamine (584 mg l^{-1}) und 10% hitzebehandeltem, fetalem Kälberserum kultiviert.
Die Brustkrebszelllinie MDA-MB-231 weist ebenfalls eine p53-Mutation (R280K) auf und wurde ursprünglich aus einem Pleuraerguss isoliert. Sie exprimiert weder Hormonrezeptoren für Östrogen und Progesteron, noch besteht eine Amplifikation von HER-2 (triple-negativ). Die Zelllinie wurde unserer Arbeitsgruppe freundlicherweise von Göran Landberg (Sahlgrenska Cancer Center, University of Gothenburg, Gothenburg, Sweden) zur Verfügung gestellt.
In allen Versuchen wurde sie mit Penicillin/Streptomycin (100 U ml^{-1})-haltigem DMEM/F12 mit L-Glutamine (365,1 mg l^{-1}) und 10% hitzebehandeltem, fetalem Kälberserum verwendet.
Die Kultivierung erfolgte bei beiden Zelllinien in einem 37°C warmen Inkubator mit 5% CO2.
Für das Waschen und Umsetzen der Zellen wurde PBS und 0,05% haltiges Trypsin verwendet.

2.2 Medikamente

Medikament	Bezugsquelle
CB-839	Selleck Chemicals, Houston, TX, USA
Cisplatin	Cayman Chemical Ann Arbor, MI, USA
DCA, Metformin	Sigma-Aldrich, Munich, Germany
NHI-2	Bio-Techne GmbH, Wiesbaden-Nordenstadt, Germany
Prima-1met, Nutlin-3, SJ 172550, YM155	Selleck Chemicals, Houston, TX, USA
Pictilisib	Absource Diagnostics GmbH, Munich, Germany
PX-478, 6-Shogaol	Hölzel Diagnostika Handels GmbH, Cologne, Germany
3-Bromopyruvat	Santa Cruz Biotechnology, Dallas, Texas, USA
Ino-C2-PAF (1-O-octadecyl-2-O-(2-(myo-inositolyl)-ethyl)-sn-glycero-3-(r/s)-phosphatidylcholine) [18]	AG Zelladhäsions-vermittelte Signaltransduktion,Institut für Biochemie, Universitätsmedizin Berlin

In destilliertem Wasser wurden 3-Bromopyruvat, Cisplatin, DCA, Metformin, PRIMA-1-met, PX-478, YM155 und Ino-C2-PAF gelöst. Dimethylsulfoxid (DMSO) wurde zur Lösung von 6-Shogaol, CB-839, NHI-2, Nutlin-3, Pictilisib und SJ-17255 verwendet. Pro Well wurde Die DMSO Konzentration 0,6% (0.6 µl pro Well) nicht überschritten.

2.3 Messung des Zellüberlebens und der Proliferation

Um das Zellüberleben zu messen, wurden je 1,5 10^4 HT-29/ MDA-MB-231 Zellen pro Well in eine 96-well Platte mit flachem Boden gegeben und 24 Stunden zu einer Konfluenz von 50% inkubiert. Danach wurden die Zellen mit den jeweiligen Einzelpräparaten oder deren Kombination mediziert und für weitere 48 Stunden inkubiert. Die Negativ-Kontrolle wurde mit

0,6 % DMSO behandelt, wobei es in Bezug auf das Zellüberleben keine Unterschiede zu nicht DMSO-behandelten Zellen gab. Danach wurden die Zellen entweder mit einem 3-(4,5-Dimethylthiazol-2-yl)-2,5-diphenyltetrazoliumbromid- (MTT) von Bio-Techne GmbH oder einem Sulforhodamin B (SRB)-Assay analysiert. Der MTT-Assay wurde wie vom Hersteller angegeben verwendet. Beim SRB-Assay wurden die Zellen mit 10 % Trichloessigsäure (w/v) behandelt und mit 0,06 % SRB in 1% Essigsäure über 30 Minuten gefärbt. Daraufhin fanden mehrere Waschzyklen mit 1% Essigsäure (v/v) statt, gefolgt von einer Auflösung in 10 mM Tris (pH 10,5). Die Proteinmasse wurde mit einem Mikroplattenleser (microplate reader) bei einer Wellenlänge von 492 nm ausgelesen. In allen Untersuchungen wurden mindestens zwei Replikate und drei separate Experimente durchgeführt. Die Dosis-Wirkungskurven wurden mit der Software GraphPad Prism statistical analysis software 7.05 berechnet. Für die mittlere effektive Konzentration (EC_{50}) der 14 Pharmaka wurde die Funktion “nonlinear regression” verwendet.

2.4 Minimalistic drug interaction screening (MDIS)

HT-29 Zellen wurden mit den 14 Substanzen in den 91 möglichen Zweier-Kombinationen mit Dosierungen im Bereich der EC_{25} behandelt. Es wurden mindestens zwei technische Replikate in drei unabhängigen Experimenten durchgeführt, sodass pro Zellline ungefähr 909 Datenpunkte (303 pro Replikat) zu Stande kamen. Zur Vorhersage synergistischer Interaktion wurde die vermutete synergistischen Potenz (CSP) berechnet. Dabei wurden die Einzeleffekte addiert und vom Kombinationseffekt abgezogen. CSP-Werte über 10% wurden als mögliche („possible“), über 15% als wahrscheinliche („likely“) und über 25% als sehr wahrscheinliche („very likely“) Synergien eingestuft. Für diese Berechnungen wurde Microsoft Excel verwendet. Die statistische Auswertung erfolgte in GraphPad Prism.

2.5 Bestätigung der Synergien

Die über das MDIS vorhergesagten Synergien wurden wie von Chou und Talalay empfohlen in drei bis sieben verschiedenen Konzentrationen über die Dosis-Wirkungs-Kurve überprüft [12]. HT-29 Zellen wurden mit den Einzelmedikamenten sowie der jeweiligen Kombination in einem konstanten EC_{50}:EC_{50} Verhältnis mediziert. Signifikante Unterschiede zwischen dem Zellüberleben von Einzeldosis und Kombination wurde durch einen ungepaarten T-Test ermittelt. Nur Konzentrationen mit einem p-Wert ≤ 0,05 im Bezug der Kombination auf beide Substanzen wurden in den Darstellungen mit einem Sternchen (*) versehen.
Die Kombination-Indices (CI) wurden mit der CompuSyn-Software berechnet [42]. Der CI ist ein quantitativer Wert für synergistische Interaktion in einer bestimmten Konzentration. Ein Wert unter 0,3 wurde als “strong”, zwischen 0, 3 – 0,7 “robust” (ursprünglich von Chou and Talalay als “synergism” bezeichnet) und zwischen 0,7 und 0,85 als “moderate” synergistisch definiert. Werte zwischen 0,9 und 1,1 weisen einen additiven Effekt nach und ein CI-Wert größer 1,1 steht für einen Antagonismus [11]. Der CI-Wert wurde wie folgt berechnet:

$$CI = \frac{(D)_1}{(Dx)_1} + \frac{(D)_2}{(Dx)_2}$$

$(D)_1$ und $(D)_2$ im Zähler stehen für die Konzentrationen von Substanz 1 und 2, die in der Kombination verwendet wurde und den Effekt (x %) auf das Zellüberleben haben. Im Nenner, $(Dx)_1$ and $(Dx)_2$, stehen die Dosen der Einzelmedikamente, die nötig sind, um den gleichen Effekt (x %) wie die Kombination zu erzielen. Diese Dosen $(Dx)_1$ und $(Dx)_2$ wurden mit CompySyn aus den Datenpunkten der Einzelsubstanzen berechnet. Um Berechnungsfehler möglichst gering zu halten, wurden vorwiegend direkte experimentelle Datenpunkte

verwendet, wie von Zhao und Kollegen empfohlen [86]. Um die “median effect plots” zu berechnen wurde die folgende Gleichung verwendet:

$$D_x = D_m \left[\frac{fa}{1 - fa} \right]^{1/m}$$

Dm ist die “median effect dose”, *m* steht für die Steigung des „median-effect plots“ und fa steht für die betroffene Fraktion des Effektes auf das Zellüberleben.

2.6 Membranlipidoxidationsrate

HT-29-Zellen wurden in eine 10cm große Petrischale ausgesetzt und nach 24 Stunden Inkubation, sowie Erreichen einer Konfluenz von ungefähr 80%, mit der EC_{50} von DCA, PX-478 sowie der Kombination mediziert. Nach einer Inkubationsperiode von weiteren 48 Stunden wurden die Zellen mit Trypsin abgelöst, pelletiert und in 500 µl hosphatgepufferter Salzlösung (PBS) resuspendiert. Die Lipidextraktion erfolgte nach Homogenisierung in einem Volumenverhältnis Methanol:Chloroform:Wasser von 2:1:1 nach einer modifizierten Bligh/Dyer Methode. Die resultierende Lipidsuspension wurde mit Argon gespült, um eine artifizielle Oxidation zu vermeiden. Danach erfolgte die alkalische Hydrolyse mit KOH und die resultierenden freien Fettsäuren wurden mit Revervse-Phase-HPLC (RP-HPLC) detektiert. Arachidonsäure und die oxidierten Derivate 10-/15- Hydroxyeicosatetraensäure (HETE) wurden durch ihre spezifischen Retentionszeiten und UV-Spektren identifiziert und mittel Integration quantifiziert [31].

2.7 Statistische Auswertung

Die statistische Auswertung erfolgte mittels ungepaartem T-Test in GraphPad Prism 7.05. P-Werte unter 0,05 wurden als signifikant angesehen. Signifikante Unterschiede zur Kontrolle wurden mit einem Sternchen (*) versehen und Werte, die signifikant unterschiedlich sowohl zur Kontrolle als auch zu den jeweiligen Einzelsubstanzen waren, erhielten zwei Sternchen (**). Alle Experimente wurden mindestens in zwei technischen Kontrollen und drei voneinander unabhängigen Experimenten durchgeführt.

3 Ergebnisse

3.1 Publikation 1: Genome reorganization in different cancer types: detection of cancer specific breakpoint regions

In dieser Studie wurden bereits publizierte SNP-Array-Daten von 111 Tumorproben (16x Malignes Melanom, 48x Mamma-, 25x Pankreaskarzinom, 22x von Pankreaskarzinom abgeleitete Zelllinien) analysiert. Als Kontrolle wurden Proben aus dem peripheren Blut gesunder Probanden verwendet.

Aus den bestehenden SNP-Daten wurden zunächst segCNV berechnet. Ein Bruchpunkt wurde definiert als zwei DNA-Segmente, die sich in ihren durchschnittlichen CNV um mehr als die log2-ratio von 0,5 unterscheiden und von denen ein Segment mindestens aus zehn und das andere mindestens aus vier SNP besteht. Zur einfacheren Auswertung wurde das Genom in 30951 Regionen à 100 kb unterteilt, von denen 19687 (63,61 %) mindestens einen Bruchpunkt aufwiesen. Es konnten 15 Top-BPR identifiziert werden. In diesen Regionen hatten mindestens 20% (23) der Tumorzellen einen Bruchpunkt. Weiterhin wiesen elf (73%) von diesen eine Assoziation zu bereits bekannten Sollbruchstellen (fragile sites) auf. Drei der Top-15-BPR (Chr. 9,13,14) traten über alle untersuchten Tumorentitäten verteilt auf, wobei der Bruchpunkt auf Chromosom 9 in 43 % aller Tumore auftrat. Weiterhin wurden sieben BPR (Chromosom 1,4,5,7,8,13) exklusiv in PDAC-Zellen und eine (Chromosom 2) exklusiv in Brustkrebsproben gefunden.

Diese Studie legt nahe, dass BPR auf einigen Abschnitte des menschlichen Genoms eine spezifische Rolle in den jeweiligen Tumorentitäten spielen. Genomische Reorganisation in anderen Abschnitten dagegen findet unspezifisch über alle Tumorentitäten verteilt und teils auch in gesunden Zellen statt.

3.2 Publikation 2: Synergisms of genome and metabolism stabilizing antitumor therapy (GMSAT) in human breast and colon cancer cell lines: a novel approach to screen for synergism

Mit dem Ziel die tumorale Mikroevolution zu verlangsamen wurden 14 Medikamente ausgewählt, die auf die Systeme Tumorstoffwechsel, genetische Instabilität und Wachstum/Überleben abzielen.

Daraufhin wurden Dosis-Wirkungskurven für Kolon- (HT-29) und Mammakarzinom (MCF-7, MDA-MB-231) Zelllinien angefertigt und die EC_{50} bestimmt. Weiterhin wurden die Medikamente in einem dafür entwickelten MDIS in allen 91 möglichen Zweier-Kombinationen in HT-29 und MCF-7 kombiniert und dem MTT-Assay ausgewertet.

Insgesamt wurden 19 (HT-29) und 27 (MCF-7) synergistische Interaktionen gefunden, bei denen die Kombinationstherapie mindestens einen 10% stärkeren Effekt hatte als die Summe der Einzeleffekte. Diese Ergebnisse wurden weiter nach ihrem CSP-Wert in die Kategorien mögliche (CSP > 10%), wahrscheinliche (CSP > 15%) und sehr wahrscheinliche (CSP > 25%) Synergien eingeteilt.

Die stärkste synergistische Interaktion wurde für der Kombination DCA und PX-478 in HT-29 Zellen mit 62,4% erreicht. Mit der Methode von Chou und Talalay wurden acht im MDIS vorhergesagte synergistische Interaktionen verifiziert von denen sechs bestätigt werden konnten. Nutlin-3 kombiniert mit PX-478 wurde in HT-29 (CI = 0,63) und MDA-MB-231 (CI = 0,62) bestätigt. Das Gleiche gilt für die Kombination von DCA und NHI-2 mit CI Werten von 0,5 (HT-29) und 0,62 (MDA-MB-231). Die Kombination von PX-478 und DCA wurde in einer separaten Studie weiterführend untersucht.

3.3 Publikation 3: Dichloroacetat and PX-478 exhibit strong synergistic effects in a various number of cancer cell lines

In dieser Studie konnten die Medikamentenkombination aus DCA und PX-478 mit der Methode von Chou und Talalay in Zelllinien der Entitäten Bronchial- (A549, H441), Mamma- (MCF-7, MDA-MB-231) Zervix- (HeLa), Kolonkarzinom (HT-29) sowie Hepatozellulärem Karzinom (HepG2) und Glioblastom (U251) als Synergie bewiesen werden.

Für HT-29 und MDA-MB-231 ergaben sich CI-Werte von 0,54 und 0,8. Die verwendeten Dosen zeigten nur minimale Effekte auf die nicht tumoröse Zelllinie HEK-293.

PX-78-behandelte HT-29 Zellen wiesen eine um 58% signifikant erhöhte Membranlipidoxidationsrate im Vergleich zur Kontrolle auf ($p = 0,04$). Bei der Kombination aus DCA und PX-478 lag die Steigerung sogar bei 109% ($p = 0,02$). Diese Oxidation beruht auf einer erhöhten ROS-Produktion wie in FACS-Analysen mit H2DCFDA bestätigt werden konnte. Western Blot Ergebnisse sowie FACS Analysen zeigen eine vermehrte Induktion von Zellzyklusarrest und Apoptose.

4 Diskussion

4.1 Genomische Veränderungen in der Tumorigenese

Genomische Veränderungen nehmen im Verlauf der Tumorigenese zu [74]. Passend zu unseren Ergebnissen konnten in einer Analyse von 2737 Proben verschiedener Tumore für jede Entität tumorspezifische Bruchpunkte gefunden werden [41]. Interessanterweise fanden Beroukhim und Kollegen in 3131 Tumorproben 158 BPR, von denen 36 mit bekannten Krebszielgenen wie FHIT and CDKN2 erklärt werden konnten [5]. In unserer Studie waren acht Gene in Breakpoints lokalisiert, die in Verbindung zu Krebs stehen [71]. C8orf33 und NBEA scheinen tumorsupprimierende Funktionen zu haben [52,63], während die anderen sechs mit Tumorprogress assoziiert sind: IBSP, MEPE, RELN, THSD7A sind mit Migration, Invasion, Infiltration und Angiogenese assoziiert [15,46,69,81] und CACNA1B sowie KIAA0513 mit Zellproliferation und Apoptose. Überexpression von CACNA1B ist zudem mit einer ungünstigeren Prognose bei nicht-kleinzelligem Bronchialkarzinom (NSCLC) [88] assoziiert und eine veränderte KIAA0513-Expression aufgrund von Methylierung stand in Korrelation zu letalen Verläufen beim Neuroblastom [52].

4.2 MDIS – ein effizientes Werkzeug auf der Suche nach synergistischen Interaktionen

Für die Durchführung des MDIS werden ausschließlich 96-Well-Platten, ein ELISA-Reader, Medikamente und ein Zellkulturlabor benötigt.
Es konnten 19 Synergien (20,9%) in HT-29 und 27 (29,7%) in MCF-7 Zellen vorhergesagt werden. Vier wahrscheinliche und sehr wahrscheinliche Synergien wurden mit der Methode von Chou und Talalay überprüft und konnten alle vier bestätigt werden. In der Gruppe der möglichen Synergien wiesen nur zwei von vier Kombinationen signifikante Synergien auf.
Somit ist bei MCF-7 von elf (12,1%) und bei HT-29 von acht (8,8%) verlässlichen Vorhersagen auszugehen. Interessanterweise wurde die Kombination aus DCA und NHI-2 in HT-29 nicht im MDIS als Synergie vorhergesagt, konnte aber mit der Methode von Chou und Talalay als Synergie identifiziert werden. Das MDIS scheint sich daher nicht gut dafür zu eignen, synergistische Interaktionen auszuschließen [62].
Borisy und Kollegen führten ein Roboter-assistiertes Screening auf synergistische Interaktion bei 30 antimykotischen Medikamenten mit 435 möglichen Zweierkombinationen in sechs verschiedenen Konzentrationen und insgesamt 31320 Datenpunkten durch [81]. Für 14 Medikamente wären das 6552 Datenpunkte im Vergleich zu 303 Datenpunkte im MDIS, was einer Reduktion des experimentellen Umfangs von 95,38% entspricht. Damit eignet sich das Werkzeug gut, um effizient einen Überblick über die synergistischen Interaktionen von Pharmaka eines Forschungsfeldes zu bekommen.

4.3 DCA und PX-478 – eine vielversprechende Kombinationstherapie

Die Kombination aus DCA und PX-478 wies von den 182 ermittelten CSP-Werten mit 62,4% in HT-29 die mit Abstand stärkste synergistische Interaktion auf. Zudem wurden für die beiden Pharmaka die meisten und stärksten synergistischen Interaktionen im MDIS nachgewiesen. Diese Synergie konnte neben HT-29 und MDA-MB-231 in allen sechs weiteren Tumorzelllinien bestätigt werden [62].
In präklinischen Studien hat sich DCA in Kombination mit diversen Zytostatika wie Paclitaxel, Doxorubicin und Cisplatin als Chemosensibilisator bewährt [71] und sich in Kombination mit dem Metformin-Analogon Phenformin effektiv in der Bekämpfung von Krebs-Stammzellen (Jiang et al., 2016) gezeigt. Passend zu diesen Ergebnissen konnte im MDIS sowohl für HT-29 als auch MCF-7 Zellen eine synergistische Interaktion zwischen DCA und Metformin als *wahrscheinlich* vorhergesagt werden [62].

Limitiert wird die klinische Anwendung von DCA bisher insbesondere durch die dosisabhängige Neurotoxizität mit Entwicklung einer peripheren Polyneuropathie. Als Ursache hierfür wird oxidativer Stress postuliert, den die normalerweise Glykolyse betreibenden Schwann-Zellen offenbar nicht kompensieren können [69]. Für DCA zeigen die Ergebnisse dieser Arbeit allerdings lediglich einen nicht signifikanten Anstieg der Membranlipidoxidationrate 21% ($p = 0,21$) in HPLC-Analysen und keinen signifikanten Anstieg der ROS-Produktion in FACS-Daten [55].
Im Fall von PX-478 konnte bereits vor über 10 Jahren am Beispiel mehrerer Lungenkarzinom Maus-Modelle gezeigt werden, dass es Progress, Tumorgröße und Metastasierung signifikant verringert [27]. Passend zu den Ergebnissen dieser Arbeit konnte in präklinischen Untersuchungen zum duktalen Pankreaskarzinom beschrieben werden, wie die Kombination von PX-478 und Arsentrioxid zu einer Proliferationshemmung und Apoptose Induktion durch ROS-Erhöhung führt [34]. Letzteres wurde durch unsere Analysen bestätigt, da das Medikament zu einer signifikanten Steigerung der Membranlipidoxidationrate in HT-29 (58%, $p = 0,04$) und ROS-Produktion von 2–12% ($p = 0,008$) in Hela-Zellen führte [55].
Interessanterweise zeigte sich in der bisher einzigen Phase-1-Studie mit PX-478 im Gegensatz zu DCA kein Hinweis auf Neurotoxizität [75]. Somit stellt sich die Frage, ob die DCA induzierte Neurotoxizität tatsächlich allein auf eine ROS-Erhöhung zurückzuführen ist.
Obwohl die orale Gabe von PX-478 in einer klinischen Phase-1 Studie als sicher und gut verträglich beschrieben wurde und in soliden Tumoren mit einer verlängerten Krankheitsstabilisierung (stable disease) assoziiert war [75], wurden bisher keine weiteren klinischen Studien durchgeführt. Aktuell wird PX-478 in präklinischen Studien als Medikament der Frühgeborenen-Retinopathie [54] und der Autoimmunmyokarditis [25] untersucht.
Die Kombinationstherapie von DCA und PX-478 kann dazu beitragen, die Einzeldosen um durchschnittlich 57% zu reduzieren [55]. Allerdings könnte die dadurch erreichte Toxizitätsverminderung durch die signifikant gesteigerte ROS-Produktion (109%, $p=0,02$) wieder relativiert werden.
Neue Forschung im Bereich von Drug-Delivery-Systemen [1] und die Gabe von Antioxidantien [69] gibt Hoffnung, diese Hürden in Zukunft zu überwinden.
Aufgrund der hier dargestellten Effektivität der Kombination von PX-478 und DCA in einer Vielzahl von Tumorentitäten empfehlen sich als nächste Schritte das Tiermodell und darauffolgend klinische Studien.

4.4 Zusammenfassung

Insgesamt konnte mit der hier präsentierten Arbeit das Potenzial neuer Therapieansätze im Bereich Genom und Tumorstoffwechsel gezeigt werden. Mit dem MDIS konnte ein effizientes Werkzeug entwickelt werden, dass es kleinen Arbeitsgruppen ermöglichen kann, neue Forschungsfelder zu explorieren.
Neben einer Vielzahl möglicher und bestätigter Synergien, die in dieser Arbeit aufgezeigt werden, konnte die Synergie aus PX-478 und DCA ihr Potenzial als Antitumor-Therapie unter Beweis stellen. Interessant wäre auch die genauere Untersuchung weiterer hier vorgestellter Synergien wie zum Beispiel der Kombination aus Nutlin-3 und PX-478 oder DCA und NHI-2.

5 Literaturverzeichnis

[1] Abánades Lázaro, I., Abánades Lázaro, S., & Forgan, R. S. (2018). Enhancing anticancer cytotoxicity through bimodal drug delivery from ultrasmall Zr MOF nanoparticles. *Chemical Communications*, *54*(22), 2792–2795. https://doi.org/10.1039/c7cc09739e

[2] Al-Lazikani, B., Banerji, U., & Workman, P. (2012). Combinatorial drug therapy for cancer in the post-genomic era. *Nat. Biotechnol.*, *30*(7), 679–692. https://doi.org/10.1038/nbt.2284

[3] Andor, N., Maley, C. C., & Ji, H. P. (2017). Genomic Instability in Cancer: Teetering on the Limit of Tolerance. *Cancer Research*, *77*(9), 2179–2185. https://doi.org/10.1158/0008-5472.CAN-16-1553

[4] Berglind, H., Pawitan, Y., Kato, S., Ishioka, C., Soussi, T. (2008). Analysis of p53 mutation status in human cancer cell lines. *Cancer Biology and Therapy*, *7(5)*, 699–708.

[5] Beroukhim, R., Mermel, C. H., Porter, D., Wei, G., Raychaudhuri, S., Donovan, J., Barretina, J., Boehm, J. S., Dobson, J., Urashima, M., Mc Henry, K. T., Pinchback, R. M., Ligon, A. H., Cho, Y.-J., Haery, L., Greulich, H., Reich, M., Winckler, W., Lawrence, M. S., Weir, B. A., Tanaka, K. E., Chiang, D. Y., Bass, A. J., Loo, A., Hoffman, C., Prensner, J., Liefeld, T., Goa, Q., Yecies, D., Signoretti, S., Maher, E., Kaye, F. J., Sasaki, H., Tepper, J. E., Fletcher, J. A., Tabernero, J., Baselga, J., Tsao, M-S., Demichelis, F., Rubin, M. A., Janne, P. A., Daly, M. J., Nucera, C., Levine, R. L., Ebert, B. L., Gabriel, S., Rustgi A. K., Antonescu, A. R., Ladanyi, M., Letai, A., Garraway, L. A., Loda, M., Beer, D. G., True, L. D., Okamoto, A., Pomeroy, S. L., Singer, S., Golub, T. R., Lander, E. S., Getz, G., Sellers, W. R., Meyerson, M. (2010). The landscape of somatic copy-number alteration across human cancers. *Nature*, *463*(7283), 899–905. https://doi.org/10.1038/nature08822

[6] Borisy, A. A., Elliott, P. J., Hurst, N. W., Lee, M. S., Lehar, J., Price, E. R., Serbedzija, G., Zimmermann, G. R., Foley, M. A., Stockwell, B. R., & Keith, C. T. (2003). Systematic discovery of multicomponent therapeutics. *Proceedings of the National Academy of Sciences of the United States of America*, *100*(13), 7977–7982. https://doi.org/10.1073/pnas.1337088100

[7] Bykov, V. J. N., Issaeva, N., Shilov, A., Hultcrantz, M., Pugacheva, E., Chumakov, P., Bergman, J., Wiman, K. G., & Selivanova, G. (2002). Restoration of the tumor suppressor function to mutant p53 by a low-molecular-weight compound. *Nature Medicine*, *8*(3), 282–288. https://doi.org/10.1038/nm0302-282

[8] Chen, Z., Lu, W., Garcia-Prieto, C., & Huang, P. (2007). The Warburg effect and its cancer therapeutic implications. *Journal of Bioenergetics and Biomembranes*, *39*(3), 267–274. https://doi.org/10.1007/s10863-007-9086-x

[9] Chisholm, R. H., Lorenzi, T., & Clairambault, J. (2016). Cell population heterogeneity and evolution towards drug resistance in cancer: Biological and mathematical assessment, theoretical treatment optimisation. *Biochimica et Biophysica Acta - General Subjects*, *1860*(11), 2627–2645. https://doi.org/10.1016/j.bbagen.2016.06.009

[10] Chou, T.-C. (2006). Theoretical basis, experimental design, and computerized simulation of synergism and antagonism in drug combination studies. *Pharmacological Reviews*, *58*(3), 621–681. https://doi.org/10.1124/pr.58.3.10.

[11] Chou, T.-C. (2008). Preclinical versus clinical drug combination studies. *Leukemia & Lymphoma*, *49*(11), 2059–2080.

[12] Chou, T. C., & Talalay, P. (1984). Quantitative analysis of dose-effect relationships: the combined effects of multiple drugs or enzyme inhibitors. *Advances in Enzyme*

Regulation, *22*, 27–55.

[13] Cluntun, A. A., Lukey, M. J., Cerione, R. A., & Locasale, J. W. (2017). Glutamine Metabolism in Cancer: Understanding the Heterogeneity. *Trends in Cancer*, *3*(3), 169–180. https://doi.org/10.1016/j.trecan.2017.01.005

[14] Dou, A., Wang, Z., Zhang, N., & Liu, J. (2017). Loss of reelin suppresses cell survival and mobility in non-Hodgkin lymphoma. *Oncology Reports*, *37*(6), 3572–3580. https://doi.org/10.3892/or.2017.5626

[15] Durkin, S. G., & Glover, T. W. (2007). Chromosome Fragile Sites. *Annual Review of Genetics*, *41*(1), 169–192. https://doi.org/10.1146/annurev.genet.41.042007.165900

[16] Essmann, F., & Schulze-Osthoff, K. (2012). Translational approaches targeting the p53 pathway for anti-cancer therapy. *British Journal of Pharmacology*, *165*(2), 328–344. https://doi.org/10.1111/j.1476-5381.2011.01570.x

[17] Evan, G. I., & Vousden, K. H. (2001). Proliferation, cell cycle and apoptosis in cancer. *Nature*, *411*(6835), 342–348. https://doi.org/10.1038/35077213

[18] Fischer, A., Müller, D., Zimmermann-Kordmann, M., Kleuser, B., Mickeleit, M., Laabs, S., Löwe, W., Cantagrel, F., Reutter, W., & Danker, K. (2006). The ether lipid inositol-C2-PAF is a potent inhibitor of cell proliferation in HaCaT cells. *ChemBioChem*, *7*(3), 441–449. https://doi.org/10.1002/cbic.200500336

[19] Foulds, L. (1954). The experimental study of tumor progression: a review. *Cancer Research*, *14*(5), 327–339.

[20] Greco, W. R., Bravo, G., & Parsons, J. C. (1995). The Search for Synergy: A Critical Review from a Response Surface Perspective. *Pharmacological Reviews, 45*(2)*,* 331-385.

[21] Gross, M. I., Demo, S. D., Dennison, J. B., Chen, L., Chernov-Rogan, T., Goyal, B., Janes, J. R., Laidig, G. J., Lewis, E. R., Li, J., MacKinnon, A. L., Parlati, F., Rodriguez, M. L. M., Shwonek, P. J., Sjogren, E. B., Stanton, T. F., Wang, T., Yang, J., Zhao, F., & Bennett, M. K. (2014). Antitumor Activity of the Glutaminase Inhibitor CB-839 in Triple-Negative Breast Cancer. *Molecular Cancer Therapeutics*, *13*(4), 890–901. https://doi.org/10.1158/1535-7163.MCT-13-0870

[22] Halatsch, M., Kast, R. E., Dwucet, A., Hlavac, M., Heiland, T., Westhoff, M., Debatin, K., Wirtz, C. R., Siegelin, M. D., & Karpel-Massler, G. (2019). Bcl-2/Bcl-xL inhibition predominantly synergistically enhances the anti-neoplastic activity of a low-dose CUSP9 repurposed drug regime against glioblastoma. *British Journal of Pharmacology*, 176(18), 3681-3694. https://doi.org/10.1111/bph.14773

[23] Hecht, F., Sutherland, G. R. (1984). Fragile sites and cancer breakpoints. *Cancer genetics and cytogenetics, 12*(2), 179-181. doi: 10.1016/0165-4608(84)90132-8.

[24] Hanahan, D., & Weinberg, R. A. (2011). Hallmarks of cancer: The next generation. *Cell*, *144*(5), 646–674. https://doi.org/10.1016/j.cell.2011.02.013

[25] Hua, X., Hu, G., Hu, Q., Chang, Y., Hu, Y., Gao, L., Chen, X., Yang, P. C., Zhang, Y., Li, M., & Song, J. (2020y). Single-cell RNA sequencing to dissect the immunological network of autoimmune myocarditis. *Circulation*, *142*(4), 384–400. https://doi.org/10.1161/CIRCULATIONAHA.119.043545

[26] Hung, J.-Y., Hsu, Y.-L., Li, C.-T., Ko, Y.-C., Ni, W.-C., Huang, M.-S., & Kuo, P.-L. (2009). 6-Shogaol, an Active Constituent of Dietary Ginger, Induces Autophagy by Inhibiting the AKT/mTOR Pathway in Human Non-Small Cell Lung Cancer A549 Cells. *Journal of Agricultural and Food Chemistry*, *57*(20), 9809–9816. https://doi.org/10.1021/jf902315e

[27] Jacoby, J. J., Erez, B., Korshunova, M. V., Williams, R. R., Furutani, K., Takahashi, O., Kirkpatrick, L., Lippman, S. M., Powis, G., O'Reilly, M. S., & Herbst, R. S. (2010). Treatment with hif-1α antagonist PX-478 inhibits progression and spread of orthotopic human small cell lung cancer and lung adenocarcinoma in mice. *Journal of Thoracic Oncology*, *5*(7), 940–949. https://doi.org/10.1097/JTO.0b013e3181dc211f

[28] Kast, R. E., Karpel-Massler, G., & Halatsch, M.-E. (2014). CUSP9* treatment protocol for recurrent glioblastoma: aprepitant, artesunate, auranofin, captopril, celecoxib, disulfiram, itraconazole, ritonavir, sertraline augmenting continuous low dose temozolomide. *Oncotarget*, *5*(18), 8052–8082. https://doi.org/10.18632/oncotarget.2408

[29] Klein, A., Guhl, E., Zollinger, R., Tzeng, Y.-J., Wessel, R., Hummel, M., Graessmann, M., & Graessmann, A. (2005). Gene expression profiling: cell cycle deregulation and aneuploidy do not cause breast cancer formation in WAP-SVT/t transgenic animals. *Journal of Molecular Medicine*, *83*(5), 362–376. https://doi.org/10.1007/s00109-004-0625-1

[30] Ko, Y. H., Pedersen, P. L., & Geschwind, J. F. (2001). Glucose catabolism in the rabbit VX2 tumor model for liver cancer: characterization and targeting hexokinase. *Cancer Letters*, *173*(1), 83–91. https://doi.org/10.1016/s0304-3835(01)00667-x

[31] Kuhn, H., Belkner, J., Wiesner, R., & Brash, A. R. (1990). Oxygenation of biological membranes by the pure reticulocyte lipoxygenase. *Journal of Biological Chemistry*, *265*(30), 18351–18361.

[32] Lambert, J. M. R., Gorzov, P., Veprintsev, D. B., Söderqvist, M., Segerbäck, D., Bergman, J., Fersht, A. R., Hainaut, P., Wiman, K. G., & Bykov, V. J. N. (2009). PRIMA-1 Reactivates Mutant p53 by Covalent Binding to the Core Domain. *Cancer Cell*, *15*(5), 376–388. https://doi.org/10.1016/j.ccr.2009.03.003

[33] Lane, D. P. (1992). p53, guardian of the genome. *Nature*, *358*(6381), 15–16. https://doi.org/10.1038/358015a0

[34] Lang, M., Wang, X., Wang, H., Dong, J., Lan, C., Hao, J., Huang, C., Li, X., Yu, M., Yang, Y., Yang, S., & Ren, H. (2016). Arsenic trioxide plus PX-478 achieves effective treatment in pancreatic ductal adenocarcinoma. *Cancer Letters*, *378*(2), 87–96. https://doi.org/10.1016/j.canlet.2016.05.016

[35] Lemos, A., Leão, M., Soares, J., Palmeira, A., Pinto, M., Saraiva, L., & Sousa, M. E. (2016). Medicinal Chemistry Strategies to Disrupt the p53-MDM2/MDMX Interaction. *Medicinal Research Reviews*, *36*(5), 789–844. https://doi.org/10.1002/med.21393

[36] Lines, C., Krueger, S. A., & Wilson, G. D. (2011). Cancer Cell Culture. *Methods*, *731*, 359–370. https://doi.org/10.1007/978-1-61779-080-5

[37] Loeb, L. A., Loeb, K. R., & Anderson, J. P. (2003). Multiple mutations and cancer. *Proceedings of the National Academy of Sciences*, *100*(3), 776–781. https://doi.org/10.1073/pnas.0334858100

[38] Loewe, S. (1953). The problem of synergism and antagonism of combined drugs. *Arzneimittel-Forschung*, *3*(6), 285–290. http://www.ncbi.nlm.nih.gov/pubmed/13081480

[39] Magenis, R. E., Hecht, F., & Lovrien, E. W. (1970). Heritable fragile site on chromosome 16: probable localization of haptoglobin locus in man. *Science (New York, N.Y.)*, *170*(3953), 85–87.

[40] Malhotra, D., & Sebat, J. (2012). CNVs: Harbingers of a rare variant revolution in psychiatric genetics. *Cell*, *148*(6), 1223–1241. https://doi.org/10.1016/j.cell.2012.02.039

[41] Marczok, S., Bortz, B., Wang, C., & Pospisil, H. (2016). Comprehensive Analysis of Genome Rearrangements in Eight Human Malignant Tumor Tissues. *PloS One*, *11*(7),

e0158995. https://doi.org/10.1371/journal.pone.0158995

[42] Chou, T.C., Martin, N. (2005). CompuSyn for Drug Combinations: PC Software and User's Guide: A Computer Program for Quantitation of Synergism and Antagonism in Drug Combinations, and the Determination of IC_{50} and ED_{50} and LD_{50} Values. ComboSyn Inc, Paramus (NJ).

[43] Mayer, L. D., & Janoff, A. S. (2007). Optimizing Combination Chemotherapy by Controlling Drug Ratios. *Molecular Interventions*, *7*(4), 216–223. https://doi.org/10.1124/mi.7.4.8

[44] Memarnejadian, A., Nikpoor, A. R., Davoodian, N., Kargar, A., Mirzadeh, Y., & Gouklani, H. (2019). HIV-1 Drug Resistance Mutations among Antiretroviral Drug-Experienced Patients in the South of Iran. *Intervirology, 62*(2), 72-79. https://doi.org/10.1159/000501255

[45] Meng, X., Zhao, Y., Wang, J., Gao, Z., Geng, Q., & Liu, X. (2017). Regulatory roles of miRNA-758 and matrix extracellular phosphoglycoprotein in cervical cancer. *Experimental and Therapeutic Medicine*, *14*(4), 2789–2794. https://doi.org/10.3892/etm.2017.4887

[46] Moore, R. D., & Chaisson, R. E. (1999). *Natural history of HIV infection in the era of combination antiretroviral therapy. AIDS, 13*(14), 1933-1942.

[47] Moses, H., Matheson, D. H. M., Cairns-Smith, S., George, B. P., Palisch, C., & Dorsey, E. R. (2015). The Anatomy of Medical Research. *JAMA*, *313*(2), 174. https://doi.org/10.1001/jama.2014.15939

[48] Murphy, W. J., Larkin, D. M., Everts-Van Der Wind, A., Bourque, G., Tesler, G., Auvil, L., Beever, J. E., Chowdhary, B. P., Galibert, F., Gatzke, L., Hitte, C., Meyers, S. N., Milan, D., Ostrander, E. A., Pape, G., Parker, H. G., Raudsepp, T., Rogatcheva, M. B., Schook, L. B., Skow, L. C., Welge, M., Womack, J. E., O'Brien, S. J., Pevzner, P. A., Lewin, H. A. (2005av). Evolution: Dynamics of mammalian chromosome evolution inferred from multispecies comparative maps. *Science*, *309*(5734), 613–617. https://doi.org/10.1126/science.1111387

[49] Nadeau, J. H., & Taylor, B. A. (1984). Lengths of chromosomal segments conserved since divergence of man and mouse. *Proceedings of the National Academy of Sciences*, *81*(3), 814–818. https://doi.org/10.1073/pnas.81.3.814

[50] Nakahara, T., Takeuchi, M., Kinoyama, I., Minematsu, T., Shirasuna, K., Matsuhisa, A., Kita, A., Tominaga, F., Yamanaka, K., Kudoh, M., & Sasamata, M. (2007). *YM155 , a Novel Small-Molecule Survivin Suppressant , Induces Regression of Established Human Hormone-Refractory Prostate Tumor Xenografts*. *17*, 8014–8021. https://doi.org/10.1158/0008-5472.CAN-07-1343

[51] O'Neal, J., Gao, F., Hassan, A., Monahan, R., Barrios, S., Lee, I., Chng, W. J., Vij, R., & Tomasson, M. H. (2009). Neurobeachin (NBEA) is a target of recurrent interstitial deletions at 13q13 in patients with MGUS and multiple myeloma. *Experimental Hematology*, *37*(2), 234–244. https://doi.org/10.1016/j.exphem.2008.10.014

[52] Olsson, M., Beck, S., Kogner, P., Martinsson, T., & Carén, H. (2016). Genome-wide methylation profiling identifies novel methylated genes in neuroblastoma tumors. *Epigenetics*, *11*(1), 74–84. https://doi.org/10.1080/15592294.2016.1138195

[53] Osborne, C. (2004). Oncogenes and Tumor Suppressor Genes in Breast Cancer: Potential Diagnostic and Therapeutic Applications. *The Oncologist*, *9*(4), 361–377. https://doi.org/10.1634/theoncologist.9-4-361

[54] Pan, X., & Lv, Y. (2020). Effects and Mechanism of Action of PX-478 in Oxygen-

Induced Retinopathy in Mice. *Ophthalmic Research*, *63*(2), 182–193. https://doi.org/10.1159/000504023

[55] Parczyk J, Ruhnau J, Pelz C, Schilling M, Wu H, Piaskowski NN, Eickholt B, Kühn H, Danker K, Klein A. Dichloroacetate and PX-478 exhibit strong synergistic effects in a various number of cancer cell lines. BMC Cancer. 2021;21(1). https://doi.org/10.1186/s12885-021-08186-9

[56] Pelz, C., Häckel, S., Semini, G., Schrötter, S., Bintig, W., Stricker, S., Mrawietz, G., Klein, A., Lucka, L., Shmanai, V., Eickholt, B., Hildmann, A., & Danker, K. (2018). Inositol-C2-PAF acts as a biological response modifier and antagonizes cancer-relevant processes in mammary carcinoma cells. *Cellular Oncology*, *41*(5), 505–516. https://doi.org/10.1007/s13402-018-0387-3

[57] Perdrix, A., Najem, A., Saussez, S., Awada, A., Journe, F., Ghanem, G., & Krayem, M. (2017). PRIMA-1 and PRIMA-1Met (APR-246): From mutant/wild type p53 reactivation to unexpected mechanisms underlying their potent anti-tumor effect in combinatorial therapies. *Cancers, 9*(12), 172. https://doi.org/10.3390/cancers9120172

[58] Pevzner, P., & Tesler, G. (2003). Human and mouse genomic sequences reveal extensive breakpoint reuse in mammalian evolution. *Proceedings of the National Academy of Sciences*, *100*(13), 7672–7677. https://doi.org/10.1073/pnas.1330369100

[59] Redon, R., Ishikawa, S., Fitch, K. R., Feuk, L., Perry, G. H., Andrews, T. D., Fiegler, H., Shapero, M. H., Carson, A. R., Chen, W., Cho, E. K., Dallaire, S., Freeman, J. L., González, J. R., Gratacòs, M., Huang, J., Kalaitzopoulos, D., Komura, D., MacDonald, J. R., Marshall, C. R., Mei, R., Montgomery, L., Nishimura, K., Okamura, K., Shen, F., Somerville, M. J., Tchinda, J., Valsesia, A., Woodwark, C., Yang, F., Zhang, J., Zerjal, T., Zhang, J., Armengol, L., Conrad, D. F., Estivill, X., Tyler-Smith, C., Carter, N. P., Aburatani, H., Lee, C., Jones, K. W., Scherer, S. W., Hurles, M. E. (2006). Global variation in copy number in the human genome. *Nature*, *444*(7118), 444–454. https://doi.org/10.1038/nature05329

[60] Research America. (2016). *U.S. Investments in Medical and Health Research and Development*. https://www.researchamerica.org/sites/default/files/2016US_Invest_R%26D_report.pdf, Accessed March 20, 2020.

[61] Roberts, J., Bebenek, K., & Kunkel, T. (1988). The accuracy of reverse transcriptase from HIV-1. *Science*, *242*(4882), 1171–1173. https://doi.org/10.1126/science.2460925

[62] Ruhnau J, Parczyk J, Danker K, Eickholt B, Klein A. Synergisms of genome and metabolism stabilizing antitumor therapy (GMSAT) in human breast and colon cancer cell lines: A novel approach to screen for synergism. BMC Cancer. 2020 Jul 2;20(1). https://doi.org/10.1186/s12885-020-07062-2

[63] Ruiz-Herrera, A., Castresana, J., & Robinson, T. J. (2006). Is mammalian chromosomal evolution driven by regions of genome fragility? *Genome Biology*, *7*(12), R115. https://doi.org/10.1186/gb-2006-7-12-r115

[64] Shao, P., Sun, D., Wang, L., Fan, R., & Gao, Z. (2017). Deep sequencing and comprehensive expression analysis identifies several molecules potentially related to human poorly differentiated hepatocellular carcinoma. *FEBS Open Bio*, *7*(11), 1696–1706. https://doi.org/10.1002/2211-5463.12310

[65] Sheng, Z., Sun, Y., Yin, Z., Tang, K., & Cao, Z. (2017). Advances in computational approaches in identifying synergistic drug combinations. *Briefings in Bioinformatics*, *19*(6), 1172–1182. https://doi.org/10.1093/bib/bbx047

[66] Shlien, A., & Malkin, D. (2009). Copy number variations and cancer. *Genome Medicine*,

1(6), 1–9. https://doi.org/10.1186/gm62

[67] Skaga, E., Skaga, I. Ø., Grieg, Z., Sandberg, C. J., Langmoen, I. A., & Vik-Mo, E. O. (2019). The efficacy of a coordinated pharmacological blockade in glioblastoma stem cells with nine repurposed drugs using the CUSP9 strategy. *Journal of Cancer Research and Clinical Oncology*, *145*(6), 1495–1507. https://doi.org/10.1007/s00432-019-02920-4

[68] Stacpoole, P W. (1989). The pharmacology of dichloroacetate. *Metabolism: Clinical and Experimental*, *38*(11), 1124–1144. http://www.ncbi.nlm.nih.gov/pubmed/2554095

[69] Stacpoole, Peter W., Martyniuk, C. J., James, M. O., & Calcutt, N. A. (2019). Dichloroacetate-induced peripheral neuropathy. *International Review of Neurobiology, 145,* 211–238. https://doi.org/10.1016/bs.irn.2019.05.003

[70] Stahl, P. R., Hoxha, E., Wiech, T., Schröder, C., Simon, R., & Stahl, R. A. K. (2017). THSD7A expression in human cancer. *Genes Chromosomes and Cancer*, *56*(4), 314–327. https://doi.org/10.1002/gcc.22440

[71] Standfuß, C., Pospisil, H., & Klein, A. (2012). SNP microarray analyses reveal copy number alterations and progressive genome reorganization during tumor development in SVT/t driven mice breast cancer. *BMC Cancer*, *12*(1), 380. https://doi.org/10.1186/1471-2407-12-380

[72] Standfuß C, Parczyk J, Ruhnau J, Klein A Genome reorganization in different cancer types: detection of cancer specific breakpoint regions. *Mol Cytogenet. 2019*;12(1):1-8. https://doi.org/10.1186/s13039-019-0435-3

[73] Swanton, C., Nicke, B., Marani, M., Kelly, G., & Downward, J. (2007). Initiation of high frequency multi-drug resistance following kinase targeting by siRNAs. *Cell Cycle*, *6*(16), 2001–2004. https://doi.org/4538

[74] Tataranni, T., & Piccoli, C. (2019). Dichloroacetate (DCA) and Cancer: An Overview towards Clinical Applications. *Oxidative Medicine and Cellular Longevity*, *Volume 2019*, Article ID 8201079. https://doi.org/10.1155/2019/8201079

[75] Tibes, R., Falchook, G. S., Von Hoff, D. D., Weiss, G. J., Iyengar, T., Kurzrock, R., Pestano, L., Lowe, A. M., & Herbst, R. S. (2010). Results from a phase I, dose-escalation study of PX-478, an orally available inhibitor of HIF-1α. *Journal of Clinical Oncology*, *28*(15_suppl), 3076–3076. https://doi.org/10.1200/jco.2010.28.15_suppl.3076

[76] Toufektchan, E., & Toledo, F. (2018). The guardian of the genome revisited: P53 downregulates genes required for telomere maintenance, DNA repair, and centromere structure. In *Cancers* (Vol. 10, Issue 5). MDPI AG. https://doi.org/10.3390/cancers10050135

[77] Vadas, O., Burke, J. E., Zhang, X., Berndt, A., & Williams, R. L. (2011). Structural Basis for Activation and Inhibition of Class I Phosphoinositide 3-Kinases. *Science Signaling*, *4*(195), re2–re2. https://doi.org/10.1126/SCISIGNAL.2002165

[78] Vander Heiden, M. G., & DeBerardinis, R. J. (2017). Understanding the Intersections between Metabolism and Cancer Biology. *Cell*, *168*(4), 657–669. https://doi.org/10.1016/j.cell.2016.12.039

[79] Vassilev, L. T., Vu, B. T., Graves, B., Carvajal, D., Podlaski, F., Filipovic, Z., Kong, N., Kammlott, U., Lukacs, C., Klein, C., Fotouhi, N., & Liu, E. A. (2004). In vivo activation of the p53 pathway by small-molecule antagonists of MDM2. *Science*, *303*(5659), 844–848. https://doi.org/10.1126/science.1092472

[80] Vogelstein, B., & Kinzler, K. W. (1993). The multistep nature of cancer. *Trends in Genetics*, *9*(4), 138–141.

[81] Weiss, A., Berndsen, R. H., Ding, X., Ho, C.-M., Dyson, P. J., van den Bergh, H., Griffioen, A. W., & Nowak-Sliwinska, P. (2015). A streamlined search technology for identification of synergistic drug combinations. *Scientific Reports*, *5*, 14508. https://doi.org/10.1038/srep14508

[82] Wheaton, W. W., Weinberg, S. E., Hamanaka, R. B., Soberanes, S., Sullivan, L. B., Anso, E., Glasauer, A., Dufour, E., Mutlu, G. M., Budigner, G. R. S., & Chandel, N. S. (2014). Metformin inhibits mitochondrial complex I of cancer cells to reduce tumorigenesis. *eLife, 3,* e02242. https://doi.org/10.7554/eLife.02242

[83] Xu, T., Qin, R., Zhou, J., Yan, Y., Lu, Y., Zhang, X., Fu, D., Lv, Z., Li, W., Xia, C., Hu, G., Ding, X., & Chen, J. (2012). High Bone Sialoprotein (BSP) Expression Correlates with Increased Tumor Grade and Predicts a Poorer Prognosis of High-Grade Glioma Patients. *PLoS ONE*, *7*(10), e48415. https://doi.org/10.1371/journal.pone.0048415

[84] Yin, Z., Deng, Z., Zhao, W., & Cao, Z. (2018). Searching synergistic dose combinations for anticancer drugs. *Frontiers in Pharmacology*, *9*(535), 1-7. https://doi.org/10.3389/fphar.2018.00535

[85] Zhang, F., Khajavi, M., Connolly, A. M., Towne, C. F., Batish, S. D., & Lupski, J. R. (2009). The DNA replication FoSTeS/MMBIR mechanism can generate genomic, genic and exonic complex rearrangements in humans. *Nature Genetics*, *41*(7), 849–853. https://doi.org/10.1038/ng.399

[86] Zhao, L., Wientjes, M. G., & Au, J. L.-S. (2004). Evaluation of combination chemotherapy: integration of nonlinear regression, curve shift, isobologram, and combination index analyses. *Clinical Cancer Research : An Official Journal of the American Association for Cancer Research*, *10*(23), 7994–8004. http://www.ncbi.nlm.nih.gov/pubmed/15585635

[87] Zhao, S., Shetty, J., Hou, L., Delcher, A., Zhu, B., Osoegawa, K., de Jong, P., Nierman, W. C., Strausberg, R. L., & Fraser, C. M. (2004). Human, mouse, and rat genome large-scale rearrangements: Stability versus speciation. *Genome Research*, *14*(10A), 1851–1860. https://doi.org/10.1101/gr.2663304

[88] Zhou, X., Wang, W., Zhang, S., Wang, X., Tang, Z., Gu, J., Li, J., & Huang, J. (2017). CACNA1B (Cav2.2) Overexpression and Its Association with Clinicopathologic Characteristics and Unfavorable Prognosis in Non-Small Cell Lung Cancer. *Disease Markers*, *2017*. https://doi.org/10.1155/2017/6136401

[89] Zinzi, L., Capparelli, E., Cantore, M., Contino, M., Leopoldo, M., & Colabufo, N. A. (2014). Small and Innovative Molecules as New Strategy to Revert MDR. *Frontiers in Oncology*, *4*, 2. https://doi.org/10.3389/fonc.2014.00002

6 Eidesstattliche Versicherung

„Ich, **Jérôme Ruhnau,** versichere an Eides statt durch meine eigenhändige Unterschrift, dass ich die vorgelegte Dissertation mit dem Thema:

Deutsch:

„Genom und Metabolismus stabilisierende Antitumor-Therapie (GMSAT) in den humanen Kolon- und Brustkrebszelllinien HT-29 und MDA-MB-231“

Englisch:

„Genome and metabolism stabilizing antitumor therapy (GMSAT) in human colon and breast cancer cell lines HT-29 and MDA-MB-231“

selbstständig und ohne nicht offengelegte Hilfe Dritter verfasst und keine anderen als die angegebenen Quellen und Hilfsmittel genutzt habe.

Alle Stellen, die wörtlich oder dem Sinne nach auf Publikationen oder Vorträgen anderer Autoren/innen beruhen, sind als solche in korrekter Zitierung kenntlich gemacht. Die Abschnitte zu Methodik (insbesondere praktische Arbeiten, Laborbestimmungen, statistische Aufarbeitung) und Resultaten (insbesondere Abbildungen, Graphiken und Tabellen) werden von mir verantwortet.

Ich versichere ferner, dass ich die in Zusammenarbeit mit anderen Personen generierten Daten, Datenauswertungen und Schlussfolgerungen korrekt gekennzeichnet und meinen eigenen Beitrag sowie die Beiträge anderer Personen korrekt kenntlich gemacht habe (siehe Anteilserklärung). Texte oder Textteile, die gemeinsam mit anderen erstellt oder verwendet wurden, habe ich korrekt kenntlich gemacht.

Meine Anteile an etwaigen Publikationen zu dieser Dissertation entsprechen denen, die in der untenstehenden gemeinsamen Erklärung mit dem/der Erstbetreuer/in, angegeben sind. Für sämtliche im Rahmen der Dissertation entstandenen Publikationen wurden die Richtlinien des ICMJE (International Committee of Medical Journal Editors; www.icmje.og) zur Autorenschaft eingehalten. Ich erkläre ferner, dass ich mich zur Einhaltung der Satzung der Charité – Universitätsmedizin Berlin zur Sicherung Guter Wissenschaftlicher Praxis verpflichte.

Weiterhin versichere ich, dass ich diese Dissertation weder in gleicher noch in ähnlicher Form bereits an einer anderen Fakultät eingereicht habe.

Die Bedeutung dieser eidesstattlichen Versicherung und die strafrechtlichen Folgen einer unwahren eidesstattlichen Versicherung (§§156, 161 des Strafgesetzbuches) sind mir bekannt und bewusst.“

Datum Unterschrift

7 Anteilserklärung an den erfolgten Publikationen

Jérôme Ruhnau hatte folgenden Anteil an den folgenden Publikationen:

Autoren:	Christoph Standfuß, Jonas Parczyk, Jérôme Ruhnau and Andreas Klein
Titel:	Genome reorganization in different cancer types: detection of cancer specific breakpoint regions
Zeitschrift:	Molecular Cytogenetics
Erscheinungsjahr:	2019
Beitrag im Einzelnen:	Datenbankauswertung zu den Ko-lokalisierten Genen Editierung und Erstellung der Abbildungen, Ergebnisdiskussion, Mitverfassung des Manuskriptes
Autoren:	Jérôme Ruhnau*, Jonas Parczyk*, Kerstin Danker, Britta Eickholt, and Andreas Klein *geteilte Erstautorenschaft
Titel:	Synergisms of genome and metabolism stabilizing antitumor therapy (GMSAT) in human breast and colon cancer cell lines: a novel approach to screen for synergism
Zeitschrift:	BMC Cancer
Erscheinungsjahr:	2020
Beitrag im Einzelnen:	Konzeption und Planung des Projektes, Literaturrecherche, Verfassen des Manuskriptes, alle Experimente (MTT-, SRB-, MDIS) mit MDA-MB-231 und HT-29 (Tabelle 1, 2, Abbildung 3, 4), Datenauswertung
Autoren:	Jonas Parczyk*, Jérôme Ruhnau*, Carsten Pelz, Max Schilling, Hao Wu, Nicole Nadine Piaskowski, Britta Eickholt, Hartmut Kühn, Kerstin Danker, Andreas Klein *geteilte Erstautorenschaft
Titel:	Dichloroacetate and PX-478 Exhibit Strong Synergistic Effects in a Various Number of Cancer Cell Lines.
Zeitschrift:	BMC Cancer
Erscheinungsjahr:	2021
Beitrag im Einzelnen:	Konzeption und Planung des Projektes, Literaturrecherche, alle MTT-, SRB-, und HPLC-Analysen mit MDA-MB-231 und HT-29, Datenauswertung, kritische Beurteilung des Manuskriptes, Supervision von Max Schilling zur Anfertigung der ROS-FACS-Analysen

Unterschrift, Datum und Stempel des/der erstbetreuenden Hochschullehrers/in

Unterschrift des Doktoranden/der Doktorandin

8 Druckexemplare der ausgewählten Publikationen

8.1 Publikation 1

Genome reorganization in different cancer types: detection of cancer specific breakpoint regions

Christoph Standfuß, Jonas Parczyk, Jérôme Ruhnau and Andreas Klein

Mol Cytogenet 12, 25 (2019). Molecular Cytogenetics volume 12, Article number: 25 (2019)
doi:10.1186/s13039-019-0435-3
Impact factor: 1.233 (2-year Impact Factor) 1.408 (5-year Impact Factor)

Standfuß et al. Molecular Cytogenetics (2019) 12:25
https://doi.org/10.1186/s13039-019-0435-3

Molecular Cytogenetics

RESEARCH Open Access

Genome reorganization in different cancer types: detection of cancer specific breakpoint regions

Christoph Standfuß[1,2], Jonas Parczyk[1], Jerome Ruhnau[1] and Andreas Klein[1*]

Abstract

Background: Tumorigenesis is a multi-step process which is accompanied by substantial changes in genome organization. The development of these changes is not only a random process, but rather comprise specific DNA regions that are prone to the reorganization process.

Results: We have analyzed previously published SNP arrays from three different cancer types (pancreatic adenocarcinoma, breast cancer and metastatic melanoma) and from non-malignant control samples. We calculated segmental copy number variations as well as breakpoint regions. Some of these regions were not randomly involved in genome reorganization since we detected fifteen of them in at least 20% of all tumor samples and one region on chromosome 9 where 43% of tumors have a breakpoint. Further, the top-15 breakpoint regions show an association to known fragile sites. The relevance of these common breakpoint regions was further confirmed by analyzing SNP arrays from 917 cancer cell lines.

Conclusion: Our analyses suggest that genome reorganization is common in tumorigenesis and that some breakpoint regions can be found across all cancer types, while others exclusively occur in specific entities.

Keywords: Pancreatic ductal adenocarcinoma, Breast cancer, Melanoma, Copy number variation, Cancer genomics, Breakpoint and genome reorganization

Background

Tumorigenesis is a stepwise process, which involves multiple genetic, epigenetic and genomic events to transform a normal cell into a tumor cell [1–6].Genomic changes like copy number variations (CNVs) or segmental copy number variations (segCNVs) increase throughout tumorigenesis [7–9] and are caused by various mechanisms, like fork stalling during replication or non-allelic homologous recombination [10–12].

These changes can affect the chromatin structure and therefore the spatial localization of specific genes, the DNA sequence like single nucleotide mutations, amplifications, deletions or translocations as well as changes of karyotypes like aneuploidies [1, 13–16].

It is also speculated that DNA regions exist which are prone for reorganization. Pevzner and Tesler stated in their seminal work "that mammalian genomes are mosaics of fragile regions with high propensity for rearrangements and solid regions with low propensity for rearrangements [17]."

Their thesis stands in contrast to the established theory of the random breakage model. The latter is based on the following two assumptions: Chromosomal segments are conserved among different species and chromosomal rearrangements are randomly distributed within the genome [18]. Indeed, it is well established that chromosomal segments exist in different species where orthologous genes are located in the same arrangement. On the other hand, it is now also established that specific DNA regions throughout the genome are prone to breakage and reorganization [17, 19–21]. Ruiz-Herrera et al stated that "certain chromosomal regions in the human genome have been repeatedly used in the evolutionary process. As a consequence, the

* Correspondence: andreas.klein@charite.de
[1]Institute of Biochemistry, Charité – Universitätsmedizin Berlin, Corporate Member of Freie Universität Berlin, Humboldt-Universität zu Berlin, and Berlin Institute of Health, Charitéplatz 1, 10117 Berlin, Germany
Full list of author information is available at the end of the article

genome is a composite of fragile regions prone to reorganization…" Well known regions exhibiting chromosomal instability are fragile sites, which were firstly described by Magenis et al 1970 [22, 23]. "Fragile sites are specific loci that form gaps, constrictions, and breaks on chromosomes exposed to partial replication stress and are rearranged in tumors [24]." Fragile sites can be divided in rare and common fragile sites (CFSs). Rare fragile sites are only expressed in a few individuals. They are associated with the expansion of micro- or minisatellite repeats and inheritable diseases like fragile X syndrome. CFSs are regular parts of chromosomes and therefore found in all humans. CFSs are hotspots for metaphase chromosomal gaps and breaks and chromosomal rearrangements. CFS instability is an early step in tumorigenesis and could be responsible for genome reorganization in cancer [23, 25–29].

In 2012, Standfuß et al observed the stepwise increase in genome reorganization in a simian virus 40 (SVT/t) transformed mouse breast cancer model. The number of genomic changes increased from non-malignant, to hyperplastic and to tumor samples of mammary glands. Moreover, distinct breakpoint regions, where genome reorganization events take place, could be detected. They argued that unique and common breakpoint regions exist in breast cancer. However, due to the small sample size, the final proof was missing [9].

In this study, we analyzed DNA SNP arrays from 20 healthy controls and 111 cancer samples as well as 917 cancer cell lines. We found unique and common breakpoint regions in different cancer entities and more strikingly, we found a breakpoint region which was common in more than one third of all tumors and cancer cell lines tested.

Thus, we addressed the questions, whether genome reorganization is a random process, and whether specific DNA regions are prone to this reorganization procedure.

Material and methods

SNP array data

We reanalyzed 131 single-nucleotide polymorphism (SNP) microarrays, produced using the Genome-Wide Human SNP Array 6.0 platform (https://tools.thermofisher.com/content/sfs/brochures/genomewide_snp6_datasheet.pdf). The 111 tumor samples compromise 25 pancreatic adenocarcinomas (PDAC) from Donahue et al [30] [GSE32688], 22 PDAC derived cell lines from Barretina et al [31] [GSE36139], 16 metastatic melanomas from Marzese et al [32] [GSE44019] and 48 breast cancer samples from [GSE26232]. The 20 non-malignant control experiments (NMCE) compromise 15 samples derived from B cells isolated from peripheral blood of healthy donors from Xie et al [33] [GSE49045] and 5 samples derived from peripheral blood cells of breast cancer patients [GSE48377]. The 15 blood samples from healthy donors were further termed as "reference" and the five peripheral blood cells from breast cancer patients were termed as "control".

Further, we analyzed 917 cancer cell line samples from the Cancer Cell Line Encyclopedia (CCLE) [31] [GSE36139]. All samples are publicly available.

Copy-number variation

Raw SNP microarray data was processed using the Affymetrix Power Tools 1.15.0 (now Oncomine™ Power Tools, Thermo Fisher Scientific) and the BRLMM-P algorithm to extract the normalized SNP signal intensities. To compare the total signal intensity distributions of all samples, intensities of both alleles for each SNP were added up. CNVs for each SNP was computed as log2-ratios of each tumor sample and the reference dataset comprising 15 blood samples from healthy donors. The reference for each SNP was calculated as the average signal intensity of the 15 reference samples.

SegCNVs for each sample were computed with the DNAcopy package (1.36.0) of Bioconductor (2.13) [34] with the following parameters: alpha = 0.001, undo.splits = "sdundo", undo.SD = 0.5, min.width = 4. The DNAcopy package implements the circular binary segmentation algorithm introduced by Olshen et al [35]. The number of segCNVs were counted for each experiment and set in relation to the number of base pairs for each chromosome. We excluded Chromosome Y (860 SNPs) and MT (411 SNPs) from our analyses. The heat map was generated using ggplot2 package of R. Hg19, provided by the University of California, Santa Cruz (UCSC), was used for human genome assembly.

Common breakpoints

The genome was divided into 30,951 bins of 100 kb size or less, if the bin represents a chromosomal end region. The occurrence of each breakpoint was counted in all 1048 analyzed samples to find regions of predisposed alterations. To enhance stringency, a breakpoint between two segCNVs was defined as follows: 1) the log2-ratio difference between both segments has to be greater than 0.5. 2) at least one segment has to include a minimum of 10 and the other of 4 SNPs.

Odds ratio

To decide whether a breakpoint event (BP) is more frequent in cancer samples than in the NMCE, we calculated the odds ratios.

oddsNMCE = (number of NMCE with BP)/(total number of NMCE - number of NMCE with BP).

oddsTumor = (number of tumors with BP)/(total number of tumors - number of tumors with BP).

oddsRatio = (oddsTumors)/(oddsNMCE)

Since some of the breakpoints were not found in the NMCE but had a high count in the tumor group odds ratio, calculations were not trivial. In accordance with the Cochrane Handbook for Systematic Reviews of Interventions we added 0.5 in those cases:

oddsNMCE = (number of NMCE with BP + 0.5)/ (total number of NMCE + 0.5 - number of NMCE with BP + 0.5).

oddsTumor = (number of tumors with BP + 0.5)/(total number of tumors + 0.5 - number of tumors with B + 0.5).

oddsRatio = (oddsTumors)/(oddsNMCE)

Fragile sites

We used the chromosomal location of the 230 fragile sites published by Mrasek et al [36] and analyzed their occurrence within our breakpoint regions. Therefore, the cytogenetic location was translated into the chromosomal location with the help of the "Ensemble Genome Browser version GRCh37.p13."

Results

SNP CNVs in different tumor entities

To study the changes in genome reorganization during tumorigenesis, we analyzed previously published SNP arrays from 111 cancer samples: 25 pancreatic ductal adenocarcinoma, 22 PDAC derived cell lines, 16 metastatic melanoma and 48 breast cancer samples. As NMCE, we used DNA from peripheral blood samples from healthy donors and from breast cancer patients.

We added up the signal intensities for SNP alleles and further determined continuous SNP CNV regions for all chromosomes using the circular binary segmentation algorithm introduced by Olshen and colleagues [35]. In order to define DNA regions with a high probability of genomic reorganization and which were common in multiple cancer samples, we divided the genome into 30,951 bins of 100 kb size and defined a breakpoint region as follows: at least two DNA segments have to differ in their average copy number values of more than a log2-ratio of 0.5 and one segment has to consist of 10 SNPs instead of the minimum of four SNPs. Thus, breakpoint regions were defined as DNA sites where segmental copy number level shifts occur. If a breakpoint is present in multiple tumor samples, we call it common breakpoint region. This approach is illustrated in Fig. 1.

In total, we found 19,687 regions (63.61%) where at least one experiment had a breakpoint. However, since most of the breakpoint regions were present in only one or two tumor samples, we focused on genomic regions in which at least 23 out of the 111 tumors (20%) had a breakpoint (Fig. 2, Table 1). The heat map shows the fifteen 100 kb sized breakpoint regions, which appear in at least 20% of all tumor samples. We highlighted breakpoints more frequent in PDAC tumor samples with

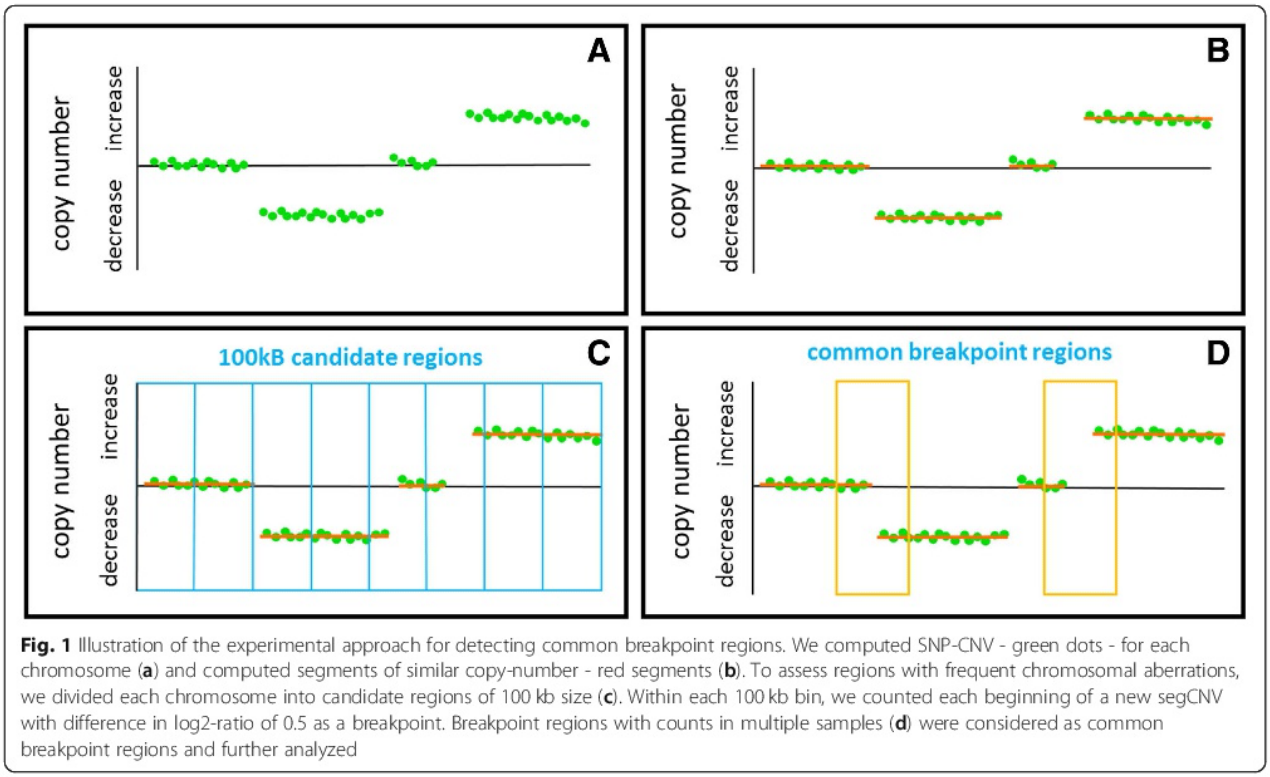

Fig. 1 Illustration of the experimental approach for detecting common breakpoint regions. We computed SNP-CNV - green dots - for each chromosome (**a**) and computed segments of similar copy-number - red segments (**b**). To assess regions with frequent chromosomal aberrations, we divided each chromosome into candidate regions of 100 kb size (**c**). Within each 100 kb bin, we counted each beginning of a new segCNV with difference in log2-ratio of 0.5 as a breakpoint. Breakpoint regions with counts in multiple samples (**d**) were considered as common breakpoint regions and further analyzed

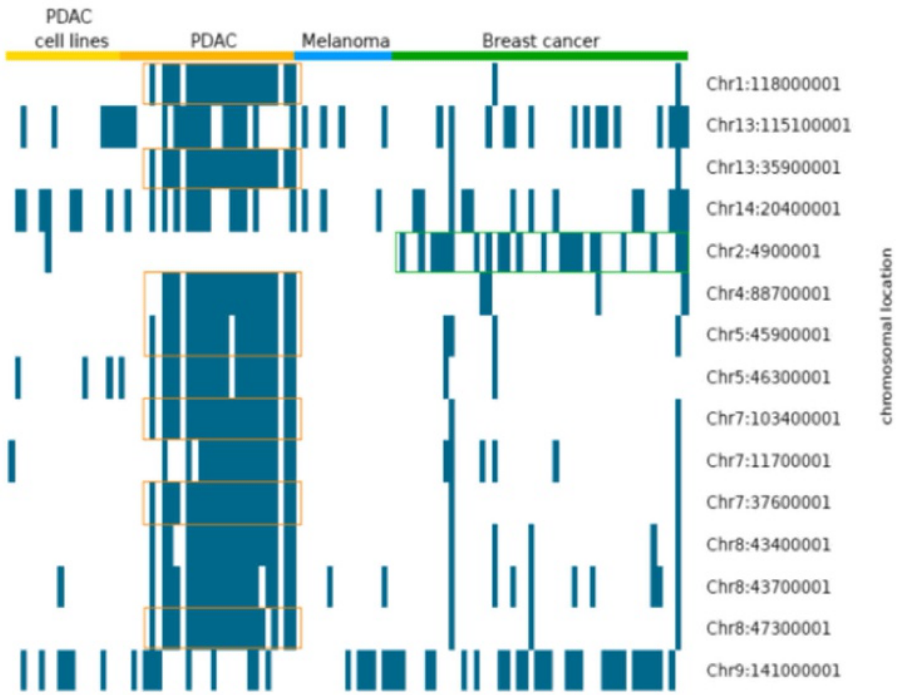

Fig. 2 To illustrate the presence (blue line) of common breakpoints within different tumor samples and tumor entities, we created a heat map. The chromosomal location is listed on the y-axis. Here, we present a heat map for all common breakpoints that appear in at least 20% of tumor samples. Breakpoints that were mainly common to PDAC tumor samples are marked by orange rectangles and green rectangles mark breakpoints common to breast cancer samples

Table 1 Chromosomal location, occurrence of breakpoint events (BP), odds ratio, located genes and association to fragile sites of the top-15 breakpoint regions. Genes that are associated with cancer in literature are marked with an asterisk

Chr	Start	End	Cytoband	BP in NMCE (20)	BP in Tumors (111)	Odds Ratio	BP in CCLE (917)	Genes	Fragile Sites
1	118000001	118100001	1p12	0	23	10,68	4	*MAN1A2*	–
2	4900001	5000001	2p25.2	0	23	10,68	26	–	FRA2M
4	88700001	88800001	4q22.1	0	24	11,26	2	*IBSP*, MPEP**	FRA4F
5	45900001	46000001	5p12	0	24	11,26	1	–	–
5	46300001	46400001	5p11	0	26	12,47	81	–	FRA5I
7	11700001	11800001	7p21.3	0	24	11,26	5	*THSD7A**	FRA7L
7	37600001	37700001	7p14.1	0	23	10,68	0	*NECAP1P1*	–
7	103400001	103500001	7q22.1	1	23	4,97	1	*RELN**	FRA7F
8	43400001	43500001	8p11.1	0	25	11,86	2	–	FRA8I
8	43700001	43800001	8p11.1	0	32	16,46	48	–	FRA8I
8	47300001	47400001	8q11.1	0	23	10,68	1	–	FRA8I
9	141000001	141100001	9q34.3	1	48	14,48	321	*CACNA1B**	FRA9N
13	35900001	36000001	13q13.3	0	23	10,68	1	*NBEA**	–
13	115100001	115106996	13q34	3	40	3,19	210	–	FRA13I
14	20400001	20500001	14q11.2	3	36	2,72	61	*OR4K1, OR4K5, OR4K14, OR4K15*	FRA14D

orange boxes, and regions more frequent in breast cancer samples with green boxes. This result indicates that some breakpoints are more frequent in only one tumor entity (like chromosomes 1, 2 and 13) whereas other regions are present in all tumor entities (like chromosomes 9 and 13). The breakpoints on Chromosomes 9 and 13 had 43 and 36% of all tumors in common. Since some breakpoints were also present in the NMCE, we verified the relevance of a breakpoint region by determining the odds ratio for being tumor specific.

Table 1 shows the odds ratio for the breakpoints illustrated in Fig. 2. In all of the top-15 breakpoint regions, we observed that on average, an odds ratio > 10 indicates a high prevalence for these breakpoints to occur in tumor samples. The two highest odds ratio values were calculated for the breakpoint of chromosome 9 present in 48 different tumor samples and one NMCE (odds ratio = 14.5) and the breakpoint on chromosome 8 (43,700,001) present only in 32 different tumor samples (odds ratio = 16.5). Twelve genes were located in eight of the top-15 breakpoint regions, and six of these genes are associated with cancer (*CACNA1B, IBSP, MEPE, NBEA, RELN and THSD7A*) (Table 1).

Cancer cell line encyclopedia (CCLE)

To further validate, the top-15 breakpoint regions, we included 917 cancer cell line samples in our analyses. We summarized in Table 2 the seven 100 kb sized breakpoint regions which appear in at least 20% of all CCLE samples The breakpoint regions on Chromosomes 9 (141,000,001) and 13 (115,100,001) which were present in all tumor entities, also had the most breakpoints in the analyzed cancer cell lines. On Chromosome 9, 321 cancer cell lines (34%) and on Chromosome 13, 210 (22%) cancer cell lines had a breakpoint within the aforementioned regions. Five genes were located in four of the seven breakpoint regions and three of these genes (*CACNA1B, C8orf33 and KIAA0513*) are associated with cancer (Table 2). Interestingly, only very few cancer cell lines (< 0.5%) had breakpoints in the seven breakpoint regions that were associated with PDAC: e.g. the region on chromosome 7 (37,600,001) had no breakpoint in cancer cell lines and the regions on chromosomes 5 (45,900,001), 7 (103,400,001), 8 (47,300,001) and 13 (35,900,001) had only one breakpoint in cancer cell lines (Table 1). The breast cancer associated breakpoint region on chromosome 2 is also only shared by 2.8% of cancer cell lines.

The presented results indicate that we created a set of common breakpoint regions with the help of PDAC, melanoma metastasis and breast cancer samples that were more highly associated with single cancer entities, whereas other breakpoint regions can be found in a variety of tumors.

Fragile site

Since fragile sites are well known regions exhibiting chromosome instability, we compared the chromosomal locations of the common breakpoint regions we found with data from chromosomal fragile sites [36]. Eleven thousand three hundred sixty out of the 19,687 breakpoint regions contained a fragile site (58%).

Since an odds ratio less than one indicates a higher likelihood of a breakpoint region to occur in NMCE, and an odds ratio above one indicates higher odds for occurring in tumor samples, we determined the percentage of a fragile site to occur in relation to the odds ratio. Out of the 19,687 breakpoint regions, 13,063 had an odds ratio of less than one and 6624 above one. A region with an odds ratio < 1 occurred in 57% (7471 out of 13,063) associated with fragile sites and a region with an odds ratio > 1 occurred in 59% (3889 out of 6624) associated with fragile sites. Thus, we could not determine a crucial difference in the association to fragile sites in the more tumor linked breakpoint regions.

However, 11 of the top-15 breakpoint regions (73%) were associated with fragile sites and 6 of the 7 CCLE related breakpoint region (86%), indicating a strong association of the top-ranked breakpoint regions to known fragile sites.

Targeted investigation

Further, we evaluated important regions known for genome reorganization from literature (e.g. loss-of

Table 2 Chromosomal location, occurrence of breakpoint events (BP), odds ratio, located genes and association to fragile sites of the top-ranked CCLE breakpoint regions. Genes that are associated with cancer in literature are marked with an asterisk. Interestingly, the breakpoint region in chromosome 2 is close to the cancer associated *SDC1* gene by about 558 bases

Chr	Start	End	Cytoband	BP in NMCE (20)	BP in Tumors (111)	Odds Ratio	BP in CCLE (917)	Gene	Fragile Sites
2	20300001	20400001	2p24.1	0	9	3,73	248	–	–
4	190900001	191000001	4q35.2	0	14	5,98	190	*FRG2*	FRA4L, FRA4M
7	159100001	159119220	7q36.3	0	22	10,11	230	–	FRA7I
8	146200001	146300001	8q24.3	0	21	9,56	238	*C8orf33**	FRA8D
9	141000001	141100001	9q34.3	1	48	14,48	321	*CACNA1B**	FRA9N
13	115100001	115106996	13q34	3	40	3,19	210	–	FRA13I
16	85000001	85100001	16q24.1	0	8	3,30	244	*KIAA0513**, *ZDHHC7*	FRA16J

heterozygosity or homozygous deletion) and looked for the relevance of those regions in our dataset concerning the occurrence of breakpoints. Fragile site FRA16D (16q23.2) is within a region of frequent loss-of-heterozygosity in breast and prostate cancers. Interestingly, we found 64 breakpoints in 13 tumor samples (11.7%) for this fragile site, whereof 61 were found in nine breast cancer samples (18.75% of all breast cancer samples). Another frequently altered chromosomal region is located on chromosome 9 (21,900,001) where the *tumor suppressor p16* (official symbol *CDKN2A*) is present. In the corresponding bins, 104 cancer cell lines had a breakpoint (11.34%) and eight tumor samples (7.2%). Interestingly, this region is part of the fragile site FRA9A. In this CFS 56 tumor samples (50.5%) had at least one breakpoint.

The most commonly known unstable CFS region is FRA3B [37]. In this CFS, spanning over 43 bins, 148 breakpoints were detected in 26 cancer samples (23.4%). It is also noteworthy that 23 out of the 26 cancer samples had a breakpoint in the region of the gene *FHIT* lying inside of FRA3B. In line with this, 243 cancer cell lines have breakpoints in FRA3B and 223 of those have breakpoints in the 16 bins containing *FHIT*.

Discussion

In this study, we examined the theory that genome reorganization during tumorigenesis is not a random process but rather a directed process, involving defined DNA regions. Therefore, we have reanalyzed 1.048 DNA SNP arrays from different cancer entities and non-malignant samples. We found an increase of DNA breakpoint regions in tumor samples compared to NMCE. Interestingly, several breakpoint regions were common in several tumor specimen (up to 43%) where as other regions seemed to be more restricted to a specific tumor entity. Surprisingly, breakpoint regions between PDCA and PDCA derived cell lines differ considerably. On the one hand, Kalinina and colleagues established a pancreatic cancer cell line from a primary tumor. Kalinina and colleagues also observed a similar CNV pattern between tumor and cell line after passaging the cell line 15–20 times, as well as a considerable number of similar large chromosomal alterations [38]. On the other hand, Burdall and colleagues stated that "Cell lines are prone to genotypic and phenotypic drift during their continual culture. This is particularly common in the more frequently used cell lines, especially those that have been deposited in cell banks for many years [39]." This might be applicable for the used cell lines in our approach, e.g. Capan 1 and 2 were established 1974 and 1975, respectively [40, 41].

It is well known that cancers develop from stem lines in a stepwise process and are characterized by chromosomal aberrations and chromosomal instability [42, 43]. The Mitelman Database of Chromosome Aberrations and Gene Fusions in Cancer currently lists 69,134 human cancers with individual clonal karyotypes [44]. In 2012, Standfuß et al found a stepwise increase in genome reorganization in a mouse breast cancer model. The number of genomic changes increased from non-malignant, to hyperplastic and to tumor samples of mammary glands [9]. Further, an analysis of 2.737 tumor samples from 8 different tumor entities (including breast cancers) showed that tumor entity-specific breakpoints could be found for all examined tumor entities. The breakpoint regions were equally distributed over all entities [45]. Further, colocalization assessment identified 20,077 CNV-affecting genes and 169 of these being known tumor-related genes. In another study, Beroukhim et al looked for somatic CNVs in 3.131 cancer specimen and found 158 regions of focal somatic CNVs of which only 36 can be explained by the presence of known cancer target genes located within this region like *FHIT* and *p16* [8]. Meaburn and Misteli also identified several genes specifically repositioned during tumorigenesis. The alterations of the spatial positioning were unrelated to gene activity [15]. In our study, genes were located in eight of the top-15 and four of the top-7 CCLE breakpoint regions. Eight of these genes are linked to cancer, but none are well characterized oncogenes or tumor suppressor genes. Interestingly, only *C8orf33* and *NBEA* seemed to have tumor suppressor functions [46, 47]. The other six genes are associated with tumor progression. *IBSP*, *MEPE*, *RELN* and *THSD7A* are associated with migration, invasion, infiltration and angiogenesis [48–51]; *CACNA1B* and *KIAA0513* are associated with cell proliferation and apoptosis. *CACNA1B* overexpression is associated with an unfavorable prognosis in non-small cellular lung cancer [52] and altered expression of *KIAA0513*, due to an aberrant methylation pattern, correlated with non-survivors in Neuroblastoma [53].

As early as 1984, several scientists postulated an association between human fragile sites and cancer breakpoints [25, 26, 54]. CFSs in cancer were considered as regions of chromosomal instability and their associated genes are frequently deleted or rearranged in cancer cells [55]. Since we found a strong correlation of our top breakpoint regions with fragile sites, we were also interested to look for breakpoints in specific CFSs described in literature. Finnis and colleagues found out that the CFS FRA16D (16q23.2) is located within regions of frequent loss-of-heterozygosity in breast and prostate cancers [56]. Here we found a breakpoint almost specific for breast cancer, since 61 from 64 breakpoints stem from breast cancer samples. 1986 Smeets and colleagues described FRA3B as the most unstable CFS region within

chromosomal band 3p14.2 [37]. This chromosomal region is a hot-spot for deletions and other alterations in a variety of different cancers. *FHIT,* a large tumor suppressor gene spanning over approximately 35% of this fragile site, is also harbored in this region [57]. While 26 tumors and 243 cancer cell lines have a breakpoint in FR3B, the majority of these breakpoints, namely 23 and 223, lay in the *FHIT* gene. Thus, it is not surprising that estimates designate *FHIT* as the most frequently altered gene in cancer [58]. Inside the CFS, FRA9A the *p16* gene is located. Cox and Colleagues found in their "survey of homozygous deletions in human cancer genomes" that *p16* was the most frequent target of homozygous deletions (24.6%) [59]. Further, they argued that genetic rearrangement in this region might signify less negative selection compared to other regions because *p16* is located adjacent to one of the largest gene-poor regions of the human genome. When looking at the direct adjacent bins of *p16*, it stands out that the area of and around *p16* is the area of FRA9A where most of the breakpoints occur. This indicates that those breakpoints occurring in this CFS might play a role for tumor development, instead of being a random side effect of genomic instability.

However, genome rearrangements are not restricted to cancer cells. Rather, they are also present in adaptive processes, such as response to selective pressures from the environment and are associated with various diseases [60–62].

Conclusion

In this study, we found that genome reorganization is more enhanced in tumor samples compared to the non-malignant controls and that some genome regions exist that are prone to rearrangements. We identified regions which may play an important role in the tumorigenesis of specific tumor entities and others that occur commonly during tumorigenesis.

For further investigations, genomic profiles could be linked to clinical data in order to produce additional prognostic markers for clinical outcome.

Abbreviations

BP: breakpoint event; CCLE: Cancer Cell Line Encyclopedia; CFS: common fragile site; CNV: copy number variation; NMCE: non-malignant control experiment; PDAC: pancreatic adenocarcinoma; segCNV: segmental copy number variation; SNP: single-nucleotide polymorphism

Acknowledgements

We gratefully acknowledge the support of Cara Reiter-Brennan for editing the English version and critical discussions of this manuscript. We acknowledge support from the German Research Foundation (DFG) and the Open Access Publication Fund of Charité – Universitätsmedizin Berlin.

Funding

N/A

Availability of data and materials

All analyzed samples are publicly available.

Authors' contributions

Conceptualization: CS and AK; Analyses and graphic design: CS, JP and JR; Project administration and supervision: AK; Writing and editing: CS, JP, JR and AK. All authors read and approved the manuscript.

Ethics approval and consent to participate

The authors have no ethical conflicts to disclose.

Consent for publication

Not applicable.

Competing interests

The authors declare that they have no competing interests.

Publisher's Note

Author details

[1]Institute of Biochemistry, Charité – Universitätsmedizin Berlin, Corporate Member of Freie Universität Berlin, Humboldt-Universität zu Berlin, and Berlin Institute of Health, Charitéplatz 1, 10117 Berlin, Germany. [2]Institute of Biochemistry, Charité – Universitätsmedizin Berlin, corporate member of Freie Universität Berlin, Humboldt-Universität zu Berlin, and Berlin Institute of Health, MTU Aero Engines, 80995 Munic, Germany.

Received: 8 February 2019 Accepted: 15 May 2019
Published online: 20 June 2019

References

1. Vogelstein B, Kinzler KW. The multistep nature of cancer. Trends Genet. 1993;9:138–41.
2. Hanahan D, Weinberg RA. Hallmarks of cancer: the next generation. Cell. 2011;144:646–74.
3. Loeb LA, Loeb KR, Anderson JP. Multiple mutations and cancer. Proc Natl Acad Sci. 2003;100:776–81.
4. Osborne C. Oncogenes and tumor suppressor genes in breast Cancer: potential diagnostic and therapeutic applications. Oncologist. 2004;9:361–77.
5. Klein A, Guhl E, Zollinger R, et al. Gene expression profiling: cell cycle deregulation and aneuploidy do not cause breast cancer formation in WAP-SVT/t transgenic animals. J Mol Med. 2005;83:362–76.
6. Foulds L. The experimental study of tumor progression: a review. Cancer Res. 1954;14:327–39.
7. Shlien A, Malkin D. Copy number variations and cancer. Genome Med. 2009;1:1–9.
8. Beroukhim R, Mermel CH, Porter D, et al. The landscape of somatic copy-number alteration across human cancers. Nature. 2010;463:899–905.
9. Standfuß C, Pospisil H, Klein A. SNP microarray analyses reveal copy number alterations and progressive genome reorganization during tumor development in SVT/t driven mice breast cancer. BMC Cancer. 2012;12:380.
10. Redon R, Ishikawa S, Fitch KR, et al. Global variation in copy number in the human genome. Nature. 2006;444:444–54.
11. Malhotra D, Sebat J. CNVs: harbingers of a rare variant revolution in psychiatric genetics. Cell. 2012;148:1223–41.
12. Zhang F, Khajavi M, Connolly AM, et al. The DNA replication FoSTeS/MMBIR mechanism can generate genomic, genic and exonic complex rearrangements in humans. Nat Genet. 2009;41:849–53.
13. Sen S. Aneuploidy and cancer. Curr Opin Oncol. 2000;12:82–8.
14. Mitelman F, Johansson B, Mertens F. The impact of translocations and gene fusions on cancer causation. Nat Rev Cancer. 2007;7:233–45.
15. Meaburn KJ, Misteli T. Locus-specific and activity-independent gene repositioning during early tumorigenesis. J Cell Biol. 2008;180:39–50.
16. Klein A, Li N, Nicholson JM, et al. Transgenic oncogenes induce oncogene-independent cancers with individual karyotypes and phenotypes. Cancer Genet Cytogenet. 2010;200:79–99.
17. Pevzner P, Tesler G. Human and mouse genomic sequences reveal extensive breakpoint reuse in mammalian evolution. Proc Natl Acad Sci. 2003;100:7672–7.
18. Nadeau JH, Taylor BA. Lengths of chromosomal segments conserved since divergence of man and mouse. Proc Natl Acad Sci. 1984;81:814–8.
19. Zhao S, Shetty J, Hou L, et al. Human, mouse, and rat genome large-scale rearrangements: stability versus speciation. Genome Res. 2004;14:1851–60.

20. Murphy WJ, Larkin DM, Everts-Van Der Wind A, et al. Evolution: Dynamics of mammalian chromosome evolution inferred from multispecies comparative maps. Science (80-) 2005; 309: 613–617.
21. Ruiz-Herrera A, Castresana J, Robinson TJ. Is mammalian chromosomal evolution driven by regions of genome fragility? Genome Biol. 2006;7:R115.
22. Magenis RE, Hecht F, Lovrien EW. Heritable fragile site on chromosome 16: probable localization of haptoglobin locus in man. Science. 1970;170:85–7.
23. Durkin SG, Glover TW. Chromosome fragile sites. Annu Rev Genet. 2007;41: 169–92.
24. Zlotorynski E, Rahat A, Skaug J, et al. Molecular basis for expression of common and rare fragile sites. Mol Cell Biol. 2003;23:7143–51.
25. Hecht F, Sutherland GR. Fragile sites and cancer breakpoints. Cancer Genet Cytogenet. 1984;12:179–81.
26. Yunis JJ, Soreng AL. Constitutive fragile sites and cancer. Science. 1984;226: 1199–204.
27. Bartkova J, Hořejší Z, Koed K, et al. DNA damage response as a candidate anti-cancer barrier in early human tumorigenesis. Nature. 2005;434:864–70.
28. Tsantoulis PK, Kotsinas A, Sfikakis PP, et al. Oncogene-induced replication stress preferentially targets common fragile sites in preneoplastic lesions. A genome-wide study. Oncogene. 2008;27:3256–64.
29. Debatisse M, Le Tallec B, Letessier A, et al. Common fragile sites: mechanisms of instability revisited. Trends Genet. 2012;28:22–32.
30. Donahue TR, Tran LM, Hill R, et al. Integrative survival-based molecular profiling of human pancreatic Cancer. Clin Cancer Res. 2012;18:1352–63.
31. Barretina J, Caponigro G, Stransky N, et al. The Cancer cell line encyclopedia enables predictive modelling of anticancer drug sensitivity. Nature. 2012; 483:603–307.
32. Marzese DM, Scolyer RA, Huynh JL, et al. Epigenome-wide DNA methylation landscape of melanoma progression to brain metastasis reveals aberrations on homeobox D cluster associated with prognosis. Hum Mol Genet. 2013;23:226–38.
33. Xie Z, Nagarajan V, Sturdevant DE, et al. Genome-wide SNP analysis of the Systemic Capillary Leak Syndrome (Clarkson disease). *Rare Dis (Austin, Tex)*; 1. Epub ahead of print 2013. DOI: https://doi.org/10.4161/rdis.27445.
34. Gentleman RC, Carey VJ, Bates DM, et al. Bioconductor: open software development for computational biology and bioinformatics. Genome Biol. 2004;5:R80.
35. Olshen AB, Venkatraman ES, Lucito R, et al. Circular binary segmentation for the analysis of array-based DNA copy number data. Biostatistics. 2004;5:557–72.
36. Mrasek K, Schoder C, Teichmann A-C, et al. Global screening and extended nomenclature for 230 aphidicolin-inducible fragile sites, including 61 yet unreported ones. Int J Oncol. 2010;36:929–40.
37. Smeets DF, Scheres JM, Hustinx TW. The most common fragile site in man is 3p14. Hum Genet. 1986;72:215–20.
38. Kalinina T, Güngör C, Thieltges S, et al. Establishment and characterization of a new human pancreatic adenocarcinoma cell line with high metastatic potential to the lung. *BMC Cancer*; 10. Epub ahead of print 2010. DOI: https://doi.org/10.1186/1471-2407-10-295.
39. Burdall SE, Hanby AM, Lansdown MRJ, et al. Breast cancer cell lines: friend or foe? Breast Cancer Res. 2003;5:89–95.
40. Kyriazis AP, Kyriazis AA, Scarpelli DG, Fogh J, Rao MSLR. Human pancreatic adenocarcinoma line Capan-1 in tissue culture and the nude mouse: morphologic, biologic, and biochemical characteristics. Am Assoc Pathol. 1982;106:250–60.
41. Kyriazis AA, Kyriazis AP, Sternberg CN, Sloane NHLJ. Morphological, biological, biochemical, and karyotypic characteristics of human pancreatic ductal adenocarcinoma Capan-2 in tissue culture and the nude mouse. Cancer Res. 1986:5810–5.
42. Thompson SL, Compton DA. Chromosomes and cancer cells. Chromosom Res. 2011;19:433–44.
43. Vargas-Rondón N, Villegas VE, Rondón-Lagos M. The role of chromosomal instability in cancer and therapeutic responses. Cancers (Basel). 2018;10:1–21.
44. https://cgap.nci.nih.gov/Chromosomes/Mitelman. Accessed 5 MAY 2019.
45. Marczok S, Bortz B, Wang C, et al. Comprehensive analysis of genome rearrangements in eight human malignant tumor tissues. PLoS One. 2016; 11:e0158995.
46. Shao P, Sun D, Wang L, et al. Deep sequencing and comprehensive expression analysis identifies several molecules potentially related to human poorly differentiated hepatocellular carcinoma. FEBS Open Bio. 2017;7:1696–706.
47. O'Neal J, Gao F, Hassan A, et al. Neurobeachin (NBEA) is a target of recurrent interstitial deletions at 13q13 in patients with MGUS and multiple myeloma. Exp Hematol. 2009;37:234–44.
48. Xu T, Qin R, Zhou J, et al. High Bone Sialoprotein (BSP) Expression Correlates with Increased Tumor Grade and Predicts a Poorer Prognosis of High-Grade Glioma Patients. PLoS One; 7. Epub ahead of print 2012. DOI: https://doi.org/10.1371/journal.pone.0048415.
49. Gao Z, Zhao Y, Geng Q, et al. Regulatory roles of miRNA-758 and matrix extracellular phosphoglycoprotein in cervical cancer. Exp Ther Med. 2017;14: 2789–94.
50. Dou A, Wang Z, Zhang N, et al. Loss of reelin suppresses cell survival and mobility in non-Hodgkin lymphoma. Oncol Rep. 2017;37:3572–80.
51. Wiech T, Hoxha E, Schröder C, et al. THSD7A expression in human cancer. Genes Chromosom Cancer. 2016;56:314–27.
52. Zhou X, Wang W, Zhang S, et al. CACNA1B (ca_v 2.2) overexpression and its association with Clinicopathologic characteristics and unfavorable prognosis in non-small cell lung Cancer. Dis Markers. 2017;2017:1–8.
53. Olsson M, Beck S, Kogner P, et al. Genome-wide methylation profiling identifies novel methylated genes in neuroblastoma tumors. Epigenetics. 2016;11:74–84.
54. Glover TW, Berger C, Coyle J, et al. DNA polymerase α inhibition by aphidicolin induces gaps and breaks at common fragile sites in human chromosomes. Hum Genet. 1984;67:136–42.
55. Glover TW, Wilson TE, Arlt MF. Fragile sites in cancer: more than meets the eye. Nat Rev Cancer. 2017;17:489–501.
56. Finnis M, Dayan S, Hobson L, et al. Common chromosomal fragile site FRA16D mutation in cancer cells. Hum Mol Genet. 2005;14:1341–9.
57. Smith DI, Zhu Y, McAvoy S, et al. Common fragile sites, extremely large genes, neural development and cancer. Cancer Lett. 2006;232:48–57.
58. Saldivar JC, Bene J, Hosseini SA, et al. Characterization of the role of Fhit in suppression of DNA damage. Adv Biol Regul. 2013;53:77–85.
59. Cox C, Bignell G, Greenman C, et al. A survey of homozygous deletions in human cancer genomes. Proc Natl Acad Sci. 2005;102:4542–7.
60. Dunham MJ, Badrane H, Ferea T, et al. Characteristic genome rearrangements in experimental evolution of Saccharomyces cerevisiae. Proc Natl Acad Sci. 2002;99:16144–9.
61. Tang Y-C, Amon A. Gene copy-number alterations: a cost-benefit analysis. Cell. 2013;152:394–405.
62. Meaburn KJ. Spatial genome organization and its emerging role as a potential diagnosis tool. Front Genet. 2016;7:1–18.

8.2 Publikation 2

Synergisms of genome and metabolism stabilizing antitumor therapy (GMSAT) in human breast and colon cancer cell lines: a novel approach to screen for synergism

Jérôme Ruhnau*, Jonas Parczyk*, Kerstin Danker, Britta Eickholt, and Andreas Klein
*geteilte Erstautorenschaft

BMC Cancer. 2020; 20: 617. Published online 2020 Jul 2.
doi: 10.1186/s12885-020-07062-2 PMCID: PMC7331156 PMID: 32615946
Impact factor: 3.15 (2-year Impact Factor) 3.432 (5-year Impact Factor)

Ruhnau et al. BMC Cancer (2020) 20:617
https://doi.org/10.1186/s12885-020-07062-2

BMC Cancer

RESEARCH ARTICLE Open Access

Synergisms of genome and metabolism stabilizing antitumor therapy (GMSAT) in human breast and colon cancer cell lines: a novel approach to screen for synergism

Jérôme Ruhnau*†, Jonas Parczyk*†, Kerstin Danker, Britta Eickholt and Andreas Klein

Abstract

Background: Despite an improvement of prognosis in breast and colon cancer, the outcome of the metastatic disease is still severe. Microevolution of cancer cells often leads to drug resistance and tumor-recurrence. To target the driving forces of the tumor microevolution, we focused on synergistic drug combinations of selected compounds. The aim is to prevent the tumor from evolving in order to stabilize disease remission. To identify synergisms in a high number of compounds, we propose here a three-step concept that is cost efficient, independent of high-throughput machines and reliable in its predictions.

Methods: We created dose response curves using MTT- and SRB-assays with 14 different compounds in MCF-7, HT-29 and MDA-MB-231 cells. In order to efficiently screen for synergies, we developed a screening tool in which 14 drugs were combined (91 combinations) in MCF-7 and HT-29 using EC_{25} or less. The most promising combinations were verified by the method of Chou and Talalay.

Results: All 14 compounds exhibit antitumor effects on each of the three cell lines. The screening tool resulted in 19 potential synergisms detected in HT-29 (20.9%) and 27 in MCF-7 (29.7%). Seven of the top combinations were further verified over the whole dose response curve, and for five combinations a significant synergy could be confirmed. The combination Nutlin-3 (inhibition of MDM2) and PX-478 (inhibition of HIF-1α) could be confirmed for all three cell lines. The same accounts for the combination of Dichloroacetate (PDH activation) and NHI-2 (LDH-A inhibition). Our screening method proved to be an efficient tool that is reliable in its projections.

Conclusions: The presented three-step concept proved to be cost- and time-efficient with respect to the resulting data. The newly found combinations show promising results in MCF-7, HT-29 and MDA-MB231 cancer cells.

Keywords: Synergism, drug combination, cancer therapy, Nutlin-3, PX-478, Dichloroacetate, NHI-2, MDA-MB-231, MCF-7, HT-29

* Correspondence: jerome.ruhnau@gmail.com; jonasparczyk@outlook.com
† Jérôme Ruhnau and Jonas Parczyk contributed equally to this work.
Charité – Universitätsmedizin Berlin, Corporate Member of Freie Universität Berlin, Humboldt-Universität zu Berlin, and Berlin Institute of Health, Institute of Biochemistry, Charitéplatz 1, 10117 Berlin, Germany

Background

Introduction

Although a lot of progress has been made in the research of potential anti-cancer agents over the last decade, secondary therapy failure and disease progression is still the major problem in most tumor entities especially in the metastatic state of solid tumors [1, 2]. The tumor microevolution gives constantly rise to new populations of cancer cells with diverse properties [3] making it difficult to target them. Therefore, we developed a combinatory therapeutic approach that targets the tumor microevolution and its driving forces.

Industrial funds become more important in research. As industrial funding [4] and the focus on commercial interests increase, research is favourably conducted on newly bioengineered and patentable drugs [5] rather than generic compounds. Therefore, we aimed to establish a cost-efficient screening strategy that is feasible for independent work groups. In order to screen a relatively high number of potential compounds for their synergistic potency, we present here a three-step approach including a minimalistic drug interaction screening (MDIS) that is cost-efficient and can easily be established with basic laboratory equipment independent of expensive high-throughput devices.

The tumor microevolution and its driving forces

Unfortunately, initial antitumor treatment frequently leaves residual disease from which the tumor regrows [6]. Microevolution of cancer cells often leads to drug resistance and tumor recurrence [7]. Important driving forces of the microevolution are the genomic instability [8], the tumor metabolism [9, 10] and a deregulated cell cycle [11] that converge in a high proliferation rate combined with a high occurrence of mutations. To treat such complex diseases, combinations of drugs that target different aspects of the disease and at best, act synergistically may be the method of choice. Another complex disease that can currently be kept in remission with a combinatory approach (combined antiretroviral therapy, *"cART"*) [12] is the infection with the human immunodeficiency virus (HIV). As HIV itself undergoes a microevolution due to the high mutagenesis by virus reverse transcriptase [13] it took decades to find an adequate multi-target treatment. And even with cART, the development of drug resistances especially for nucleotide reverse transcriptase inhibitors (NRTI) is still a major problem [14]. Due to the complexity of cancer, it can be anticipated that more sophisticated combinatory approaches are needed. An example for such a concept is CUSP9 where multiple drugs that are approved for non-cancer indications are combined as a treatment approach for recurrent glioblastoma [15–17]. The combination of compounds can lead to a broader effect on different tumor subtypes which may reduce chances of relapses or keep the tumor in a progression free state [18].

Genome and metabolism stabilizing antitumor therapy (GMSAT)

The here presented combinatory approach aims to counteract the tumor microevolution by targeting the genome, tumor metabolism as well as growth and survival (Fig. 1). PRIMA-1met and Nutlin-3 are two compounds targeting p53 which is often referred to as the "guardian of the genome" [19]. PRIMA-1met binds and reactivates mutated p53 [20] whereas Nutlin-3 increases p53 levels by disrupting the p53-MDM2 interaction and thereby inhibiting its degradation [21]. Likewise, SJ172550 counteracts the p53-MDM4 interaction which also leads to elevated p53 levels [22]. Compounds that modulate metabolism include Dichloroacetate (DCA) which aims to reverse the Warburg effect via activation of pyruvate dehydrogenase (PDH) by inhibition of pyruvate dehydrogenase kinase, promoting the entry of pyruvate into tricarboxylic acid cycle [23]. Other important metabolism targeting compounds used for our study are the hypoxia-inducible factor 1α (HIF-1α) inhibitor PX-478 (Koh et al. 2008), Metformin, which inhibits complex 1 of the respiratory chain [24], the inhibitor of lactate dehydrogenase A (LDH-A) NHI-2 (Allison et al. 2014) and the hexokinase 2 (HK2) inhibitor 3-Bromopyruvate (Ko, Pedersen, and Geschwind 2001). Another important energy source in cancer is Glutamine metabolism [25] which is targeted by the Glutaminase inhibitor CB-839 [26]. Finally, compounds targeting growth and survival are the survivin inhibitor YM155 [27], the phosphatidylinositol 3-kinase (PI3K) inhibitor pictilisib/GDC-0941 [28], InoC2PAF [29, 30] and the ginger derivate 6-Shogaol targeting the AKT/mTOR pathway [31].

Screening for and evaluation of synergisms

In order to screen for potent synergisms, various successful methods have been tested and published recently [32, 33]. While some are relying on high throughput [34, 35] others are partially computerised to reduce the amount of actual experimental data points being investigated like the Feedback System Control [36–38]. There are also methods investigating synergism via mostly computerised analyses (Stochastic Searching Model, Statistical Model and Multi-Scale Agent-Based Model) [33, 39]. In literature, more than 10 different ways of defining synergism are described [40]. First referred to as the Loewe Additivity [41], quantification of synergistic drug interaction by the combination index (CI) is nowadays widely accepted. A precise method to estimate the specific dosages of fractional effects needed to calculate the CI, is the median effect method of Chou and Talalay that is derived from the mass action law [42, 43]. Quantification of synergisms via the CompuSyn software [44] based on multiple concentrations across the dose response curves is a well-established procedure [45].

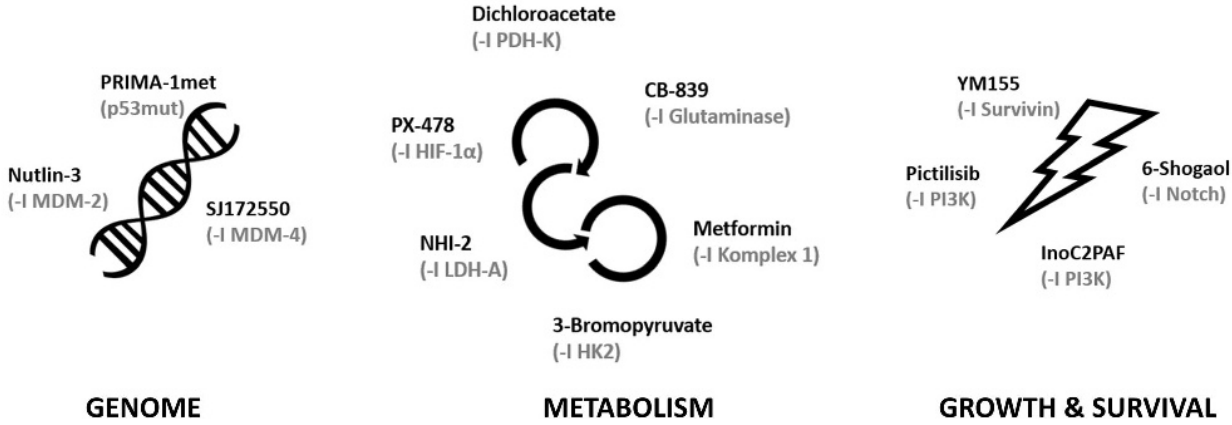

Fig. 1 13 genome, metabolism and growth–/ survival targeting agents according to the GMSAT concept as well as Cisplatin as a reference to conventional chemotherapy are illustrated with their respective target structures in brackets. "**-I** "stands for inhibition

Methods

Cell culture

MCF-7 breast cancer cells express p53 wild-type, are estrogen (ER) and progesterone receptor (PR) positive and express low levels of human epidermal growth factor receptor 2 (HER2) [46, 47]. MDA-MB-231 breast cancer cells that were originally isolated from a human breast cancer pleural effusion express a p53-mutation (R280K), are negative for ER and PR and express no amplification of HER2 [46, 48]. Both breast cancer cell lines were a kind gift of Göran Landberg (Sahlgrenska Cancer Center, University of Gothenburg, Gothenburg, Sweden) and were initially purchased from ATCC (Catalogue number: CRL-3435 and HTB-26). The primary colon cancer cell line HT-29 was isolated in 1964 by Fogh and Trempe. HT-29 cells carry a p53 mutation (R273H) and are deregulated for c-MYC [48]. HT-29 was a kind gift from Karsten Parczyk (Bayer AG) and initially purchased from ATCC (Catalogue number: HTB-38). All cell lines were routinely tested for mycoplasma contamination. For testing of mycoplasma contamination either PCR (GATC Biotech) or staining with Hoechst 33342 dye (Sigma-Aldrich, Steinheim, Germany) was conducted. HT-29 and MCF-7 cells were cultured in DMEM and the MDA-MB-231 in DMEM/F12 containing penicillin/streptomycin (100 U ml^{-1}), L-glutamine (DMEM: 584 mg l^{-1}, DMEM/F12: 365,1 mg l^{-1}) and 10% heat-inactivated fetal calf serum (FCS) at 37 °C in a humidified incubator with 5% CO2. Cells were harvested using 0.05% trypsin/0.02% EDTA in PBS.

Compounds

Fourteen compounds were used: Prima-1met, Nutlin-3, SJ 172550, YM155 (Selleck Chemicals, Houston, TX, USA), 6-Shogaol (Hölzel Diagnostika Handels GmbH, Cologne, Germany), Pictilisib (Absource Diagnostics GmbH, Munich, Germany), Ino-C2-PAF (1-O-octadecyl-2-O-(2-(myo-inositolyl)-ethyl)-sn-glycero-3-(r/s)-phosphatidyl-choline) [29], PX-478 (Hölzel Diagnostika Handels GmbH, Cologne, Germany), DCA, Metformin-hydrochloride (Sigma-Aldrich, Munich, Germany), CB-839 (Selleck Chemicals, Houston, TX, USA), 3-Bromopyruvate (Santa Cruz Biotechnology, Dallas, Texas, USA), NHI-2 (Bio-Techne GmbH, Wiesbaden-Nordenstadt, Germany) and Cisplatin (Cayman Chemical Ann Arbor, MI, USA). 3-Bromopyruvate, Cisplatin, Dichloroacetate, Metformin, PRIMA-1-met, PX-478, YM155 and Ino-C2-PAF were solved in distilled water. Dimethyl sulfoxide (DMSO) was used to solubilize 6-Shogaol, CB-839, NHI-2, Nutlin-3, Pictilisib and SJ-17255. Finally, DMSO concentration was kept under 0.6 μl per well (0.6%).

All data collected in this study can be found in the additional file (Additional file 1). This includes all data produced for dose response curves and all combination experiments.

Cell viability assay and cell proliferation assay

0.5×10^4 MCF-7, 1.5 10^4 HT-29 and 1.5 10^4 MDA-MB-231 cells per well were seeded in flat bottom 96-well plates. After 24 h and reaching a cell-confluence of approximately 50%, the respective compound or combination was added. As a negative control, cells were cultured in the presence of 0.6% DMSO. However, we could not detect any differences in cell viability between 0.6% DMSO and no DMSO. After 48 h of further incubation, either MTT assay (3-(4,5-dimethylthiazol-2-yl)-2, 5-diphenyltetrazolium bromide, a tetrazole assay, Bio-Techne GmbH, Germany) or SRB (Sulforhodamin B) assay were applied. The MTT assay was performed according to the manufacturer's instructions. For the SRB assay, cells were treated with 10% trichloroacetic acid (w/v) and stained with 0.06% SRB in 1% acetic acid for 30 min. Cells were then repeatedly washed using 1% acetic acid (v/v) followed by dissolution in 10 mM Tris

(pH 10.5). Protein mass was monitored using a microplate reader at an optical density of 492 nm. All experiments were performed at least with two replicates in three independent experiments.

Dose response curves were obtained for 14 compounds using GraphPad Prism statistical analysis software 7.05. EC_{50} of the respective compounds was determined via nonlinear regression.

Minimalistic drug interaction screening (MDIS)

MCF-7 and HT-29 cells were treated with 14 single and their 91 pairwise combinations at dosages of approximately EC_{25}. All experiments were performed at least with three biological and two technical replicates. Thus, for one cell lines we produced about 909 data points (303 per biological replicate). The conjectured synergistical potency (CSP) of a combination was quantified by adding up the effect of the single compounds and subtracting the result from the combination's effect. E.g.: Single dose A: 20% cell viability-reduction, single dose B: 10% cell viability-reduction and the combination of A and B exhibit cell viability-reduction of 37%. Thus, the combination of A and B reduces the cell viability 7% more than it is expected from simply adding up the effects of the single compounds (CSP = 7). Analyses were performed with Graph pad prism and Microsoft Excel.

Confirmation of synergism

Synergism predicted by MDIS was evaluated with three to seven concentrations as suggested by Chou and Talalay [49].

MCF-7 and HT-29 cells were treated with the respective combination of compounds at a constant EC_{50}:EC_{50} ratio as well as the same concentrations of each drug individually. Significant differences between single compound viabilities and combination viability was assessed by unpaired t-test. Only concentrations with p-values ≤0.05 for both compounds were considered as significant and marked by an asteriks (*) in the figures.

The combination indices (CI) were calculated using the CompuSyn software [44]. The CI is a quantitative value for the synergism of a drug combination at specific concentrations. A value below 0.3 indicates a *"strong"*, 0.3–0.7 a *"robust"* (originally referred to as "synergism" by Chou and Talalay), 0.7 to 0.85 a *"moderate" and 0.85 to 0.9 a "slight"* synergism. Values from 0.9 to 1.1 show an *"additive"* effect and a CI above 1.1 indicates *"antagonism"* [50, 51]. The CI was calculated as follows:

$$CI = \frac{(D)_1}{(Dx)_1} + \frac{(D)_2}{(Dx)_2}$$

In the numerators, $(D)_1$ and $(D)_2$, are the concentrations of drug 1 and drug 2 in the drug-combination which have a certain effect on cell viability (x %). In the denominators, $(Dx)_1$ and $(Dx)_2$, stand for the concentration of each drug alone (drug 1 or drug 2) that is necessary to obtain the same effect (x %) as the drug-combination (drug 1 and drug 2). The concentrations $(Dx)_1$ and $(Dx)_2$ were calculated by CompySyn referring to individual cell-viability data of the concerning compounds. To enhance rigidity, $(Dx)_1$ and $(Dx)_2$ were predominantly generated via direct experimental data points. This way, potential calculation errors are ruled out as suggested by Zhao et al. [45]. To produce the median effect plots the following equation was used:

$$D_x = D_m\left[\frac{fa}{1-fa}\right]^{1/m}$$

Dm is the median effect dose, m counts for the slope of the median-effect plot and fa stands for fraction affected.

Results

Three-step concept to identify synergisms between selected compounds

In this work, we applied the following three steps to identify synergisms between the compounds for our combinatory approach (Fig. 2).

1. Dose response curves aiming to detect the single drug effect in cancer cell lines and calculate fractional effects like EC_{50} or EC_{25}.
2. The minimalistic drug interaction screening (MDIS) to identify potential synergies.
3. Verification by the method of Chou and Talalay to reliably prove the projected synergisms.

Following these steps, we identified 27 potential synergisms in MCF-7 (29.7%) and 19 in HT-29 (20.9%) of the 91 pairwise combinations. A selection of combinations was further analysed by the method of Chou and Talalay.

Dose response curves in MCF-7, MDA-MB-231 and HT-29 cells

Dose response experiments were conducted in order to identify the dose range for MDIS and evaluate the antitumor effects of the single compounds in different cell lines. Therefore, MCF-7, MDA-MB-231 and HT-29 cells were cultivated for 24 h before being treated with increasing concentrations of the 14 different compounds (Fig. 1). After an additional cultivation period of 48 h, cell viability or protein mass were quantified using the MTT or SRB assay. In Fig. 3, we exemplarily illustrated the dose response curves of Nutlin-3 and DCA for all three cell lines. Furthermore, we calculated the median effective concentration (EC_{50}) for all compounds with

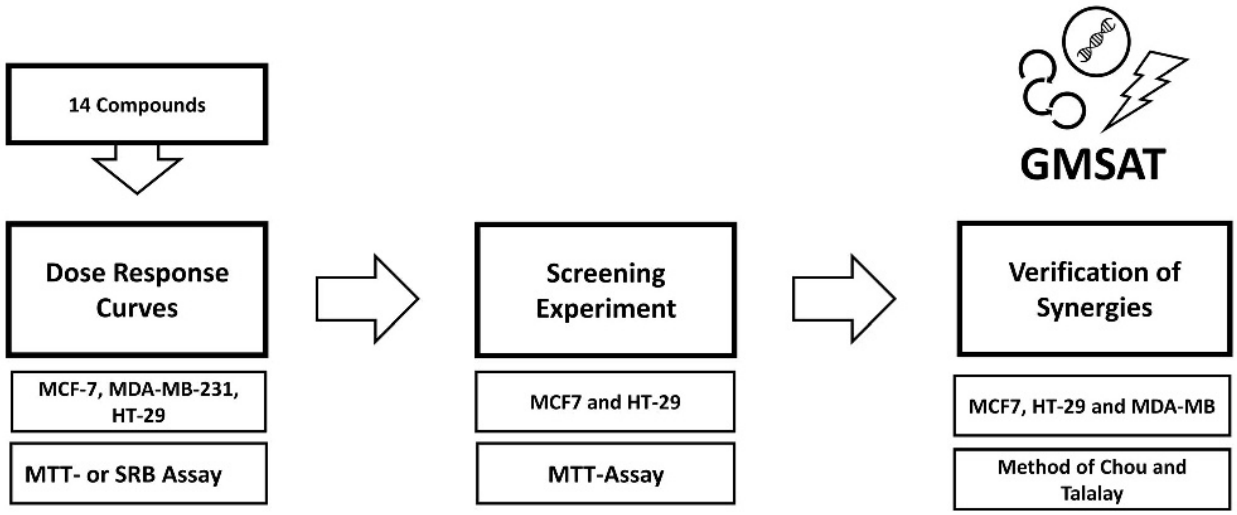

Fig. 2 14 compounds were selected and analysed using MTT- or SRB Assay in HT-29, MCF-7 and MDA-MB-231 cells in order to obtain dose response curves and EC_{50}. A minimalistic drug interaction screening (MDIS) was applied to detect synergies in the 91 possible combinations. The combinations with the most synergistic potential were then further verified

the help of GraphPad Prism (Table 1). Data for all dose respond curves can be found in the Additional file 1.

Overall, we observe that the triple negative breast cancer cell line MDA-MB-231 is the most resistant cell line requiring the highest dosages in 11 out of the 14 tested compounds. Although Prima-1met is intended to stabilize p53-mut, the strongest efficacy is shown in the p53 wild-type cell line MCF-7. YM155 is effective at very low concentrations at EC_{50} in a nM range in all three cell lines.

Minimalistic drug interaction screening (MDIS)

To identify synergistic actions of compound combinations, we developed a minimalistic drug interaction screening (MDIS). For this experiment, HT-29 and MCF-7 cells were treated with 14 different compounds in all 91 possible pairwise combinations. In this approach, dosages of approximately EC_{25} were used for all compounds. The conjectured synergistical potency (CSP) of a combination was quantified adding up the effect of the single compounds and subtracting the result from the combination's effect (c.f. Material and Methods). We applied this rather simple mathematical approach not to prove synergisms, but to narrow down the number of effective combinations. The overall average standard deviations in MDIS were 7.5% for MCF-7 and 10.6% for HT-29 respectively. CSP values above 10 were chosen as a cut off for a 'possible' (+) synergism, 15 for a *"likely"* (++) and 25 for a *"very likely"* (+++) synergism (Fig. 4). Pure numerical values can be found in Additional file 1.

For HT-29 cells, a total amount of 19 synergistic projections out of the 91 combinations (20.9%) were predicted. Eleven of the latter were *"possible"* (12.1%), seven *"likely"* (7.7%) and one a "*very likely*" synergism (1.1%). For the p53 wild type breast cancer cell line MCF-7, a total of 27 combinations (29.7%) were identified, including 16 *"possible"* (17.6%), ten *"likely"* (11.0%) and one *"very likely"* (1.1%) synergism.

The highest CSP could be achieved in HT-29 for the combination of DCA + PX-478 which led to an average increase in inhibition of cell growth of 62.4% compared to the sum of the single dose effects determined for both drugs. Therefore, we performed deeper investigations with the combination of DCA + PX-478 in different cancer cell lines in a separate study. The second highest value was obtained for DCA + NHI-2 (43.4%) in MCF-7. Four combinations were projected to be synergistic in both cell lines: Nutlin-3 + YM155, DCA + Metformine, DCA + PX-478 and Nutlin-3 + PX-478.

DCA, PX-478, Nutlin-3 and NHI-2 exhibit highest potential for synergistic interactions in MDIS

There were substantial differences in the count of potential synergies and their strength for the 14 compounds. The total number of "+" attributed to a compound by MDIS illustrates the synergistic potential of a compound since it summarizes quantity and quality of predicted synergistic interactions. With a total of 19 "+" the two compounds DCA and PX-478 have the highest synergistic potential. While PX-478 has the highest count of possible synergisms [12], DCA compensates a lower count [10] with stronger predictions (one vs. two *"very likely"* synergisms).

Additionally, with a total of 11 projections each, Nutlin-3 with 16 "+" and NHI-2 with 15 "+" show high synergistic potential. The lowest count of synergistic interaction was identified for the two PI3K-pathway

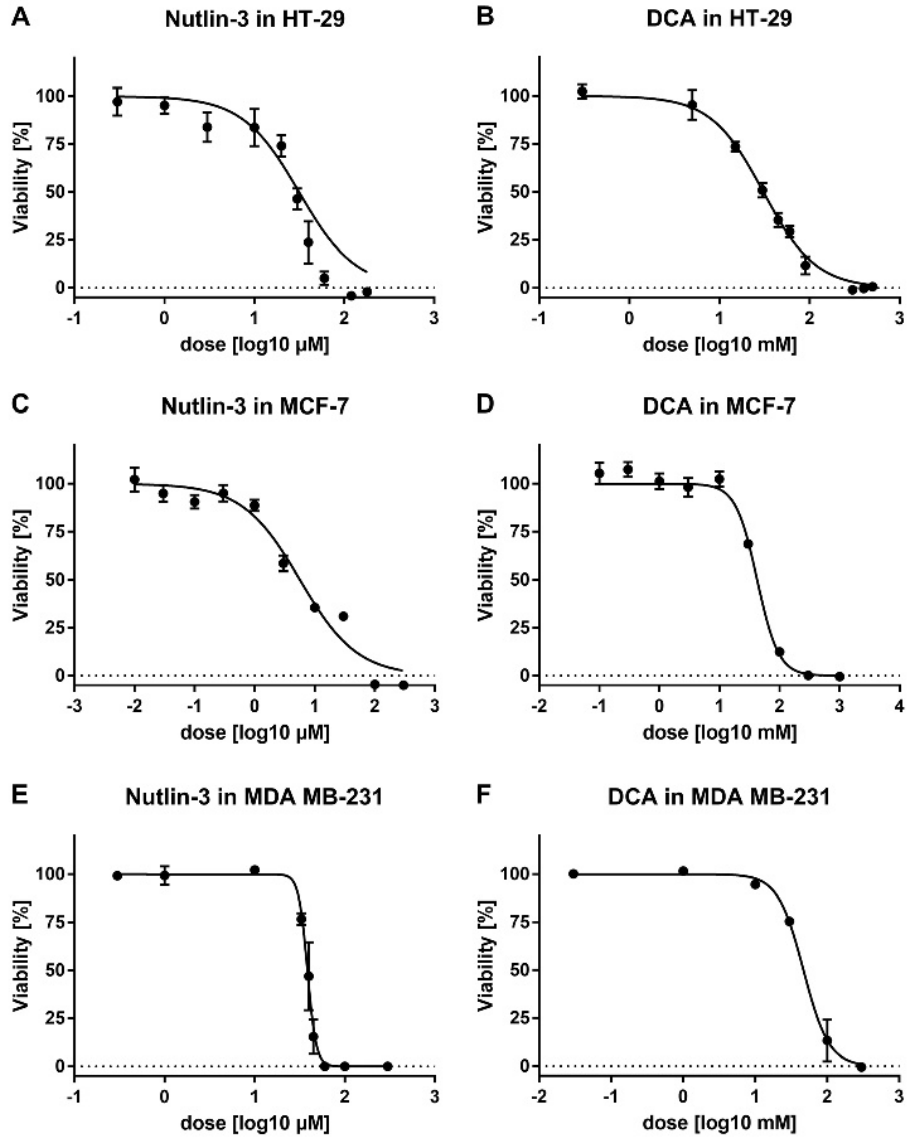

Fig. 3 dose response curves Cells were seeded into a 96 well plate at a density of 1.5 (HT-29, MDA-MB) and 0.5 × 10^4/well (MCF-7), incubated 24 h to a confluence of 50%, then cells were treated with increasing concentrations of the 14 selected drugs for 48 h. Viability was assessed using the MTT-Assay and curves were obtained using the four-parameter variable slope function of Graphpad Prism. Exemplarily the resulting curves for Nutlin-3 and DCA are shown for the three cell lines

targeting drugs Pictilisib and InoC2PAF with 0 and 2 predictions, respectively. YM155 had seven projections in MCF-7 and only one in HT-29. For 6-Shogaol, the opposite was the case: Five predictions in HT-29 and none in MCF-7.

Analysis of the synergies by the method of Chou and Talalay

For further evaluation of these predicted synergisms according to the method of Chou and Talalay, we used the CompuSyn Software to calculate the combination indices (CI). The CI is a quantitative value for the synergism of a drug combination at specific concentrations. A value below 0.9 indicates synergism and the lower a CI, the stronger a synergism: A value below 0.3 indicates a "strong", 0.3 to 0.7 a "robust" 0.7 to 0.85 a "moderate" and 0.85 to 0.9 a "slight "synergism. Values from 0.9 to 1 show a nearly "additive" effect and a CI above 1.1 indicates "antagonism". Furthermore, significance in the differences between a combination and the respective single compounds was evaluated by unpaired T-test. We evaluated seven combinations projected by MDIS

Table 1 EC_{50} of the 14 compounds

Compound	Unit	HT-29 EC50	MCF-7 EC50	MDA-MB-231 EC50
Prima-1met	[μM]	64.9	18.1	71.1
Nutlin-3	[μM]	28.8	6.0	39.2
SJ172550	[μM]	15.4	15.6	229.5
YM155	[**n**M]	50.9	2.54	23.6
6-Shogaol	[μM]	29.7	148.9	503.5
Pictilisib	[μM]	19.8	0.16	532.8
InoC2PAF	[μM]	7.4	9.5	91.7
PX-478	[μM]	77.4	15.92	164.3
DCA	[**m**M]	34.9	40.7	48.7
CB-839	[μM]	3.3	6.0	13.3
3-BP	[μM]	15.6	110.7	554.8
Metformin	[**m**M]	6.9	13.4	100
NHI-2	[μM]	32.7	29.82	26.14
Cisplatin	[μM]	549.8	84.35	484.5

Cells were seeded into a 96 well plate at a density of 1.5 (HT-29, MDA-MB) and 0.5×10^4/well (MCF-7), incubated 24 h to a confluence of 50%, then incubated with increasing concentrations of the 14 selected drugs for 48 h. Then, viability was assessed using the MTT-Assay and EC_{50} was calculated using Graphpad Prism

(Table 2). Five of the latter could be confirmed by the method of Chou and Talalay, while two combinations, PRIMA-1met + Nutlin-3 and Nutlin-3 + 3-Bromopyruvate did not reach significant p-values in detected synergisms (CI = 0.89 and 0.72 respectively). Since the combination of DCA + NHI-2 was promising in MCF-7 cells in both the screening trial (CSP = 43) and the method of Chou and Talalay (CI = 0.27), we further verified it in HT-29 (Table 2 and Fig. 6-C, D). Although it could not be detected by MDIS, we found the combination to be synergistic in HT-29 cells (CI = 0.50). Furthermore, we verified the most promising synergisms in MDA-MB-231 by calculating the CI-value using the dose response curves and equation of Loewe [41]. Thereby, we could confirm the top synergies DCA + NHI-2 (CI = 0.) and Nutlin-3 + PX-478 (CI = 0.62). Since we found a *"likely"* synergism between DCA + Nutlin-3 in p53 wild-type MCF-7 cells (Fig. 4), we checked the combination of p53mut binding PRIMA-1met + DCA in the p53-mutated MDA-MB-231 cells. Interestingly, a synergy exclusively found in MDA-MB-231 cells could be confirmed (CI = 0.78). After the evaluation of MDIS, we named synergies with CSP values between ten and 15 *"possible"*, 15 and 25 *"likely"* and greater than 25 *"very likely"* synergisms. Out of the seven verified synergies, we could prove all *"likely"* and *"very likely"* (4/4) but only two of the four possible synergisms. Thus, we detected eight (8.8%) and 11 (12.1%) *"likely"* and *"very likely"* synergisms in HT-29 and MCF-7 respectively.

Interpretation of the combination index

When analysing drug interactions, looking at certain concentrations alone may lead to a false interpretation of synergism [42, 45]. The example of the synergism between PRIMA-1met + YM155 illustrates the principle of the CI-value interpretation (Fig. 5). At first sight, the combination of Prima-1met + YM155 shown in Fig. 5-D seems to exhibit stronger synergistic effects compared to lower dosages presented in Fig. 5-B. Contrarily to that assumption, the opposite is the case: 5-B shows indeed a *"robust"* synergism (CI = 0.34) while the effects shown in Fig. 5-D are not even *"additive"* (CI = 1.19). The explanation for this counter-intuitive finding is that doubling the single doses of PRIMA-1met + YM155 in EC_{50} results in a much stronger effect than the combination of both drugs at EC_{50} (Fig. 5-D, E). Therefore, one can conclude that the shape of and position on the curve is important to accurately describe and interpret synergisms. The easiest method to interpret synergistic effects of these curves consists in doubling the fractions of EC_{50}. As a result, the CI calculations are mainly based on experimental data and can easily be interpreted by studying the curve progression. This method also helps minimizing errors that might occur with mathematical dose fitting [45].

The combinations of Nutlin-3 + PX-478 and DCA + NHI-2 act synergistically in MCF-7, MDA-MB and HT-29 cells

The combination Nutlin-3 (inhibition of MDM-2) + PX-478 (inhibition of HIF-1α) was predicted to be synergistic by MDIS for HT-29 and MCF-7 cells. Via the method of Chou and Talalay, we analysed this synergism over the whole dose response curve. Exemplarily, we show in Fig. 6a and b the dose response curves for the combination Nutlin-3 + PX-478 and the single compounds. Best CI-values were 0.33 for MCF-7 (Fig. 6a) as well as 0.63 and 0.62 for HT-29 and MDA-MB-231, respectively (Table 2). In the reduction of protein mass (Fig. 6b) as well as the reduction of viability (Fig. 6a) it was mainly synergistic at 0.125x, 0.25x and 0,5x EC_{50}.

Further, we confirmed the synergism of DCA + NHI-2 (PDH activation and LDH-A inhibition) in all three cell lines (Fig. 6c and d for MCF-7 and Table 2 for HT-29 and MDA-MB-231). A *"strong"* synergism was identified for the cell line MCF-7 (CI = 0.27) whereas a *"robust"* synergism could be found in HT-29 (CI = 0.50) and MDA-MB-231 (CI = 0.62).

Discussion

We present here a three-step concept to systematically screen for and reliably describe synergies between a high number of compounds at a minimal cost and time budget. With that concept, we identified five synergistic combinations of genome and metabolism stabilizing compounds of which Nutlin-3 + PX-478 as well as DCA + NHI-2 were

Fig. 4 minimalistic drug interaction screening. HT-29 and MCF-7 cells were seeded into a 96 well plate at a density of 1.5 (HT-29) or 0.5×10^4/well (MCF-7) and incubated 24 h to a confluence of 50%. Then, cells were incubated with 14 single compounds and the respective 91 combinations at a concentration about EC_{25} for 48 h. Viability was assessed using the MTT-Assay and the CSP (conjectured synergistical potency) values were calculated. CSP of a combination was quantified by adding up the effect of the single compounds and subtracting the result from the combination's effect. All CSP values above ten are highlighted in green. Values between ten and 15 are marked by one plus (+), between 15 and 25 by two plus (++), greater than 25 by three plus (+++) and referred to as "possible", "likely" and "very likely" synergism respectively. The number of total "+" is given in the first column below the name of the compounds and summarizes the number and strength of projected synergistic interactions

found in all three cell lines MCF-7, MDA-MB-231 (breast cancer) and HT-29 (colon cancer).

In contrast to the here presented approach, Borisy and colleagues designed a sophisticated high-throughput robot-assisted approach where 30 antifungal drugs and their 435 pairwise combinations were screened for potential synergistic interactions. For their screening experiment, six different concentrations with two technical replicates were used, resulting in a total of 31,320 data points [34]. For 14 compounds the same experimental design would result in 6552 compared to 303 data points with MDIS. While this approach provides a substantial amount of valuable information, it is material, cost and time intensive. Thus, optimization in material use and number of conducted experiments is needed to make drug interaction research feasible for a broader range of work groups.

Dose-ratio based screening

Yin and colleagues reviewed, how computational based approaches such as the Feedback System Control [37] or Stochastic Searching Model with an heuristic idea can help to minimize costs of mainly experimental approaches [32]. Both approaches incorporate different dose-ratios already in the screening process. This design respects the fact that compounds interacting synergistically at a specific dose ratio may be antagonistic at other ratios [35]. Consequently, a screening without different dose-ratios may fail to detect synergisms that have antagonistic, additive or just slightly synergistic effects in the tested dose-ratio. In the here presented minimalistic drug interaction screening, this phenomenon is reflected in the fact that DCA + NHI-2 has not been projected to be synergistic by MDIS in HT-29 but could be proved by the method of Chou and Talalay (CI = 0.50). The

Table 2 Verified synergies

Combination	Cell line	MDIS	C & T	MDA-MB
DCA + NHI-2	MCF-7	+++	0.27*	0.62*
	HT-29	–	0.50*	
Nutlin-3 + PX-478	MCF-7	+++	0.33*	0.62*
	HT-29	+	0.63*	
PRIMA-1met + YM155	MCF-7	++	0.34*	n.d.
DCA + Metformin	MCF-7	++	0.51*	n.d.
PRIMA-1met + NHI-2	HT-29	+	0.24*	n.d.
Nutlin-3 + PRIMA-1met	HT-29	+	0.89	n.d.
Nutlin-3 + 3-Bromopyruvate	MCF-7	+	0.72	n.d.

Table 2 shows the seven combinations that were selected for further verification by the method of Chou and Talalay. The third column shows the predictions by MDIS: + indicates a "possible" ++ a "likely", +++ a "very likely" synergism and – no synergism. The respective best CI-values calculated by the method of Chou and Talalay (C & T) are listed in the fourth column. They were marked with an * if unpaired T-test was significant for the respective concentration of the combination in comparison with the single compounds. A CI-value indicates the quality of a synergism at a specific concentration. A value below 0.3 indicates a *"strong"*, 0.3 to 0.7 a *"robust"* and 0.7 to 0.85 a *"moderate"* synergism. In the case of MDA-MB cells, CI-values were calculated by the method of Loewe with the help of the earlier obtained dose response curves and Graphpad Prism. The resulting CI-values are listed in the fifth column. Combinations that were not analysed in MDA-MB-231 cells are marked with n.d. Out of the seven verified synergies, we could prove all "likely" and "very likely" (4/4) but only two of the four "possible" synergisms (two combinations had no significant CI-value below 0.9). Details concerning the combinations (the complete dose response curve and all the respective CI-values) can be found in Figs. 5 and 6 as well as in the Additional file 1.

opposite accounts for PRIMA-1met + YM155 which is synergistic in low doses (e.g. 0.125x EC_{50}) and antagonistic at 8x EC_{50}. Nevertheless, MDIS represents a substantial decrease in experimental scope: If for example three concentrations (e.g. EC_{25}, EC_{50} and EC_{75}) and all possible dose-ratios are used instead of one, the number of combinations increases from one to nine. Additionally, MDIS resulted in a total of 19 potential synergisms in HT-29 and 27 in MCF-7, a number that requires immense efforts to further verify and describe. Even when selecting only *"likely"* (++) and *"very likely"* (+++) synergisms, nine (HT-29) and 11 (MCF-7) combinations remain (Fig. 4). The focus on mechanistically interesting and most solid combinations in different cell lines is necessary to select most promising candidates. A dose-ratio based screening method is likely to detect even weak synergisms at an optimized dose-ratio and in that way it multiplies the number of projections. Therefore, we recommend the here presented cost-efficient design for projects that aim to evaluate interesting compounds of newly anticipated antitumor concepts for their synergistic potency. We recommend verifying the synergy over the entire dose-response curve at a constant dose-ratio before the determination of the optimal dose-ratios. Dose-ratio based screening might rather be appropriate for detailed analyses in order to optimize therapies of already implemented compounds [34].

Synergy interpretation

After performing the three phases of the here proposed concept, we consider *"likely"* and *"very likely"* synergisms predicted by MDIS as the most relevant and solid results. In HT-29, we detected eight (8.8%) and in MCF-7 11 (12.1%) *"likely"* and *"very likely"* synergisms. Out of this group, we could confirm four of four tested synergisms (Table 2). In the case of *"possible"* synergisms, only two of four tested combinations could be confirmed. Nutlin-3 + PRIMA-1met and Nutlin-3 + 3-Bromopyruvate did reach synergistic CI values at some concentrations (CI: 0.89 and 0.72 respectively), but without significance. Furthermore, the CI-values over the whole dose-respond curve of these combinations were mainly additive or even antagonistic. Another "possible" synergisms detected by MDIS in MCF-7 is Metformin + Nutlin-3 which has already been described for mesothelioma cells by Shimazu et al. [52]. In general, *"possible"* synergisms might be worth examining as the *"robust"* synergistic effect between Nutlin-3 + PX-478 in HT-29 (CI = 0.63) illustrates (Table 2).

Out of the five detected and proven synergies, two top combinations were synergistic in all three cell lines. Nutlin-3 inhibits p53 degradation [21] while PX-478 modulates metabolism by inhibiting HIF-1α and thereby aerobic glycolysis [53]. While a mechanistic overlap is described in literature, we were – to the best of our knowledge - the first to detect this synergism. Lee and colleagues reported in 2009 that Nutlin-3 inhibits HIF-1α in a p53 dependent and vascular endothelial growth factor (VEGF) in a p53 independent manner [54]. These findings are supported by the fact that the Nutlin-3 + PX-478 showed the strongest synergism in the p53 wild-type cell line MCF-7 (CI = 0.33) compared to the p53 mutated cell lines HT-29 (CI = 0.63) and MDA-MB (CI = 0.62).

The second combination present in all three cell lines is DCA (PDH activation [55]) + NHI-2 (LDH-A inhibition [56]) which showed a *"strong"* synergism for the cancer cell line MCF-7 (CI = 0.27) and *"robust"* synergisms for HT-29 (CI = 0.50) and MDA-MB-231 (CI = 0.62). This combination has not been described in literature yet and is particularly interesting as both compounds target the "Warburg" effect [55], inhibiting the conversion of pyruvate to lactate and promoting its entrance into the tricarboxylic acid cycle. Out of the other four synergisms we were able to identify and prove, DCA + Metformine was already described thoroughly in literature [57].

Validation of conjectured synergies

For the verification of the synergisms projected by MDIS, the widely accepted median-effect principle of the mass

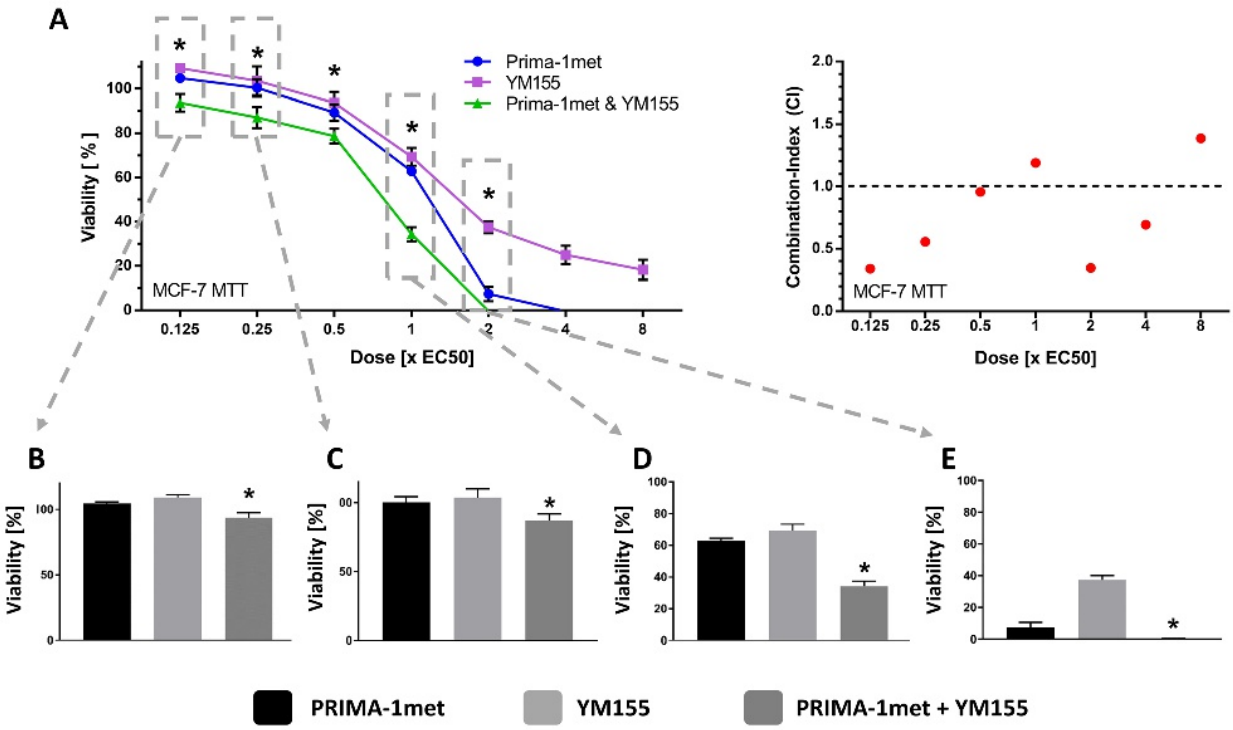

Fig. 5 Synergy interpretation. HT-29 and MCF-7 cells were seeded into a 96 well plate at a density of 1.5 (HT-29) and 0.5 × 10^4/well (MCF-7), incubated 24 h to a confluency of 50%, then medicated with increasing concentrations of PRIMA-1met, YM155 and their combination for 48 h. Cell viability was assessed using the MTT-Assay and curve was further analysed using Graphpad Prism. CI-Values were calculated by CompuSyn and illustrated with red dots in the diagram on the right. Each dot corresponds to the respective combination shown in the graph to the left. CI-values underneath the dashed line (< 1) imply a synergism. Viability data were also illustrated in a bar-chart design at 0.125x (B) 0.25x (C), 1x (D) and 2x EC_{50} (E)

action law implemented in the method of Chou and Talalay was used [58]. To keep the transformation error low, we decided not to simplify our experiments by the overextended use of calculation and curve fitting for the determination of synergism [45]. In detail, we combined our compounds in a constant ratio of EC_{50} to EC_{50}, stepwise doubling the dosages. We favour this method as the data necessary to calculate the CI-values have a solid empirical base. When a combination commends itself for further investigation, we suggest the following analyses:

1. The dose-ratio is crucial in the description of synergisms but cost and time expensive. Therefore, we suggest evaluating the most effective dose-ratios after a synergy has successfully been identified and proven.
2. To further evaluate the effectiveness of the detected combination, we recommend utilizing cell lines with different properties (e.g. p53 status) and or in different tumor entities [35].

Limitations

In this work, we focused intensively on synergistic drug interaction in the detection of potential combinatory approaches. Synergistic effects are desirable, but additive effects or in some cases even compounds with slight antagonisms might be useful as well [18, 59]. For example, if the necessary single dose cannot be reached in vivo for pharmacodynamics reasons or dose limiting toxicity, a combination with a higher cumulative dose might result in a better outcome.

With respect to the genome and metabolism stabilizing antitumor approach, we conducted a systematic literature research to identify matching compounds. In contrast, large-scale prediction of drug combinations via different databases [18, 39] is another promising way of narrowing down the field of potential compounds. Generally, we based the calculation of the CI-values on substantial experimental data. If only half of the curve is measured experimentally while the other parts are calculated via curve fitting, changes in slope might be missed which could lead to false low CI-values [45]. Therefore, the amount of experimental data points and EC-range covered must be considered in the interpretation of the resulting CI-values.

Clinical implications

To further evaluate promising combinations, taking already conducted clinical trials of the respective single compounds

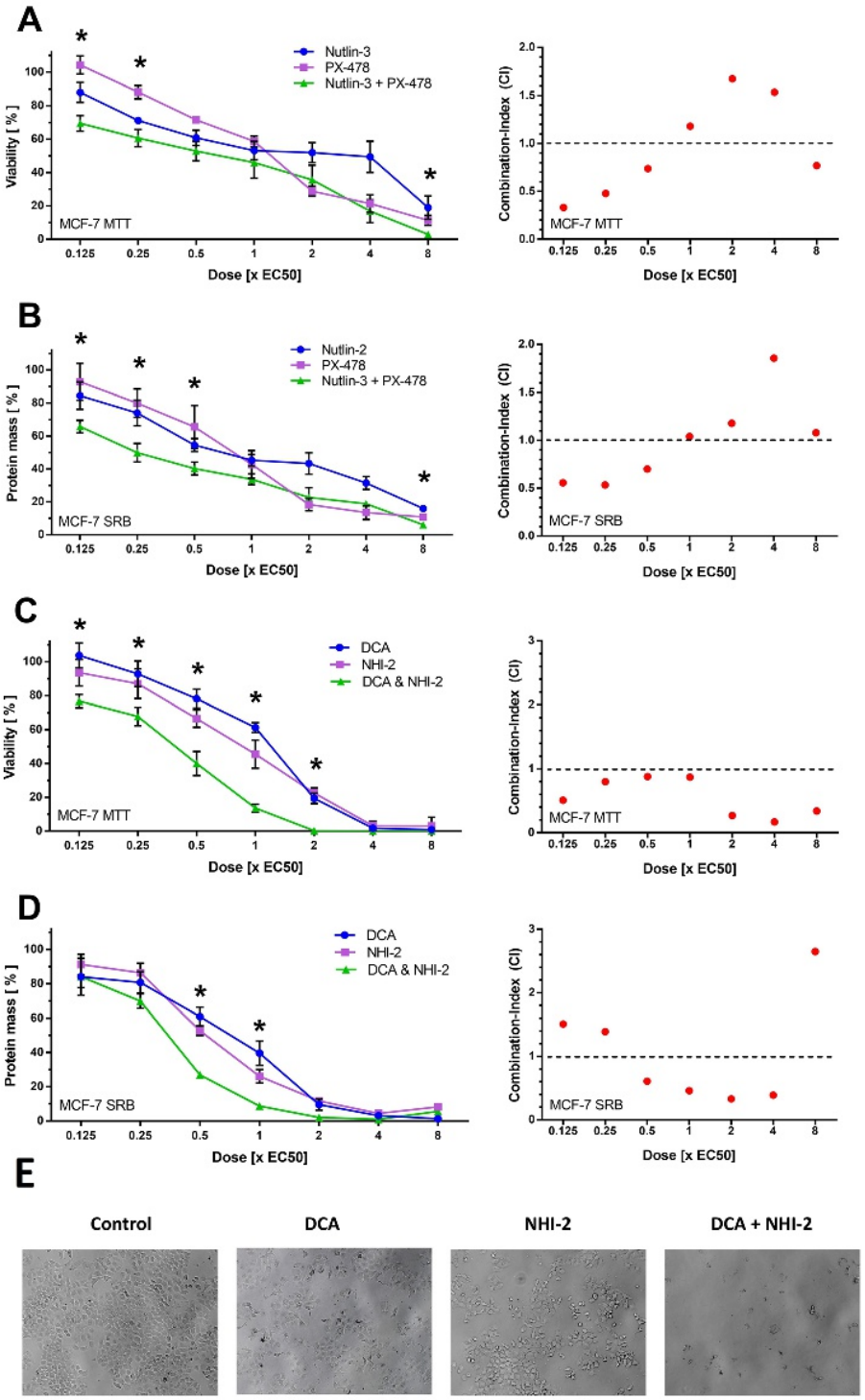

Fig. 6 Nutlin-3 + PX-478 and DCA + NHI-2. MCF-7 cells were seeded into a 96 well plate at a density of 0.5×10^4/well (MCF-7), incubated 24 h to a confluency of 50%, then incubated with increasing concentrations of Nutlin-3, PX-478 and their combination (**a**, **b**) as well as DCA, NHI-2 and their combination (**c**, **d**) and) for 48 h. Then, viability was assessed using MTT assay (**a**, **c**) and protein mass was assessed using SRB assay (**b**, **d**). CI-Values were calculated by CompuSyn and illustrated with red dots in the diagram on the right. Each dot corresponds to the respective combination shown in the graph to the left. The effects of EC_{50} *of* DCA, NHI-2 and DCA + NHI-2 on the cell confluency is illustrated on the bottom (**e**)

into account is important to identify potential obstacles and problems in the translational phase. When looking at DCA, "clinicaltrials.gov" does list 37 studies in the context of cancer and 81 studies in total. In one trial where patients with previously treated metastatic breast or non-small cell lung cancer were treated with DCA, the authors concluded that DCA should be used for patients with longer life expectancy and potentially in combination [60] (ClinicalTrials.gov Identifier: NCT01029925). PX-478 seems to be abandoned since the last clinical trial was conducted in 2010 (ClinicalTrials.gov Identifier: NCT00522652). In this phase 1 clinical trial PX-478 has been well tolerated in low doses with consistent HIF-1α inhibition in patients with advanced solid tumors [61]. A sufficient effect with well tolerated doses to commence with a phase 2 clinical trial seemed to be missing although a HIF-1α inhibition was achieved. As a conclusion, it can be stated that these two drugs are tolerated in the respectively needed dose while a convincing effect on cancer was missing. We believe that synergism is an important way to successfully include promising compounds like DCA and or PX-478 in the therapy of cancer. The synergisms with NHI-2 or Nutlin-3 identified in this study may be a solution in this context. For NHI-2 and Nutlin-3 no literature on clinical trials is available. However, it also seems that the effect of NHI-2 and Nutlin-3 on normal non-cancerous cells is tolerable. In vitro treatment with Nutlin-3 induced a significant cytotoxicity on primary CD19(+) B-CLL cells, but not on normal CD19(+) B lymphocytes, peripheral-blood mononuclear cells or bone marrow hematopoietic progenitors [62]. As for the molecular mechanism of NHI-2, Calvaresi et al. stated that LDH-A inhibition is unlikely to harm normal tissues [63].

Conclusion

The here presented three-step concept proved to be cost and time efficient with respect to the resulting data at the example of our combinatory approach. *"Likely"* and *"very likely"* synergisms proved to be reliable predictions of MDIS after verification by the method of Chou and Talalay. The combination of Nutlin-3 + PX-478 as well as DCA + NHI-2 could be identified in all three cell lines. In vivo experiments are required to evaluate the potential of these combinations for clinical studies.

Supplementary information

Supplementary information accompanies this paper at https://doi.org/10.1186/s12885-020-07062-2.

Additional file 1. Combination experiments, MCF-7 dose-respond-curves, HT-29 dose respond curves, MDA-MB dose respond curves and MDIS (minimalistic drug interaction screening). In this file all data concerning the combination experiments, the dose respond curves of the three cell lines and the MDIS can be found.

Abbreviations

CSP: Conjectured Synergistical Potency; CI: combination index; DCA: Dichloroacetat; GMSAT: Genome and Metabolism Stabilizing Antitumor Therapy; HIF-1α: hypoxia inducible factor α; MDIS: Minimal Drug Interaction Screening; PI3K: phosphatidylinositol 3-kinase; w/v: weight per volume; v/v: volume per volume

Acknowledgements

We gratefully acknowledge the support of Sarra Amroune for editing the English version and for critical discussions of this manuscript. We acknowledge support from the German Research Foundation (DFG) and the Open Access Publication Fund of Charité – Universitätsmedizin Berlin. Thanks for the support throughout the project to Dr. Jutta Hinke-Ruhnau, Dr. Karsten Parczyk and Lilith Marie Bechinger.

Authors' contributions

Conceptualization of the project was done by JP, JR and AK. Experiments were performed by JP and JR. AK was responsible for project administration and supervision. Writing and editing was done by JP, JR, AK, BE and KD. All authors read and approved the manuscript.

Funding

Jonas Parczyk received a 6-month scholarship by the Berlin Institute of Health during his doctoral thesis.

Availability of data and materials

All data generated or analysed during this study are included in this published article and its supplementary information file (Additional file 1).

Ethics approval and consent to participate

None of our cell lines required ethics approval.

Consent for publication

Not applicable.

Competing interests

The authors declare that they have no competing interests.

Received: 9 December 2019 Accepted: 11 June 2020
Published online: 02 July 2020

References

1. Society AC. American Cancer Society. Cancer Facts & Figures 2018 (p14-15, p26-27). Atlanta: American Cancer Society; 2018. Available from: https://www.cancer.org/content/dam/cancer-org/research/cancer-facts-and-statistics/annual-cancer-facts-and-figures/2018/cancer-facts-and-figures-2018.pdf.
2. Güth U, Magaton I, Jane D, Fisher R, Schötzau A, Vetter M. Primary and secondary distant metastatic breast cancer : two sides of the same coin. The Breast. 2014;23(1):26–32 Available from: https://doi.org/10.1016/j.breast.2013.10.007.
3. Nowell P. The clonal evolution of tumor cell populations. Science (80-). 1976;194(4260):23–8. [cited 2019 Aug 10] Available from: http://www.ncbi.nlm.nih.gov/pubmed/959840.
4. Research America. U.S. Investments in Medical and Health Research and Development. 2016 [cited 2019 Jul 22]. Available from: https://www.researchamerica.org/sites/default/files/2016US_Invest_R%26D_report.pdf.
5. Moses H, Matheson DHM, Cairns-Smith S, George BP, Palisch C, Dorsey ER. The Anatomy of Medical Research. JAMA. 2015 [cited 2019 Jul 22];313(2):174. Available from: http://www.ncbi.nlm.nih.gov/pubmed/25585329.
6. Swanton C, Nicke B, Marani M, Kelly G, Downward J. Initiation of high frequency multi-drug resistance following kinase targeting by siRNAs. Cell Cycle. 2007;6(16):2001–4.
7. Chisholm RH, Lorenzi T, Clairambault J. Cell population heterogeneity and evolution towards drug resistance in cancer: biological and mathematical assessment, theoretical treatment optimisation. Biochim Biophys Acta - Gen Subj. 2016;1860(11):2627–45 Available from: https://doi.org/10.1016/j.bbagen.2016.06.009.
8. Andor N, Maley CC, Ji HP. Genomic Instability in Cancer: Teetering on the Limit of Tolerance. Cancer Res. 2017;77(9):2179–85. [cited 2019 Aug 15] Available from: http://www.ncbi.nlm.nih.gov/pubmed/28432052.

9. Vander Heiden MG, DeBerardinis RJ. Understanding the Intersections between Metabolism and Cancer Biology. Cell. 2017;168(4):657–69. [cited 2019 Aug 15] Available from: http://www.ncbi.nlm.nih.gov/pubmed/28187287.
10. Roy D, Sheng GY, Herve S, Carvalho E, Mahanty A, Yuan S, et al. Interplay between cancer cell cycle and metabolism: Challenges, targets and therapeutic opportunities. Biomed Pharmacother. 2017;89:288–96. [cited 2019 Aug 15] Available from: https://www.sciencedirect.com/science/article/abs/pii/S0753332216320923?via%3Dihub.
11. Evan GI, Vousden KH. Proliferation, cell cycle and apoptosis in cancer. Nature. 2001;411(6835):342–8. [cited 2019 Aug 15] Available from: http://www.nature.com/articles/35077213.
12. Moore RD, Chaisson RE. Natural history of HIV infection in the era of combination antiretroviral therapy. 1999;(June).
13. Roberts J, Bebenek K, Kunkel T. The accuracy of reverse transcriptase from HIV-1. Science (80-). 1988;242(4882):1171–3. [cited 2019 Jul 23] Available from: http://www.ncbi.nlm.nih.gov/pubmed/2460925.
14. Memarnejadian A, Nikpoor AR, Davoodian N, Kargar A, Mirzadeh Y, Gouklani H. HIV-1 Drug Resistance Mutations among Antiretroviral Drug-Experienced Patients in the South of Iran. Intervirology. 2019;1–8. [cited 2019 Jul 23] Available from: http://www.ncbi.nlm.nih.gov/pubmed/31311021.
15. Kast RE, Karpel-Massler G, Halatsch M-E. CUSP9* treatment protocol for recurrent glioblastoma: aprepitant, artesunate, auranofin, captopril, celecoxib, disulfiram, itraconazole, ritonavir, sertraline augmenting continuous low dose temozolomide. Oncotarget. 2014;5(18):8052–82.
16. Skaga E, Skaga IØ, Grieg Z, Sandberg CJ, Langmoen IA, Vik-Mo EO. The efficacy of a coordinated pharmacological blockade in glioblastoma stem cells with nine repurposed drugs using the CUSP9 strategy. J Cancer Res Clin Oncol. 2019;145(6):1495–507. [cited 2019 Aug 23] Available from: http://www.ncbi.nlm.nih.gov/pubmed/31028540.
17. Halatsch M, Kast RE, Dwucet A, Hlavac M, Heiland T, Westhoff M, et al. Bcl-2/Bcl-xL inhibition predominantly synergistically enhances the anti-neoplastic activity of a low-dose CUSP9 repurposed drug regime against glioblastoma. Br J Pharmacol. 2019;bph.14773. [cited 2019 Aug 23] Available from: http://www.ncbi.nlm.nih.gov/pubmed/31222722.
18. Al-Lazikani B, Banerji U, Workman P. Combinatorial drug therapy for cancer in the post-genomic era. Nat Biotechnol. 2012;30(7):679–92 Available from: http://www.ncbi.nlm.nih.gov/pubmed/22781697%5Cnhttp://www.pubmedcentral.nih.gov/articlerender.fcgi?artid=4320499&tool=pmcentrez&rendertype=abstract.
19. Lane DP. p53, guardian of the genome. Nature. 1992;358(6381):15–6. [cited 2019 Aug 2] Available from: http://www.nature.com/articles/358015a0.
20. Bykov VJN, Issaeva N, Shilov A, Hultcrantz M, Pugacheva E, Chumakov P, et al. Restoration of the tumor suppressor function to mutant p53 by a low-molecular-weight compound. Nat Med. 2002;8(3):282–8. [cited 2019 Jul 23] Available from: http://www.ncbi.nlm.nih.gov/pubmed/11875500.
21. Vassilev LT, Vu BT, Graves B, Carvajal D, Podlaski F, Filipovic Z, et al. In vivo activation of the p53 pathway by small-molecule antagonists of MDM2. Science. 2004;303(5659):844–8. Available from: http://www.ncbi.nlm.nih.gov/pubmed/14704432.
22. Lemos A, Leão M, Soares J, Palmeira A, Pinto M, Saraiva L, et al. Medicinal Chemistry Strategies to Disrupt the p53-MDM2/MDMX Interaction. Med Res Rev. 2016;36(5):789–844. [cited 2018 Oct 14] Available from: http://www.ncbi.nlm.nih.gov/pubmed/27302609.
23. Chen Z, Lu W, Garcia-Prieto C, Huang P. The Warburg effect and its cancer therapeutic implications. J Bioenerg Biomembr. 2007;39(3):267–74. [cited 2019 Jul 23] Available from: http://link.springer.com/10.1007/s10863-007-9086-x.
24. Wheaton WW, Weinberg SE, Hamanaka RB, Soberanes S, Sullivan LB, Anso E, et al. Metformin inhibits mitochondrial complex I of cancer cells to reduce tumorigenesis; 2014. p. 1–18.
25. Cluntun AA, Lukey MJ, Cerione RA, Locasale JW. Glutamine Metabolism in Cancer: Understanding the Heterogeneity. Trends in cancer. 2017 [cited 2019 Sep 11];3(3):169–80. Available from: http://www.ncbi.nlm.nih.gov/pubmed/28393116.
26. Gross MI, Demo SD, Dennison JB, Chen L, Chernov-Rogan T, Goyal B, et al. Antitumor Activity of the Glutaminase Inhibitor CB-839 in Triple-Negative Breast Cancer. Mol Cancer Ther. 2014;13(4):890–901. [cited 2018 Oct 15] Available from: http://www.ncbi.nlm.nih.gov/pubmed/24523301.
27. Nakahara T, Takeuchi M, Kinoyama I, Minematsu T, Shirasuna K, Matsuhisa A, et al. YM155, a Novel Small-Molecule Survivin Suppressant , Induces Regression of Established Human Hormone-Refractory Prostate Tumor Xenografts 2007;(17):8014–8021.
28. Vadas O, Burke JE, Zhang X, Berndt A, Williams RL. Structural Basis for Activation and Inhibition of Class I Phosphoinositide 3-Kinases. Sci Signal. 2011;4(195):re2–re2. [cited 2019 Jul 24] Available from: https://stke.sciencemag.org/content/4/195/re2.long.
29. Fischer A, Müller D, Zimmermann-Kordmann M, Kleuser B, Mickeleit M, Laabs S, et al. The ether lipid inositol-C2-PAF is a potent inhibitor of cell proliferation in HaCaT cells. ChemBioChem. 2006;7(3):441–9.
30. Pelz C, Häckel S, Semini G, et al. Inositol-C2-PAF acts as a biological response modifier and antagonizes cancer-relevant processes in mammary carcinoma cells. Cell Oncol (Dordr). 2018;41(5):505–16. Available from: https://pubmed.ncbi.nlm.nih.gov/30047091/.
31. Hung J-Y, Hsu Y-L, Li C-T, Ko Y-C, Ni W-C, Huang M-S, et al. 6-Shogaol, an Active Constituent of Dietary Ginger, Induces Autophagy by Inhibiting the AKT/mTOR Pathway in Human Non-Small Cell Lung Cancer A549 Cells. J Agric Food Chem. 2009 28;57(20):9809–16. [cited 2019 Jul 24] Available from: https://pubs.acs.org/doi/10.1021/jf902315e.
32. Yin Z, Deng Z, Zhao W, Cao Z. Searching synergistic dose combinations for anticancer drugs. Front Pharmacol. 2018;9(MAY):1–7.
33. Sheng Z, Sun Y, Yin Z, Tang K, Cao Z. Advances in computational approaches in identifying synergistic drug combinations. Brief Bioinform. 2017;19(6):1172–82. [cited 2019 Jul 26] Available from: http://www.ncbi.nlm.nih.gov/pubmed/28475767.
34. Borisy AA, Elliott PJ, Hurst NW, Lee MS, Lehar J, Price ER, et al. Systematic discovery of multicomponent therapeutics. Proc Natl Acad Sci U S A. 2003;100(13):7977–82. [cited 2019 Jul 29] Available from: http://www.ncbi.nlm.nih.gov/pubmed/12799470.
35. Mayer LD, Janoff AS. Optimizing Combination Chemotherapy by Controlling Drug Ratios. Mol Interv. 2007;7(4):216–23. [cited 2019 Jul 29] Available from: http://www.ncbi.nlm.nih.gov/pubmed/17827442.
36. Weiss A, Berndsen RH, Ding X, Ho C-M, Dyson PJ, van den Bergh H, et al. A streamlined search technology for identification of synergistic drug combinations. Sci Rep. 2015;5:14508. [cited 2019 Jul 26] Available from: http://www.ncbi.nlm.nih.gov/pubmed/26416286.
37. Nowak-Sliwinska P, Weiss A, Ding X, Dyson PJ, van den Bergh H, Griffioen AW, et al. Optimization of drug combinations using Feedback System Control. Nat Protoc. 2016;11(2):302–15. [cited 2019 Jul 29] Available from: http://www.ncbi.nlm.nih.gov/pubmed/26766116.
38. Weiss A, Ding X, van Beijnum JR, Wong I, Wong TJ, Berndsen RH, et al. Rapid optimization of drug combinations for the optimal angiostatic treatment of cancer. Angiogenesis. 2015;18(3):233–44. [cited 2019 Aug 21] Available from: http://www.ncbi.nlm.nih.gov/pubmed/25824484.
39. Li P, Huang C, Fu Y, Wang J, Wu Z, Ru J, et al. Large-scale exploration and analysis of drug combinations. Bioinformatics. 2015;31(12):2007–16.
40. Greco WR, Bravo G, Parsons JC. The Search for Synergy: A Critical Review from a Response Surface Perspective*. 1995 . [cited 2019 Jul 24] Available from: http://pharmrev.aspetjournals.org/content/pharmrev/47/2/331.full.pdf.
41. LOEWE S. The problem of synergism and antagonism of combined drugs. Arzneimittelforschung. 1953;3(6):285–90. [cited 2019 Aug 27] Available from: http://www.ncbi.nlm.nih.gov/pubmed/13081480.
42. Chou T-C. Theoretical basis, experimental design, and computerized simulation of synergism and antagonism in drug combination studies. Pharmacol Rev. 2006;58(3):621–81. [cited 2015 Sep 26] Available from: http://www.ncbi.nlm.nih.gov/pubmed/16968952.
43. Lines C, Krueger SA, Wilson GD. Cancer Cell culture. Methods. 2011;731:359–70 Available from: http://www.springerlink.com/index/10.1007/978-1-61779-080-5.
44. Martin N, Trials HIVC, Tumor X, Nude I, Basis T, Design E, et al. CompuSyn by Ting-Chao Chou. 2010;2005(D):3–4.
45. Zhao L, Wientjes MG, Au JL-S. Evaluation of combination chemotherapy: integration of nonlinear regression, curve shift, isobologram, and combination index analyses. Clin Cancer Res. 2004;10(23):7994–8004. [cited 2016 Apr 13] Available from: http://www.ncbi.nlm.nih.gov/pubmed/15585635.
46. Dai X, Cheng H, Bai Z, Li J. Breast cancer cell line classification and its relevance with breast tumor subtyping. J Cancer. 2017;8(16):3131–41.
47. Comşa Ş, Cîmpean AM, Raica M. The story of MCF-7 breast Cancer Cell line: 40 years of experience in research. Anticancer Res. 2015;35(6):3147–54. Available from: http://www.ncbi.nlm.nih.gov/pubmed/26026074.
48. Berglind H, Pawitan Y, Kato S. Analysis of p53 mutation status in human cancer cell lines. Cancer Biol … 2008;(April):701–10. Available from: http://www.landesbioscience.com/journals/cbt/14BerglindCBT7-5.pdf.
49. Chou TC, Talalay P. Quantitative analysis of dose-effect relationships: the combined effects of multiple drugs or enzyme inhibitors. Adv Enzyme

Regul. 1984;22:27–55. [cited 2016 mar 8] Available from: http://www.ncbi.nlm.nih.gov/pubmed/6382953.
50. Chou T-C. Preclinical versus clinical drug combination studies. Leuk Lymphoma. 2008;49(11):2059–80. [cited 2016 Apr 9] Available from: http://www.ncbi.nlm.nih.gov/pubmed/19021049.
51. Chou T. Preclinical versus clinical drug combination studies. 2016;8194(April).
52. Shimazu K, Tada Y, Morinaga T, Shingyoji M, Sekine I, Shimada H, et al. Metformin produces growth inhibitory effects in combination with nutlin-3a on malignant mesothelioma through a cross-talk between mTOR and p53 pathways. BMC Cancer. 2017;17(1):309. [cited 2018 Jun 9] Available from: http://bmccancer.biomedcentral.com/articles/10.1186/s12885-017-3300-y.
53. Koh MY, Spivak-Kroizman T, Venturini S, Welsh S, Williams RR, Kirkpatrick DL, et al. Molecular mechanisms for the activity of PX-478, an antitumor inhibitor of the hypoxia-inducible factor-1. Mol Cancer Ther. 2008;7(1):90–100. [cited 2018 Apr 13] Available from: http://www.ncbi.nlm.nih.gov/pubmed/18202012.
54. Lee YM, Lim JH, Chun YS, Moon HE, Lee MK, Huang LE, et al. Nutlin-3, an Hdm2 antagonist, inhibits tumor adaptation to hypoxia by stimulating the FIH-mediated inactivation of HIF-1α. Carcinogenesis. 2009;30(10):1768–75.
55. Li B, Zhu Y, Sun Q, Yu C, Chen L, Tian Y, et al. Reversal of the Warburg effect with DCA in PDGF-treated human PASMC is potentiated by pyruvate dehydrogenase kinase-1 inhibition mediated through blocking Akt/GSK-3β signalling. Int J Mol Med. 2018;42(3):1391–400. [cited 2019 Jul 23] Available from: http://www.ncbi.nlm.nih.gov/pubmed/29956736.
56. Allison SJ, Knight JRP, Granchi C, Rani R, Minutolo F, Milner J, et al. Identification of LDH-A as a therapeutic target for cancer cell killing via (i) p53/NAD(H)-dependent and (ii) p53-independent pathways. Oncogenesis. 2014;3(5):e102 Available from: http://www.pubmedcentral.nih.gov/articlerender.fcgi?artid=4035693&tool=pmcentrez&rendertype=abstract.
57. Li B, Li X, Ni Z, Zhang Y, Zeng Y, Yan X, et al. Dichloroacetate and metformin synergistically suppress the growth of ovarian cancer cells. Oncotarget. 2016;7(37):1–13 Available from: http://www.ncbi.nlm.nih.gov/pubmed/27449090.
58. Chou T. Preclinical versus clinical drug combination studies. Leuk Lymphoma. 2008;49(11):2059–80. [cited 2016 Apr 9] Available from: http://www.ncbi.nlm.nih.gov/pubmed/19021049.
59. Zimmermann GR, Lehár J, Keith CT. Multi-target therapeutics: when the whole is greater than the sum of the parts. Drug Discov Today. 2007;12(1–2):34–42.
60. Garon EB, Christofk HR, Hosmer W, Britten CD, Bahng A, Crabtree MJ, et al. Dichloroacetate should be considered with platinum - based chemotherapy in hypoxic tumors rather than as a single agent in advanced non - small cell lung cancer; 2014. p. 443-52 .
61. Tibes R, R, Falchook GS, Von Hoff DD, Weiss GJ, Iyengar T, Kurzrock R, et al. Results from a phase I, dose-escalation study of PX-478, an orally available inhibitor of HIF-1α. J Clin Oncol. 2010 20;28(15_suppl):3076–3076. [cited 2019 Jul 22] Available from: http://ascopubs.org/doi/10.1200/jco.2010.28.15_suppl.3076.
62. Secchiero P, Barbarotto E, Tiribelli M, Zerbinati C, Di Iasio MG, Gonelli A, et al. Functional integrity of the p53-mediated apoptotic pathway induced by the nongenotoxic agent nutlin-3 in B-cell chronic lymphocytic leukemia (B-CLL). Blood. 2006;107(10):4122–9.
63. Calvaresi EC, Granchi C, Tuccinardi T, et al. Dual targeting of the Warburg effect with a glucose-conjugated lactate dehydrogenase inhibitor. Chembiochem. 2013;14(17):2263–7. Available from: https://pubmed.ncbi.nlm.nih.gov/24174263/.

Publisher's Note

8.3 Publikation 3

Dichloroacetate and PX-478 Exhibit Strong Synergistic Effects in a Various Number of Cancer Cell Lines.

Jonas Parczyk*, Jérôme Ruhnau*, Carsten Pelz, Max Schilling, Hao Wu, Nicole Nadine Piaskowski, Britta Eickholt, Hartmut Kühn, Kerstin Danker, Andreas Klein
*geteilte Erstautorenschaft

BMC Cancer. 2021
doi: 10.21203/rs.3.rs-88933/v1
Impact factor: 3.15 (2-year Impact Factor) 3.432 (5-year Impact Factor)

Parczyk et al. BMC Cancer (2021) 21:481
https://doi.org/10.1186/s12885-021-08186-9

BMC Cancer

RESEARCH ARTICLE Open Access

Dichloroacetate and PX-478 exhibit strong synergistic effects in a various number of cancer cell lines

Jonas Parczyk*†, Jérôme Ruhnau*†, Carsten Pelz, Max Schilling, Hao Wu, Nicole Nadine Piaskowski, Britta Eickholt, Hartmut Kühn, Kerstin Danker and Andreas Klein

Abstract

Background: One key approach for anticancer therapy is drug combination. Drug combinations can help reduce doses and thereby decrease side effects. Furthermore, the likelihood of drug resistance is reduced. Distinct alterations in tumor metabolism have been described in past decades, but metabolism has yet to be targeted in clinical cancer therapy. Recently, we found evidence for synergism between dichloroacetate (DCA), a pyruvate dehydrogenase kinase inhibitor, and the HIF-1α inhibitor PX-478. In this study, we aimed to analyse this synergism in cell lines of different cancer types and to identify the underlying biochemical mechanisms.

Methods: The dose-dependent antiproliferative effects of the single drugs and their combination were assessed using SRB assays. FACS, Western blot and HPLC analyses were performed to investigate changes in reactive oxygen species levels, apoptosis and the cell cycle. Additionally, real-time metabolic analyses (Seahorse) were performed with DCA-treated MCF-7 cells.

Results: The combination of DCA and PX-478 produced synergistic effects in all eight cancer cell lines tested, including colorectal, lung, breast, cervical, liver and brain cancer. Reactive oxygen species generation and apoptosis played important roles in this synergism. Furthermore, cell proliferation was inhibited by the combination treatment.

Conclusions: Here, we found that these tumor metabolism-targeting compounds exhibited a potent synergism across all tested cancer cell lines. Thus, we highly recommend the combination of these two compounds for progression to in vivo translational and clinical trials.

Keywords: PX-478, HIF-1α inhibition, Dichloroacetate, Synergism, Cancer therapy, Drug combination, Cancer cell lines, Metabolism

* Correspondence: jonasparczyk@outlook.com; jerome.ruhnau@gmail.com
† Jonas Parczyk and Jérôme Ruhnau contributed equally to this work.
Charité – Universitätsmedizin Berlin, Corporate Member of Freie Universität Berlin, Humboldt-Universität zu Berlin, and Berlin Institute of Health, Charitéplatz 1, 10117 Berlin, Germany

Introduction

In the last decade, combinatorial approaches for cancer therapy have become increasingly popular [1]. Drugs designed to act against individual molecular targets can hardly combat a multigenic disease such as cancer [2]. However, synergistic drug combinations can lead to reduced drug doses with less pronounced side effects, increased response rates and attenuated likelihoods of drug resistance [1–3].

In a previous work [4], we screened 14 selected compounds, including dichloroacetate (DCA) and PX-478, for synergistic interactions in cancer cell lines. The combination of DCA and PX-478 displayed significantly stronger effects on cell viability than either single compound. Therefore, we aimed to further investigate this combination using a widely accepted method of quantifying synergism over the whole dose-response curve introduced by Chou and Talalay [5].

Compounds

DCA, a chlorinated carboxylic acid that was originally administered in the treatment of hereditary lactate acidosis [6], is an inhibitor of pyruvate dehydrogenase kinase (PDK). Thus, it leads to increased pyruvate dehydrogenase activity and therefore to an increase in pyruvate decarboxylation to acetyl-CoA, partially reversing the Warburg effect [7]. The Warburg effect describes alterations in tumor metabolism that lead to enhanced aerobic glycolysis and a reduction in oxidative phosphorylation. These alterations, while being less energy efficient, provide the necessary building blocks the tumor needs for proliferation [8, 9]. Furthermore, the reduction in cell respiration results in suppression of the mitochondrial-K^+ channel axis and thus hyperpolarisation of the mitochondrial membrane. Consequently, the release of cytochrome c and AIF is impaired, leading to apoptosis resistance [10]. DCA was found to normalise this axis and thereby induce the apoptosis of cancer cells [11, 12]. In addition to its effects on the mitochondrial membrane potential, DCA is believed to lead to a significant increase in reactive oxygen species (ROS) generation, which plays an important role in the induction of apoptosis [13–17]. In contrast, other authors reported that DCA may function as a sensitiser for ROS-induced alterations but did not significantly increase ROS production per se [16, 18]. In addition, DCA has been shown to positively regulate p53 as well as to downregulate autophagy, thereby leading to enhanced tumor cell apoptosis and attenuated cell proliferation [19, 20].

PX-478 is a small molecule that interferes with the transcription and translation of hypoxia-inducible factor-1α (HIF-1α) and leads to diminished deubiquitination of HIF-1α [21]. HIF-1α is physiologically activated by hypoxia and mediates multiple cellular alterations via transactivation of various target genes, such as GLUT1, LDHA and VEGF, and hence increases aerobic glycolysis in order for the cell to sustain hypoxic conditions [22]. Hence, PX-478-mediated inhibition of HIF-1α was found to induce apoptosis and cell cycle arrest in cancer cells [23, 24]. In oesophageal squamous cell cancer, PX-478 induces apoptosis, reduces cell proliferation and inhibits epithelial-mesenchymal transition [25]. Welsh et al. identified that the antitumor effect of PX-478 is positively correlated with HIF-1α levels in human xenografts [26]. In a study by Lang et al., PX-478 acted synergistically with an ROS inducer, ATO, leading to more efficient ROS-induced apoptosis via blocking ROS clearance by the HIF-1/FOXO1/SESN3 pathway [24].

HIF-1α-mediated inhibition of mitochondrial ROS production (as a reaction to ROS accumulation, hypoxia and cytokine stimulation) is achieved partially through a decrease in the production of acetyl-CoA via upregulation of PDK-1 and -3, the direct targets of DCA [27, 28]. Additionally, DCA-mediated inhibition of PDK leads to HIF-1α inhibition and, thereby supresses angiogenesis [14].

Apart from preliminary results indicating a likely synergism [4], the anticipated interplay of DCA and PX-478 regarding ROS generation, apoptosis and proliferation makes this combination especially interesting for further investigations.

In this study, we examined the effects of the combination of DCA and PX-478 on eight cancer cell lines and the non-cancerous cell line HEK-293. In addition, we studied the impact of the combination on ROS generation, apoptosis induction and cell cycle arrest.

Methods

Cell culture

The breast cancer cell lines MCF-7 and MDA MB-231 were a kind gift from Göran Landberg (Sahlgrenska Cancer Center, University of Gothenburg, Gothenburg, Sweden). The colon cancer cell line HT-29, the hepatocellular cancer cell line HEPG2, the cervical cancer cell line HeLa and the adenocarcinoma lung cancer cell lines A549 and H441, as well as the non-cancerous cell line HEK-293, were purchased from the American Type Culture Collection (ATCC). The glioblastoma cell line U251 was a kind gift from Kai Murk (Charité Berlin, Germany). A549, HEK-293, HeLa, HEPG2, HT-29, MCF-7 and U251 cells were cultured in DMEM, and H441 and MDA-MB-231 cells were cultured in DMEM/F12. All media contained penicillin/streptomycin (100 U ml^{-1}), L-glutamine (DMEM: 584 mg l^{-1}, DMEM/F12: 365.1 mg l^{-1}) and 10% heat-inactivated foetal calf serum (PAN Biotech, Germany). The humidified incubator was set at 37 °C with 5% CO_2. Cells were harvested using 0.05% trypsin/0.02% ethylenediaminetetraacetic acid (EDTA) in PBS.

Compounds

PX-478 (Hölzel Diagnostika Handels GmbH, Cologne, Germany) and DCA (Sigma-Aldrich, Munich, Germany) were dissolved in distilled water.

Cell viability and cell proliferation assays

A total of 0.75×10^4 A549, 1×10^4 HEK-293, 0.3×10^4 HeLa, 0.6×10^4 HEPG2, 1.5×10^4 HT-29, 0.5×10^4 MCF-7, 1.5×10^4 MDA-MB-231, 1×10^4 H441 and 0.3×10^4 U251 cells per well were seeded in flat bottom 96-well plates. After 24 h, when the cells were approximately 50% confluent, DCA, PX-478 or the combination was added. After 48 h of further incubation, a sulforhodamine B (SRB) assay was performed. For the SRB assay, cells were fixed with 10% trichloroacetic acid (w/v) and stained with 0.06% SRB in 1% acetic acid for 30 min. Cells were then repeatedly washed with 1% acetic acid (v/v) and dissolved in 10 mM Tris (pH 10.5). The protein mass was measured by determining the optical density at a wavelength of 492 nm in a microplate reader. Additionally, in HT-29 cell MTT assays were performed according to the manufacture's instructions (data are shown in additional file 1). All experiments were performed independently three times with at least 2 technical triplicates (mostly with 3).

Dose-response curves were generated using GraphPad Prism 7.05 statistical analysis software. The half-maximal effective concentration (EC_{50}) of each compound was determined via nonlinear regression.

Confirmation of synergism

Synergism was evaluated with four to seven different concentrations (mostly with 6), as suggested by Chou and Talalay [5].

Cells were treated with the combination of DCA and PX-478 at a constant EC_{50}:EC_{50} ratio as well as with the single compounds alone. Significant differences between each single compound and the combination were assessed by an unpaired t-test. Only concentrations with *p*-values of ≤0.05 for both single compounds compared to the combination were considered to exhibit significant differences and are marked with an asterisk (*) in the figures.

Combination indices (CIs) were calculated using CompuSyn software [29]. The CI is a quantitative value indicating the synergism of a drug combination at specific concentrations. A value of less than 0.9 indicates synergism (the lower the CI, the stronger the synergism). Values from 0.9 to 1 indicate a nearly additive effect, and a CI value of greater than 1.1 indicates antagonism [30]. CI values were calculated as follows:

$$CI = \frac{(D)_1}{(Dx)_1} + \frac{(D)_2}{(Dx)_2}$$

In the numerators, $(D)_1$ and $(D)_2$ are the concentrations of drug 1 and drug 2, respectively, in the drug combination that have a certain effect on cell viability (x %). In the denominators, $(Dx)_1$ and $(Dx)_2$ are the concentrations of each drug alone (drug 1 or drug 2, respectively) that are necessary to obtain the same effect (x %) as the drug combination (both drug 1 and drug 2). The concentrations $(Dx)_1$ and $(Dx)_2$ were calculated by CompuSyn with reference to the cell viability data for the respective compounds. To enhance analytical robustness, most concentrations of the compounds were doubled. Therefore, potential calculation errors were minimised, as suggested by Zhao et al. [31]. To generate the median-effect plots, the following equation was used:

$$D_x = D_m \left[\frac{fa}{1-fa}\right]^{1/m}$$

where Dm is the median effective dose, m is the slope of the median-effect curve, and fa is the fraction affected. Since calculation of a CI value is appropriate only when neither single compound has an effect close to 100%, the respective CI values are not shown in the Results section [31]. All data collected in this study can be found in additional file 1 (additional file 1).

Membrane lipid oxidation rate

HT-29 cells were seeded in 10 cm diameter Petri dishes and treated with the EC_{50} dose of DCA, the EC_{50} dose of PX-478 or the combination after 24 h when the cells were approximately 80% confluent. After incubation for an additional 48 h, cells were harvested with trypsin, pelleted and resuspended in 500 µl of PBS. For lipid extraction, cells were homogenised in a mixture of methanol: chloroform:water (2:1:1 by volume) using a modified Bligh/Dyer method. The extracted lipid suspension was bubbled with argon to prevent artificial oxidation. Then, alkaline hydrolysis was carried out, and the resulting free fatty acids were analysed by reversed-phase HPLC (RP-HPLC). Arachidonic acid and its oxygenated derivative 10–/15-hydroxyeicosatetraenoic acid (HETE) were identified by their specific retention times and UV spectra and were quantified via integration [32].

Flow cytometric analysis

Samples were analysed with BD FACS Calibur and Cell Quest.

Detection of intracellular ROS

Intracellular ROS were detected via an oxidation-sensitive fluorescent probe (2′,7′-dichlorodihydrofluorescein diacetate [H2DCFDA], Bio-Techne GmbH, Germany). HeLa and MCF-7 cells were seeded in 6 cm diameter Petri dishes and treated after 24 h at a confluence of 50%. Cells were treated with the EC_{50} dose of DCA, PX-478 or the combination for 48 h. Then, cells were harvested and

washed twice with PBS. Next, the cells were incubated with 50 μM H2DCFDA at 37 °C for 20 min in the dark and were then placed on ice. Cells were washed 2 more times before being analysed by flow cytometry.

Evaluation of apoptosis by Annexin-V-FITC and propidium iodide staining

HeLa and MCF-7 cells were seeded in 6 cm diameter Petri dishes and incubated for 24 h to a confluence of approximately 60%. After 24 h, cells were treated with PX-478, DCA or the combination and harvested 48 h later. The following concentrations were used: HeLa cells—EC_{50} DCA and 0.5 x EC_{50} PX-478; MCF-7 cells—EC_{50} DCA and EC_{50} PX-478. Cells were washed twice with PBS, placed on ice immediately, transferred to binding buffer (10 mM Hepes, 140 mM NaCl, 2.5 mM $CaCl_2$; pH 7.4) and stained with Annexin-V-FITC (Hölzel Diagnostika Handels GmbH, Germany) in the dark according to the manufacturer's instructions. After 15 min, propidium iodide (50 μg/ml) was added, and the cells were analysed by flow cytometry.

Western blot analysis

For Western blotting, cells were seeded in 6 cm diameter Petri dishes, grown to approximately 80% confluence and treated with the noted compounds. 24 h later, the cells were washed with PBS and lysed with lysis buffer (50 mM β-glycerophosphate pH 7.6, 1.5 mM EGTA, 1.0 mM EDTA, 1% (v/v) Triton X-100, 0.2% (v/v) protease inhibitor cocktail, 0.4% (v/v) PMSF, 100 mM sodium vanadate, 500 mM NaF). The samples were separated under reducing conditions by 10% SDS-PAGE and transferred to nitrocellulose membranes (Thermo Fisher, Rockford, USA). The primary antibodies and the corresponding working concentrations are listed in Table 1. Proteins were detected using SuperSignal West Pico Chemiluminescent Substrate (Pierce, Thermo Fisher Scientific, Bonn, Germany). Signals were visualised using a VersaDoc™ 4000 MP and QuantityOne® 4.6.5 software (BioRad Laboratories, Munich, Germany) and quantified using ImageJ 1.52a software (National Institute of Health, USA; version 1.8.0_112).

Metabolic assays

MCF-7 cells were seeded in an XF 96-well culture microplate (Agilent, Santa Clara, USA) at 3×10^4 cells per well in 180 μl of prewarmed assay medium. After 24 h, a mitochondrial respiration assay or glycolytic rate assay was performed with a Seahorse XFe96 Analyzer (Agilent Technologies). For the mitochondrial respiration assay, the oxygen consumption rate (OCR) was measured using the mitochondrial stress test procedure in XF media (nonbuffered DMEM containing 10 mm glucose, 2 mm L-glutamine and 1 mm sodium pyruvate). The glycolytic rate was measured in accordance with the Agilent Seahorse XFp Glycolytic Stress Test Kit instructions. After four measurements of either the baseline OCR or baseline extracellular acidification rate (ECAR), DCA solution was injected into the appropriate wells to the desired working concentration. Before each measurement, the assay medium was gently mixed to restore normal oxygen tension and pH in the microenvironment surrounding the cells. Two hours after treatment with DCA (6 measurements), the actual mitochondrial respiration assay or glycolytic stress test was performed. When metabolic analysis was complete, the cells were immediately fixed, and an SRB assay was performed as described above for data normalisation. Graphs were produced using GraphPad Prism 7.05 statistical analysis software. Glycolytic capacity and maximal respiration (Fig. 5) were calculated as follows:

- maximal respiration (OCR) = (maximum rate measured after injection of carbonyl cyanide-4-(trifluoromethoxy)phenylhydrazone [FCCP]) − (non-mitochondrial respiration rate)
- non-mitochondrial respiration (OCR) = minimum rate measured after injection of rotenone & antimycin A)
- Glycolytic capacity (ECAR) = (maximum rate measured after injection of oligomycin) − (non-glycolytic acidification rate)
- non-glycolytic acidification (ECAR) = minimum rate measured after injection of 2-deoxy-D-glucose (2DG).

Statistical analysis

Statistical analysis was performed using unpaired T-tests in GraphPad Prism 7.05 statistical analysis software. Differences with a p-value of ≤0.05 were considered significant: significant differences compared to the control are marked with an asterisk (*), while significant differences

Table 1 List of antibodies

Antibody raised against	Purchased from	Source	Dilution
β-actin	Cell Signaling (Danvers, USA)	Mouse	1:4000
PARP/cleaved PARP (9542)	Cell Signaling (Danvers, USA)	Rabbit	1:1000
Retinoblastoma p795 (9301)	Cell Signaling (Danvers, USA)	Rabbit	1:1000
Cyclin D1 (DCS-6)	Thermo Scientific (Waltham, USA)	Mouse	1:200

between the combination and both the control and each single compound are marked with two asterisks (**). All experiments were performed with at least 2 technical and 3 biological replicates.

Results

The combination of DCA and PX-478 produces synergistic effects in eight cancer cell lines and shows only minimal effects on the non-cancerous cell line HEK-293

In this study, we evaluated the effects of DCA and PX-478 on eight cancer cell lines, including lung (A549 and H441), breast (MCF-7 and MDA-MB-231), cervical (HeLa), hepatocellular (HepG2), colon cancer (HT-29) and glioblastoma (U251) cell lines (Fig. 1). The EC_{50} values used for treatment in the combinatorial experiments were determined for all cell lines in preceding experiments and are henceforth referred to as the approximated half-maximal effective concentration (EC_{50}a) values [4] (see additional file 1). The actual EC_{50} values for the experiments conducted herein were calculated afterwards (see Table 2).

While the combination showed synergistic effects in six investigated tumor entities, the combination exhibited synergistic effects over the complete dose-response curve in A549 (lung adenocarcinoma) and HEPG2 (hepatocellular carcinoma) cells with CI values ranging from 0.61 to 0.87 and 0.56 to 0.79, respectively.

EC_{50} data and best CI values are listed in Table 2. As illustrated, the synergism between DCA and PX-478 was observed in all analysed cell lines, with the lowest CI value in MCF-7 at 0.125 x EC_{50} (CI = 0.4). To minimise extrapolation errors, we calculated CI values relying on experimental data and eliminated CI values for concentrations where the effect of either single compound was too close to 100%, as suggested by Zhao et al. [31]. Interestingly, the combination of DCA and PX-478 strongly

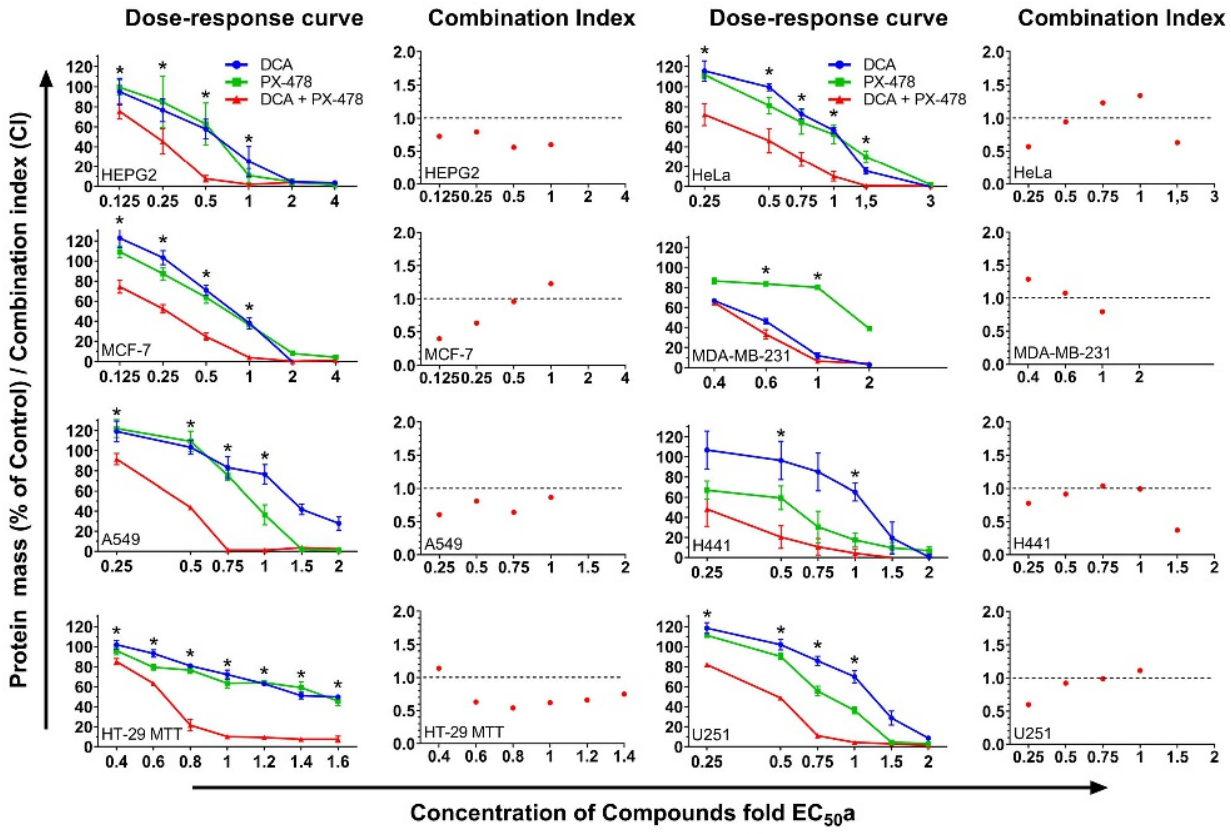

Fig. 1 Synergistic interactions between DCA and PX-478 in eight cancer cell lines. Figure 1 shows the dose-response curves for DCA, PX-478 and their combination in eight different cell lines as well as the respective CIs (shown to the right of each dose-response curve). Cells were seeded in 96-well plates and treated at a confluence of approximately 50%. Forty-eight hours later, an SRB (protein mass) assay was performed. If applicable, a CI was calculated with CompuSyn for each concentration. A CI of less than 0.9 indicates synergism, a CI between 0.9 and 1.1 indicates a nearly additive effect, and a CI of greater than 1.1 indicates antagonism. Approximated EC_{50} values were used (EC_{50}a) at a constant EC_{50}a:EC_{50}a ratio. Concentrations for which the effect of combination was significantly different from that of both single compounds and the control ($p \leq 0.05$, unpaired T-Test) are marked with an asterisk (*). Synergistic interactions were confirmed for all cancer cell lines, as indicated by the CI values and predominant left shifts of the curves. Without exception, the effects of the drug combination surpassed the effects of each single compound

Table 2 EC_{50} values for the single compounds and the combination

Cell line	EC_{50} DCA (mM)	EC_{50} PX-478 (μM)	EC_{50} Combination DCA (mM)/PX-478 (μM)	Best CI
A549 (lung)	41.9	30	14.2/15.8	0.61
H441 (lung)	38.6	23.5	8.3/11.9	0.78
HeLa (cervical)	21.2	13.4	8.9/5.8	0.57
HEPG2 (hepatocellular)	21.4	17.7	8.4/6.3	0.56
HT-29 (colon)	26.5	75.6	18.1/28.2	0,65
MCF-7 (breast)	31.5	11.2	10.2/4	0.4
MDA-MB-231 (breast)	26.1	276	23.4/79	0.8
U251 (glioblastoma)	25	30.5	9.5/16.8	0.6

affected cell viability or the protein mass in all cell lines, leading to a left shift in the dose-response curves. The combination treatment allowed the concentration of each single drug to be noticeably reduced (Table 2). For example, in MCF-7 cells, the EC_{50} values of DCA and PX-478 were reduced by 68 and 64%, respectively. Collectively considering all cell lines, the EC_{50} values of the compounds were profoundly reduced by an average of 60.7% when used in combination relative to when used as single agents.

Comparison of the EC_{50} values of PX-478 in HT-29 and MDA-MB-231 cells indicates that noticeably higher doses were needed in these cell lines than in the other cell lines, indicating resistance to PX-478. For MDA-MB-231 cells, the resistance to PX-478 resulted in the highest CI value compared to the other cell lines. Interestingly, the dose-response curve for DCA was close to that for the combination (Table 2 and Fig. 1). However, a stronger synergism was shown for HT-29 cells even though a higher dose of PX-478 was required (CI = 0.65).

The six cell lines that were sensitive to PX-478 were significantly more sensitive to the combination of DCA and PX-478 than the immortalised non-cancerous cell line HEK-293 at a comparable concentration (Fig. 2). For example, in MCF-7 cells, 10 mM DCA and 4 μM PX-478 led to a reduction of 48% in the protein mass, while 15 mM DCA and 15 μM PX-478 led to a reduction of only 3% in HEK-293 cells ($p = 0.000007$). Since we detected a PX-478 resistance in MDA MB-231 and HT-29 cells, we did not use concentrations of PX-478 in comparable dosages for the combination.

Table 2 lists the EC_{50} values for DCA, PX-478 and the combination of both in all tested cell lines. The EC_{50} values were calculated via curve fitting with the program GraphPad Prism. In the last column, the lowest CI value indicating synergism (CI < 0.9) is listed.

The combination of DCA and PX-478 increases ROS levels and leads to apoptosis and cell cycle arrest

The existing data for PX-478 and DCA suggest some theories concerning the mechanisms underlying their

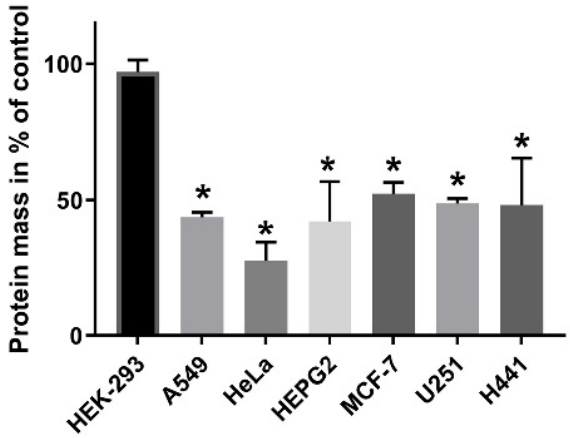

Fig. 2 The combination of DCA and PX-478 shows significantly lower effects on the non-cancerous cell line HEK-293 than on the six PX-478-sensitive cancer cell lines (A549, HeLa, HEPG2, MCF-7, U251 and H441). HEK-293 cells were seeded in 96-well plates and treated with 15 mM DCA and 15 μM PX-478 or the combination at a confluence of approximately 50%. Forty-eight hours later, an SRB assay was performed. The combination had no significant effect (97% protein mass) compared to the control ($p = 0.3$). The effect of the combination of 15 mM DCA and 15 μM PX-478 on HEK-293 cells was compared to the effect of similar or lower concentrations of the combination on the tested cancer cell lines (A549: 15 mM and 16.5 μM, HeLa: 15.5 mM and 10 μM, HEPG2: 10.5 mM and 8 μM, MCF-7: 10 mM and 4 μM, U251: 10 mM and 18.5 μM and H-441: 9 mM and 12.5 μM respectively). Data points used to generate the dose-response curves in Fig. 1 were used for comparison. The bars are marked with an asterisk when the effect on a cancer cell line was significantly stronger than that on HEK-293 cells. All six PX-478-sensitive cancer cell lines were significantly more sensitive than HEK-293 cells to the combination of DCA and PX-478. HT-29 and MDA-MB-231 cells were not compared, since due to the described resistance, no doses of PX-478 close to 15 μM were used. This figure is not applicable for comparing effects between the different cancer cell lines, since different concentrations of the compounds were used. For comparisons of synergism, please see Fig. 1 and Table 2

synergism. In the following experiments, the effects of this combination on increasing reactive oxygen species generation, arresting the cell cycle and inducing apoptosis were investigated.

The combination of DCA and PX-478 increases ROS levels in HT-29, MCF-7 and HeLa cell lines

To investigate the relevance of the combination to ROS production, we performed HPLC measurements with HT-29 cells to analyse the oxidation of arachidonic acid derivatives (Fig. 3a). DCA-treated cells showed a non-significant (21%, $p = 0.21$) increase in the 5- and 10-HETE levels compared to those in control cells. In cells treated with PX-478, the oxidation ratio was significantly increased by 58% compared to that in control cells ($p = 0.04$). The combination treatment led to a 109% increase in the oxidation ratio, which was significantly higher than that observed for the control treatment ($p = 0.02$) but did not differ significantly from that observed for PX-478 alone ($p = 0.22$).

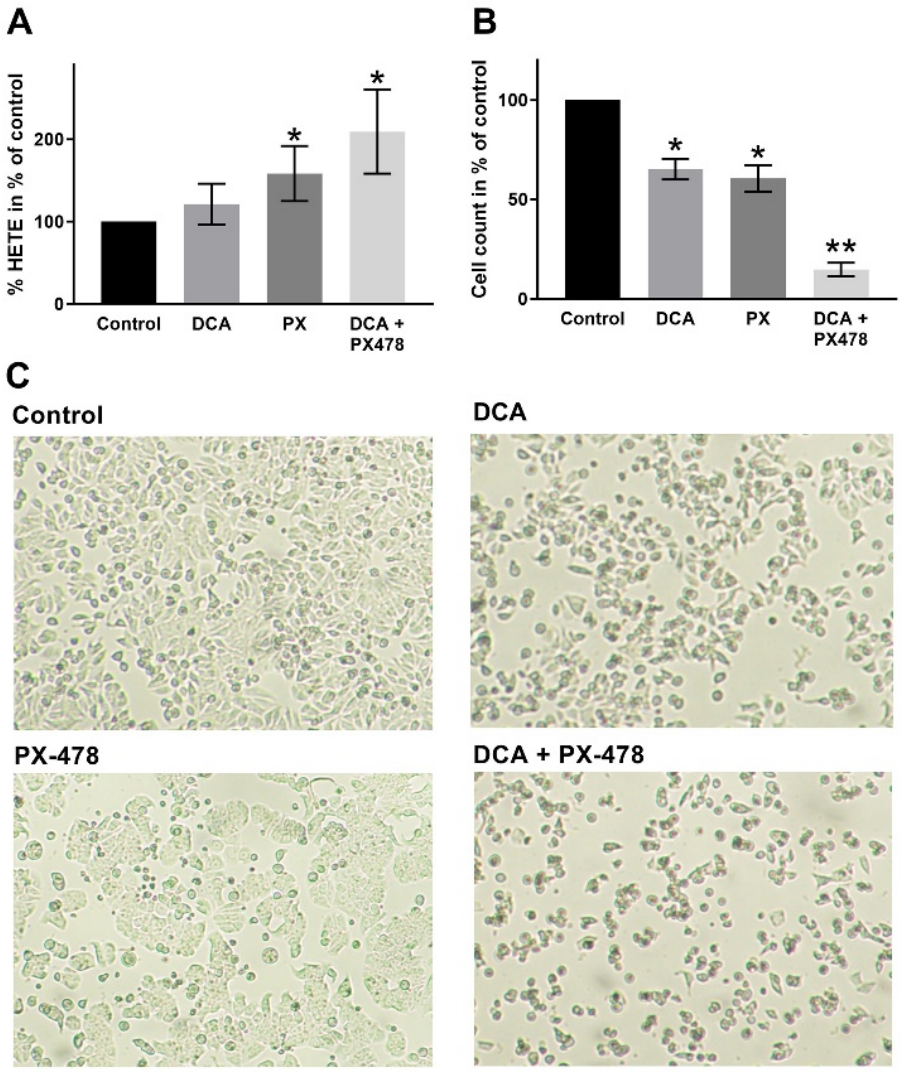

Fig. 3 The combination of DCA and PX-478 leads to increased ROS activity in HT-29 cells. Figure 3 shows HPLC analysis results and cell counts for HT-29 cells. **a**: HPLC results for the proportion of arachidonic acid to its oxygenated derivatives 10–/15-HETE for drug treatment compared to the control treatment are presented. Cells were treated with either the EC_{50} dose of DCA, the EC_{50} dose of PX-478 or the combination. Cells treated with PX-478 alone and with the combination of DCA and PX-478 showed a significant increase in the oxidation ratio compared to that in control cells, although the difference between the combination and PX-478 was noticeable but not significant. **b**: The cell count as a percentage of the control cell count is presented. Treatment with the single compounds DCA and PX-478 led to significant reductions of 65 and 61%, respectively. Only 15% of the control cells remained after the combination treatment. Significant differences from the control are marked with an asterisk (*), while significant differences from both the control and each single compound are marked with two asterisks (**). **c**: The profound effects of DCA, PX-478 and DCA + PX-478 on cell confluency are shown. All cells were imaged at 40× magnification with a Nikon D90

Furthermore, we evaluated the relevance of this combination to ROS via FACS analysis with H2DCFDA in HeLa, MCF-7 and HT-29 cells (Fig. 4). H2DCFDA reacts with ROS, and fluorescent dichlorofluorescein (DCF) can be measured in the FL1 channel. The results shown in Fig. 4b confirmed our HPLC results in HT-29 cells. FACS analysis showed that compared to the control treatment, DCA did not affect ROS activity in any cell line. ROS production was significantly increased in HeLa cells (2 to 12%, $p = 0.008$) but not in MCF-7 cells (3 to 4%, $p = 0.37$) or HT-29 cells (7 to 10%, $p = 0.089$) treated with PX-478 alone compared to control cells. Compared to the single compounds, the combination led to significant increases of 28% ($p = 0.021$), 16% ($p = 0.0002$) and 37% ($p = 0.014$) in HeLa, MCF-7 and HT-29 cells, respectively. Thus, as our results in HeLa, MCF-7 and HT-29 cells suggest, increased ROS is likely to play an important role in the synergism of DCA + PX-478 combination treatment.

The combination of DCA and PX-478 leads to apoptosis and a reduction in proliferation

Western blot analyses of PARP/cleaved PARP, Ser795-phosphorylated Retinoblastoma protein (pRB1) and Cyclin D1 were performed in HT-29 and MCF-7 cells (Fig. 5). In MCF-7 cells, two concentrations of DCA and PX-478 (EC_{50} and 0.5 x EC_{50}) and the respective combinations were analysed. In HT-29 cells (DCA EC_{50} and PX-478 0.5 x EC_{50}), the level of cleaved PARP was significantly higher in cells treated with the combination than in cells treated with the single compounds ($p = 0.002$). In MCF-7 cells, the combination led to the highest levels of cleaved PARP at both doses, with significant differences compared to control and DCA-treated cells but non-significant differences compared to PX-478-treated cells ($p = 0.086$ and $p = 0.087$). However, via FACS analysis with Annexin-V-FITC staining, we identified significantly increased levels of programmed cell death for the combination of DCA and PX-478 in MCF-7 cells compared to PX-478-treated cells (Fig. 6). While 12% of PX-478-treated cells were Annexin-V-FITC-positive, the percentage increased to 20% after combination treatment ($p = 0.004$). Thus, we concluded that apoptosis is a relevant factor for this synergism in HT-29 and MCF-7 cells.

For both cell lines, pRB1 levels were significantly lower in combination-treated cells than in single compound-treated cells and control cells (Fig. 5). Furthermore, we observed an interesting effect of the combination in

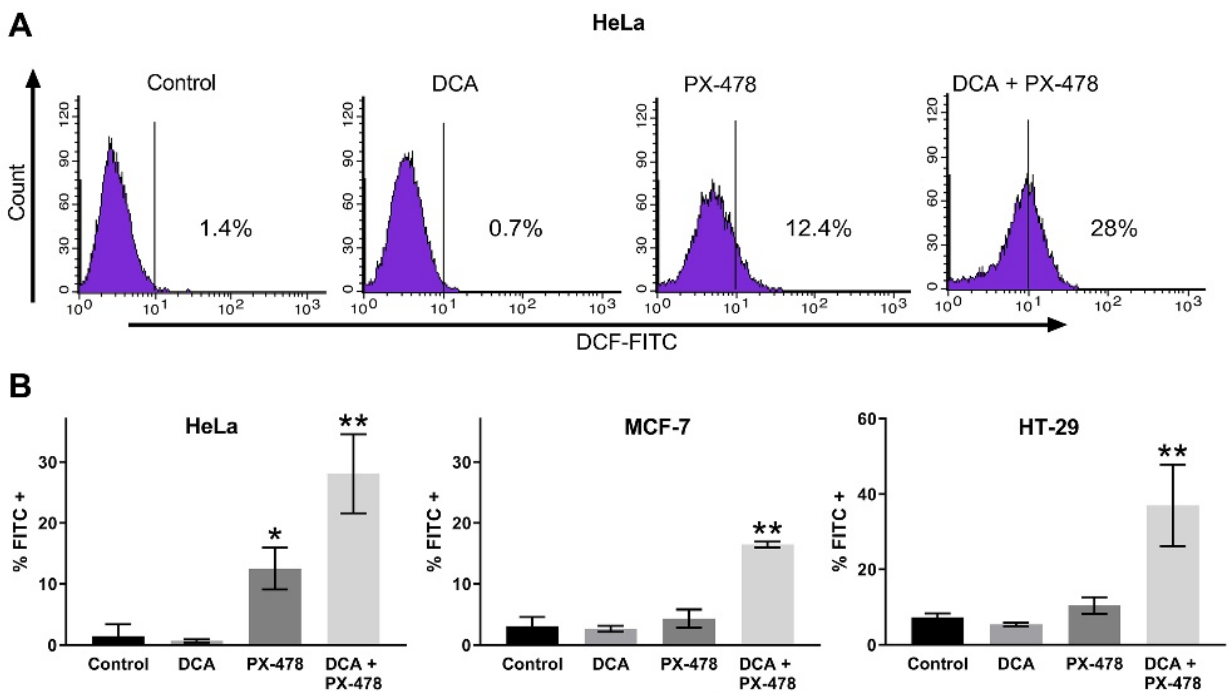

Fig. 4 The combination of DCA and PX-478 leads to increased ROS activity. Figure 3 shows the ROS activity assessed by flow cytometric analysis with H2DCFDA in HeLa, MCF-7 and HT-29 cells. Cells were incubated to a confluence of 50% and were then treated with either DCA, PX-478 or the combination for 48 h. The following concentrations of the compounds were used: HeLa—DCA and PX-478, EC_{50}; MCF-7 and HT-29—DCA, EC_{50} and PX-478, 0.5 x EC_{50}. Panel **a** shows representative histograms for the analysis of DCF-FITC in HeLa cells. Panel **b** shows the results in HeLa, MCF-7 and HT-29 cells as bar graphs. Three independent experiments were performed. Significant results compared to the control are marked with an asterisk (*). The combination of DCA and PX-478 led to the highest ROS activity in all cell lines, which was significantly increased compared to that in the corresponding control, DCA-treated and PX-478-treated cells (marked with two asterisks [**])

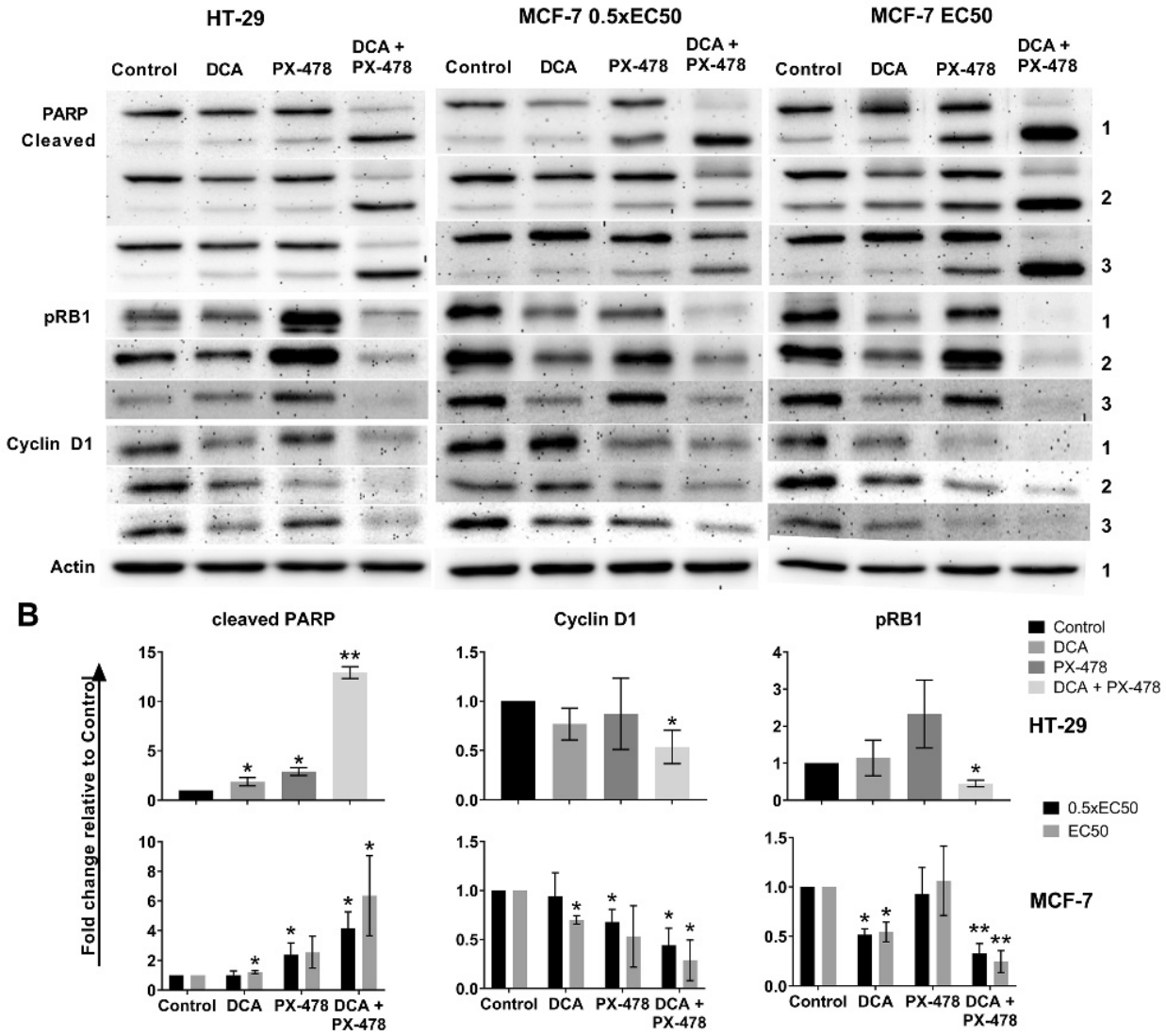

Fig. 5 The combination of DCA and PX-478 leads to increased levels of cleaved PARP and reduced levels of Cyclin D1 and pRB1 in HT-29 and MCF-7 cells. Cells were incubated to a confluence of approximately 80% and treated with DCA and PX-478 at the following concentrations: HT-29—DCA, EC_{50} and PX-478, 0.5 x EC_{50}; MCF-7—either DCA and PX-478, 0.5 x EC_{50} or EC_{50}. Twenty-four hours later, the cells were harvested, and Western blot analyses were performed. **a**: Three independent Western blots are shown for each antibody except for β-actin (only one representative blot is shown here). The blots presented here are cropped; please see additional file 2 for full-length blots. **b**: The results are presented as the fold change relative to the control. Significant differences are marked with an asterisk (*). The level of cleaved PARP was significantly increased in HT-29 cells treated with the combination ($p = 0.00002$) compared to HT-29 cells treated with the single compounds. For MCF-7 cells, a clear trend was visible for both concentrations ($p = 0.086$ or $p = 0.087$, respectively). Significant differences compared to the control are marked with an asterisk (*); significant differences between the combination of DCA and PX-478 and each single compound are marked with two asterisks (**). The combination of DCA and PX-478 significantly reduced cyclin D1 and pRB1 levels in both cell lines and at both concentrations in MCF-7 cells

MCF-7 cells: while PX-478 alone did not affect the level of pRB1 at 0.5 x EC_{50} and EC_{50}, DCA led to decreased levels of pRB1 (52 and 54%, respectively). For the combination, pRB1 levels were reduced to 33% compared to control at the lower concentration and 25% at the higher concentration ($p = 0.027$ and 0.046 compared to the single compounds, respectively). These data suggest that DCA alone has limited effects on pRB1 levels in MCF-7 cells while the combination affects RB1 phosphorylation more strongly.

Furthermore, we used Western blotting to evaluate the impact of the compounds on Cyclin D1 levels. In HT-29 and MCF-7 cells, the level of Cyclin D1 exhibited the greatest reduction for the combination treatment ($p = 0.009$ and $p = 0.005$, respectively, compared to control treatment). However, the differences with respect to

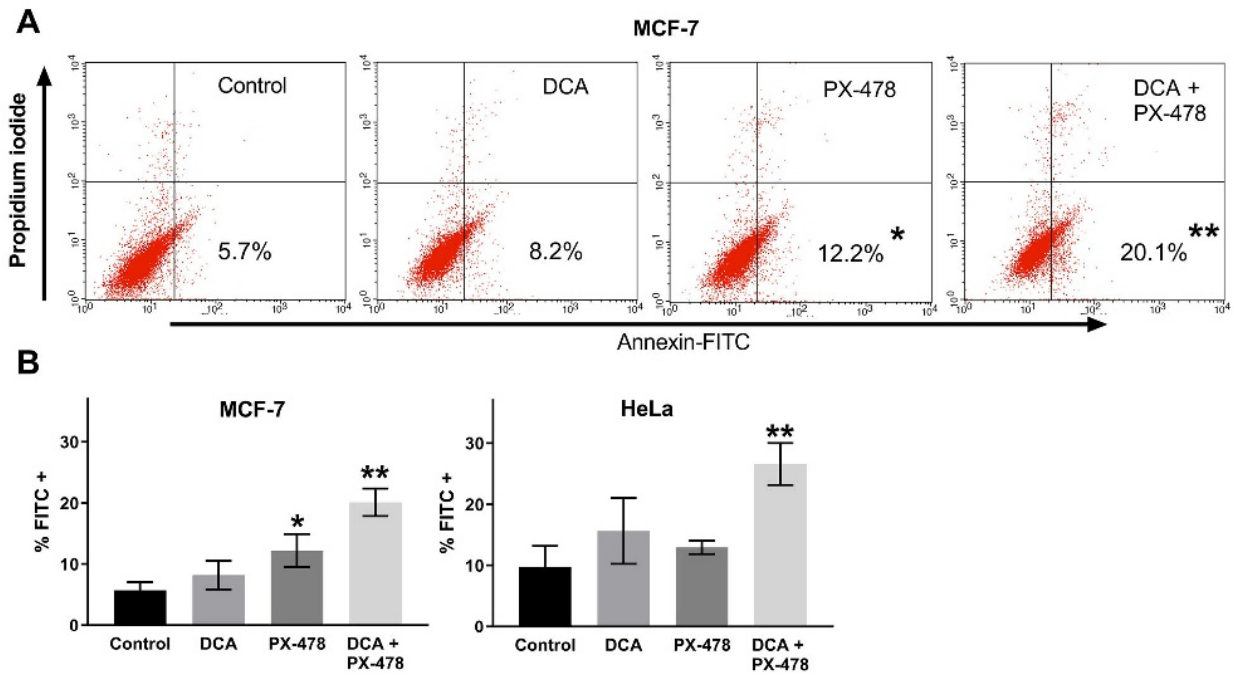

Fig. 6 DCA + PX-478 induced significantly higher levels of apoptosis than DCA or PX-478 alone in MCF-7 and HeLa cells. Figure 6 shows the results of flow cytometric analysis with Annexin-V-FITC and propidium iodide in MCF-7 and HeLa cells. At 60% confluence, MCF-7 cells were treated with either the EC_{50} dose of DCA or the EC_{50} dose of PX-478, while HeLa cells were treated with the EC_{50} dose of DCA and 0.5 times the EC_{50} dose of PX-478. Three independent experiments were performed. Panel **b** shows bar graphs indicating the percentages of Annexin-VF-ITC-positive MCF-7 and HeLa cells. Significant differences compared to the control are marked with an asterisk (*). Representative dot plots are shown for MCF-7 cells in panel **a**. The combination of DCA and PX-478 led to the greatest percentage of Annexin-V-FITC-positive cells, and the percentage was significantly different from that of control, DCA-treated and PX-478-treated cells for both cell lines (**) ($p = 0.004$ and 0.042 for MCF-7 cells and HeLa cells, respectively)

each single compound were non-significant (Fig. 5). Collectively, these data suggest that the combination of DCA and PX-478 synergistically reduces cell proliferation.

The effect of DCA was verified via real-time measurement of metabolism (seahorse XFe96)

To verify the effects of DCA on glycolysis, studies with the Seahorse XFe96 Analyzer were performed (Fig. 7). We measured real-time changes in the oxygen consumption rate (OCR) and the extracellular acidification rate (ECAR). Two hours after treatment with DCA, the protocols for the mitochondrial respiration assay and the glycolytic rate assay were performed. The results supported the hypothesis that DCA increases the influx of pyruvate into mitochondria, which led to a 42% increase in maximal respiration ($p = 0.004$). In addition, we observed a 73% reduction in glycolytic capacity when DCA was added ($p = 0.0001$).

Discussion

In this study, we demonstrate that DCA and PX-478 are a potent combination that exerts synergistic effects in all tested cancer cell lines and proved thereby to be effective in various tumor entities in vitro including colorectal, lung, breast, cervical, liver and brain cancer while having limited effects on the non-cancerous cell line HEK-293 (Figs. 1 and 2). We found the combination to induce cell cycle arrest and apoptosis as well as increasing the generation of ROS in a colorectal and a breast cancer cell line (HT-29 and MCF-7).

The EC_{50} of PX-478 ranged from 11.2 to 276 μM, indicating a drug resistance for MDA MB-231 cells (276 μM). Interestingly, this resistance does not inhibit synergism, with a CI value of 0.8. However, best CI values where lower in all other cell lines. Via its effect on HIF-1α, PX-478 has already shown synergistic potential with different compounds. In combination with arsenic trioxide (ATO), PX-478 increases ROS and, likely, ROS-induced apoptosis [24]. As our data suggest, this mechanism might also apply to the combination of DCA + PX-478. Interestingly, both DCA and PX-478 mediate antitumoral effects through inhibition of PDKs, which can partially explain the synergism observed here. While DCA suppresses PDK-1, HIF-1α increases PDK-1 expression [27, 28]. Thus, PX-478 reinforces the primary

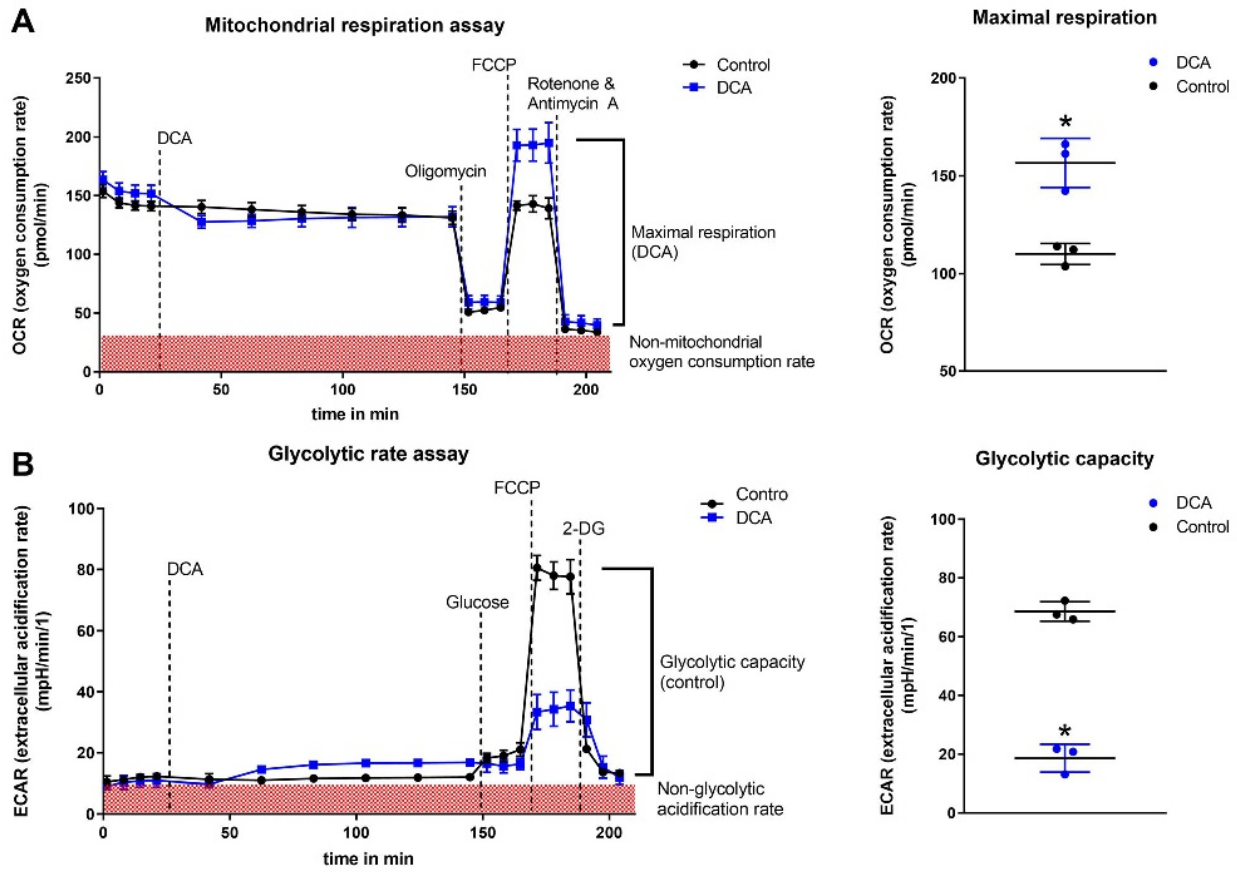

Fig. 7 Mitochondrial respiration assay and glycolytic stress test with DCA. Figure 7 shows the results of the mitochondrial respiration assay (**a**) and glycolytic stress test (**b**) of DCA-treated MCF-7 cells performed with a Seahorse XFe96 analyzer. Three independent experiments were performed with at least four technical replicates. After measurement of the baseline OCR and ECAR, the EC_{50} dose of DCA was injected. After six measurement cycles, oligomycin (inhibition of ATP synthase), FCCP (uncoupling agent) and rotenone & antimycin A (inhibition of respiratory chain) were added for the mitochondrial respiration assay (**a**), and glucose, oligomycin and 2-DG (inhibition of glycolysis) were added for the glycolytic rate assay (**b**). Three measurement cycles were performed after each chemical was added. **a:** As shown, DCA increased the maximal OCR and thereby the maximal respiration of MCF-7 cells. **b:** Furthermore, DCA reduced the maximal ECAR and thereby the glycolytic capacity. See the Methods section for the exact calculation procedures and definitions of glycolytic capacity, maximal respiration, non-mitochondrial OCR and non-glycolytic acidification rate. In MCF-7 cells, DCA increased the maximal respiration by 42% and decreased the glycolytic capacity by 73% ($p = 0.004$ and 0.0001, respectively)

effect of DCA indirectly, thereby synergistically increasing ROS production when combined with DCA, as our data suggest (Figs. 3 and 4). These results are in line with the findings of Lang et al. and support the hypothesis that PX-478, as a HIF-1α inhibitor, may be beneficial for different therapeutic approaches.

The EC_{50} of DCA ranged from 21.2 mM to 41.9 mM (Fig. 2). A heterogeneity of the DCA-mediated effects in different cancer cell lines can be seen when our real-time metabolic assay results are compared with those of Tataranni et al. and Lucido et al. [17, 33]. DCA strongly increased maximal respiration and decreased glycolytic capacity in MCF-7 cells (Fig. 7), while in pancreatic carcinoma as well as head and neck squamous cell cancer, both glycolytic capacity and maximal respiration were decreased. Consistent with our findings however, Ma et al. found increased maximal respiration in non-small cell lung cancer cells treated with DCA [34].

Hence, literature as well as our data suggest that DCA mediates heterogenic metabolic modulation depending on the metabolic status of a cancer cell. Interestingly, cells primarily undergoing oxidative phosphorylation as well as cells relying primarily on aerobic glycolysis can both be sensitive to DCA [35–39].

As DCA has attracted considerable attention in recent years, many examples of synergism have been detected. 5-Fluorouracil, a platinum-based chemotherapy, a SIRT2 inhibitor, metformin, omeprazole + tamoxifen, sorafenib, erlotinib and gefitinib have shown synergistic effects in combination with DCA in vivo and in vitro [15, 34, 40–48].

Clinical trials with DCA in cancer therapy, congenital lactic acidosis and pulmonary arterial hypertension have

been performed in recent decades and are ongoing [49–51]. Although DCA has not yet been implemented in clinical cancer treatment regimens, interest in DCA has not decreased. Authors of clinical trials with DCA suggest DCA in combination with chemotherapy in previously treated metastatic breast cancer and non-small cell lung cancer (ClinicalTrials.gov Identifier: NCT01029925) [45] and as an apoptosis sensitiser for recurrent solid tumors (ClinicalTrials.gov Identifier: NCT00566410) in less advanced disease stage [52].

Although a phase 1 clinical trial of PX-478 conducted in 2010 in patients with advanced solid tumors showed that PX-478 was well tolerated at low doses, with consistent HIF-1α inhibition and prolonged duration of stable disease [53], it seems to have been abandoned as an anticancer drug, as no further clinical trials with PX-478 have been registered. If PX-478 is used in combination with DCA, obstacles such as its dose-limiting toxicity could be eliminated. We believe that synergism is an important strategy for successfully including promising compounds such as DCA and/or PX-478 in cancer therapy. Our data indicates that the concentrations of DCA and PX-478 could be reduced by an average of approximately 60.7%. Considering the concentrations of DCA achieved in clinical studies and our EC_{50} values in the different cell lines tested, we conclude that combination of DCA and PX-478 can help attain the concentrations needed for a therapeutic effect.

Limitations

In this study, we focused on the effect of the specific compounds and their combination rather than identifying whether a certain effect can be directly linked to a specific mode of action of a single compound. These conclusions must be drawn considering the existing data for single compounds.

While DCA exerts an immediate effect via PDH activation (see the results of the real-time metabolic assays, Fig. 7), PX-478-mediated inhibition of the transcription factor HIF-1α consequently shows relatively delayed effects. HIF-1α, having a short half-life of eight to 20 min itself [54], regulates more than 100 proteins, exemplarily GLUT1 and VEGFA, with half-lifes of approximately 7–8 h [55, 56].

We performed Western blot analysis after 24 or 48 h of incubation to partially address this issue, but we did not consistently quantify the individual effects of DCA and PX-478 at the respective time points. Consequently, we did not analyse the dynamics of this combination.

Conclusion

In summary, we found synergistic effects of the combination DCA and PX-478 in all analysed cancer cell lines, including colorectal, lung, breast, cervical, liver and brain cancer. Induction of apoptosis, generation of ROS and inhibition of proliferation played important roles in this synergism. Considering the promising synergism between the two compounds presented here and the evidence generated by various research groups about the effects of DCA and PX-478, commencement of in vivo trials (e.g. xenografts) is recommended.

Abbreviations

CI: Combination index; DCA: Dichloroacetate; FACS: Fluorescence-activated cell sorting; HPLC: High performance liquid chromatography; HIF-1α: Hypoxia inducible factor α; ROS: Reactive oxygen species; w/v: Weight per volume; v/v: Volume per volume

Supplementary Information

The online version contains supplementary material available at https://doi.org/10.1186/s12885-021-08186-9.

Additional file 1. Includes data of: Combination experiments with DCA and PX-478, flow cytometric analysis, HPLC analysis, Western blot analysis and Seahorse analysis.

Additional file 2. Includes all Western Blots.

Acknowledgements

We acknowledge support from the German Research Foundation (DFG) and the Open Access Publication Fund of Charité – Universitätsmedizin Berlin. Thanks for the support throughout the project to Gudrun Mrawietz, Klaus-Dieter Irrgang, Kai Murk, Juliane Schiweck, Marjann Schäfer, Gustav Steinemann, Laura Michalick, Lothar Lucka, Kim Stolte, Marlon Tilgner and Michael Fähling. This work is dedicated to Ralf Redemund and Jutta Hinke-Ruhnau.

Authors' contributions

Conceptualisation of the project was done by JP, JR and AK. Experiments were performed by JP, JR, CP, MS, HW, NN, HK and AK. AK and JP were responsible for project administration and supervision. Writing and editing was done by JP, JR, AK, BE and KD. All authors read and approved the manuscript.

Funding

Jonas Parczyk received a stipend by the Berlin Institute of Health. Open Access funding enabled and organized by Projekt DEAL.

Availability of data and materials

All data generated or analysed during this study are included in this published article and its supplementary files (additional file 1 and additional file 2).

Declarations

Ethics approval and consent to participate

Not applicable.

Consent for publication

Not applicable.

Competing interests

The authors declare that they have no competing interests.

Received: 30 September 2020 Accepted: 14 April 2021
Published online: 30 April 2021

References

1. Schweim JK, Schweim HG. Status quo and future developments of combinations of medicinal products. Synergy 2014;1(1):70–75. Available from: http://dx.doi.org/https://doi.org/10.1016/j.synres.2014.07.007

2. Zimmermann GR, Lehár J, Keith CT. Multi-target therapeutics: when the whole is greater than the sum of the parts. Drug Discov Today. 2007;12(1–2):34–42. https://doi.org/10.1016/j.drudis.2006.11.008.
3. Al-Lazikani B, Banerji U, Workman P. Combinatorial drug therapy for cancer in the post-genomic era. Nat Biotechnol. 2012;30(7):679–92. Available from: http://www.ncbi.nlm.nih.gov/pubmed/22781697%5Cnhttp://www.pubmedcentral.nih.gov/articlerender.fcgi?artid=4320499&tool=pmcentrez&rendertype=abstract. https://doi.org/10.1038/nbt.2284.
4. Ruhnau J, Parczyk J, Danker K, Eickholt B, Klein A. Synergisms of genome and metabolism stabilizing antitumor therapy (GMSAT) in human breast and colon cancer cell lines: a novel approach to screen for synergism. BMC Cancer. 2020;20(1):617. Available from: /pmc/articles/PMC7331156/?report=abstract. [cited 2020 Sep 13].
5. Chou TC, Talalay P. Quantitative analysis of dose-effect relationships: the combined effects of multiple drugs or enzyme inhibitors. Adv Enzyme Regul. 1984;22:27–55 [cited 2016 mar 8] Available from: http://www.ncbi.nlm.nih.gov/pubmed/6382953.
6. Abdelmalak M, Lew A, Ramezani R, Shroads AL, Coats BS, Langaee T, et al. Long-term safety of dichloroacetate in congenital lactic acidosis. Mol Genet Metab. 2013;109(2):139–43 [cited 2016 Mar 22] Available from: http://www.pubmedcentral.nih.gov/articlerender.fcgi?artid=3751427&tool=pmcentrez&rendertype=abstract.
7. Stacpoole PW. The pharmacology of dichloroacetate. Metabolism. 1989;38:1124–44.
8. Chen Z, Lu W, Garcia-Prieto C, Huang P. The Warburg effect and its cancer therapeutic implications. J Bioenerg Biomembr . 2007;39(3):267–274. [cited 2019 Jul 23] Available from: http://link.springer.com/https://doi.org/10.1007/s10863-007-9086-x
9. Warburg O, Wind F, Negelein E. The metabolism of tumors in the body. J Gen Physiol. 1927;8(6):519–30. https://doi.org/10.1085/jgp.8.6.519.
10. Bonnet S, Archer SL, Allalunis-Turner J, Haromy A, Beaulieu C, Thompson R, et al. A mitochondria-K+ channel Axis is suppressed in Cancer and its normalization promotes apoptosis and inhibits Cancer growth. Cancer Cell. 2007;11(1):37–51. https://doi.org/10.1016/j.ccr.2006.10.020.
11. Bonnet S, Archer SL, Allalunis-Turner J, Haromy A, Beaulieu C, Thompson R, et al. A mitochondria-K+ channel axis is suppressed in cancer and its normalization promotes apoptosis and inhibits cancer growth. Cancer Cell. 2007;11(1):37–51 [cited 2018 Jun 13] Available from: https://www.sciencedirect.com/science/article/pii/S1535610806003722?via%3Dihub.
12. Wong JYY, Huggins GS, Debidda M, Munshi NC, De Vivo I. Dichloroacetate induces apoptosis in endometrial cancer cells. Gynecol Oncol. 2008;109(3):394–402. https://doi.org/10.1016/j.ygyno.2008.01.038.
13. Saed GM, Fletcher NM, Jiang ZL, Abu-Soud HM, Diamond MP. Dichloroacetate induces apoptosis of epithelial ovarian cancer cells through a mechanism involving modulation of oxidative stress. Reprod Sci. 2011;18(12):1253–61 [cited 2020 Jan 20] Available from: http://www.ncbi.nlm.nih.gov/pubmed/21701041.
14. Sutendra G, Dromparis P, Kinnaird A, Stenson TH, Haromy A, Parker JMR, McMurtry MS, Michelakis ED Mitochondrial activation by inhibition of PDKII suppresses HIF1a signaling and angiogenesis in cancer. Oncogene 2013;32(13):1638–1650. Available from: http://dx.doi.org/https://doi.org/10.1038/onc.2012.198
15. Ward NP, Poff AM, Koutnik AP, D'Agostino DP. Complex I inhibition augments dichloroacetate cytotoxicity through enhancing oxidative stress in VM-M3 glioblastoma cells. PLoS One. 2017;12(6):1–18.
16. Lu H, Lu Y, Xie Y, Qiu S, Li X, Fan Z. Rational combination with PDK1 inhibition overcomes cetuximab resistance in head and neck squamous cell carcinoma. JCI Insight. 2019;4(19):1–16.
17. Tataranni T, Agriesti F, Pacelli C, Ruggieri V, Laurenzana I, Mazzoccoli C, et al. Dichloroacetate affects mitochondrial function and Stemness-associated properties in pancreatic Cancer cell lines. Cells. 2019;8(5):478. https://doi.org/10.3390/cells8050478.
18. Alkarakooly Z, Al-Anbaky QA, Kannan K, Ali N. Metabolic reprogramming by Dichloroacetic acid potentiates photodynamic therapy of human breast adenocarcinoma MCF-7 cells. PLoS One. 2018;13(10):e0206182.
19. Lu X, Zhou D, Hou B, Liu QX, Chen Q, Deng XF, et al. Dichloroacetate enhances the antitumor efficacy of chemotherapeutic agents via inhibiting autophagy in non-small-cell lung cancer. Cancer Manag Res. 2018;10:1231–41. https://doi.org/10.2147/CMAR.S156530.
20. Agnoletto C, Melloni E, Casciano F, Rigolin GM, Rimondi E, Celeghini C, et al. Sodium dichloroacetate exhibits anti-leukemic activity in B-chronic lymphocytic leukemia (B-CLL) and synergizes with the p53 activator Nutlin-3. Oncotarget. 2014;5(12):4347–60 Available from: http://www.pubmedcentral.nih.gov/articlerender.fcgi?artid=4147328&tool=pmcentrez&rendertype=abstract.
21. Koh MY, Spivak-Kroizman T, Venturini S, Welsh S, Williams RR, Kirkpatrick DL, et al. Molecular mechanisms for the activity of PX-478, an antitumor inhibitor of the hypoxia-inducible factor-1alpha. Mol Cancer Ther. 2008;7(1):90–100 [cited 2019 Dec 22] Available from: http://www.ncbi.nlm.nih.gov/pubmed/18202012.
22. Semenza GL. Targeting HIF-1 for cancer therapy. Nat Rev Cancer. 2003;3(10):721–32. https://doi.org/10.1038/nrc1187.
23. Palayoor ST, Mitchell JB, Cerna D, Degraff W, John-Aryankalayil M, Coleman CN. PX-478, an inhibitor of hypoxia-inducible factor-1alpha, enhances radiosensitivity of prostate carcinoma cells. Int J Cancer. 2008;123(10):2430–7 [cited 2018 Apr 13] Available from: http://www.ncbi.nlm.nih.gov/pubmed/18729192.
24. Lang M, Wang X, Wang H, Dong J, Lan C, Hao J, et al. Arsenic trioxide plus PX-478 achieves effective treatment in pancreatic ductal adenocarcinoma. Cancer Lett. 2016;378(2):87–96 [cited 2018 Apr 13] Available from: http://www.ncbi.nlm.nih.gov/pubmed/27212442.
25. Zhu Y, Zang Y, Zhao F, Li Z, Zhang J, Fang L, et al. Inhibition of HIF-1α by PX-478 suppresses tumor growth of esophageal squamous cell cancer in vitro and in vivo. Am J Cancer Res. 2017;7(5):1198–212 [cited 2020 Jan 19] Available from: http://www.ncbi.nlm.nih.gov/pubmed/28560067.
26. Welsh S, Williams R, Kirkpatrick L, Paine-Murrieta G, Powis G. Antitumor activity and pharmacodynamic properties of PX-478, an inhibitor of hypoxia-inducible factor-1alpha. Mol Cancer Ther. 2004;3(3):233–44.
27. Kim JW, Tchernyshyov I, Semenza GL, Dang CV. HIF-1-mediated expression of pyruvate dehydrogenase kinase: a metabolic switch required for cellular adaptation to hypoxia. Cell Metab. 2006;3(3):177–85. https://doi.org/10.1016/j.cmet.2006.02.002.
28. Kirito K, Hu Y, Komatsu N. HIF-1 prevents the overproduction of mitochondrial ROS after cytokine stimulation through induction of PDK-1. Cell Cycle. 2009;8(17):2844–9. https://doi.org/10.4161/cc.8.17.9544.
29. Chou TC, Martin N. CompuSyn for Drug Combinations: PC Software and User's Guide: A Computer Program for Quantitation of Synergism and Antagonism in Drug Combinations, and the Determination of IC50 and ED50 and LD50 Values. Paramus: ComboSyn Inc; 2005.
30. Chou T-C. Preclinical versus clinical drug combination studies. Leuk Lymphoma. 2008;49(11):2059–80 [cited 2016 Apr 9] Available from: http://www.ncbi.nlm.nih.gov/pubmed/19021049.
31. Zhao L, Wientjes MG, Au JL-S. Evaluation of combination chemotherapy: integration of nonlinear regression, curve shift, isobologram, and combination index analyses. Clin Cancer Res. 2004;10(23):7994–8004 [cited 2016 Apr 13] Available from: http://www.ncbi.nlm.nih.gov/pubmed/15585635.
32. Kuhn H, Belkner J, Wiesner R, Brash AR. Oxygenation of biological membranes by the pure reticulocyte lipoxygenase. J Biol Chem. 1990;265(30):18351–61. https://doi.org/10.1016/S0021-9258(17)44759-4.
33. Lucido CT, Miskimins WK, Vermeer PD. Propranolol promotes glucose dependence and synergizes with dichloroacetate for anti-cancer activity in HNSCC. Basel: Cancers. 2018;10(12):476.
34. Ma W, Zhao X, Wang K, Liu J, Huang G. Dichloroacetic acid (DCA) synergizes with the SIRT2 inhibitor Sirtinol and AGK2 to enhance anti-tumor efficacy in non-small cell lung cancer. Cancer Biol Ther. 2018 Sep 2;19(9):835–46. https://doi.org/10.1080/15384047.2018.1480281.
35. Schoonjans CA, Joudiou N, Brusa D, Corbet C, Feron O, Gallez B. Acidosis-induced metabolic reprogramming in tumor cells enhances the anti-proliferative activity of the PDK inhibitor dichloroacetate. Cancer Lett. 2020 Feb 1;470:18–28. https://doi.org/10.1016/j.canlet.2019.12.003.
36. Zhou L, Liu L, Chai W, Zhao T, Jin X, Guo X, et al. Dichloroacetic acid upregulates apoptosis of ovarian cancer cells by regulating mitochondrial function. Onco Targets Ther. 2019;12:1729–39. https://doi.org/10.2147/OTT.S194329.
37. Chaudhary AK, Bhat TA, Kumar S, Kumar A, Kumar R, Underwood W, et al. Mitochondrial dysfunction-mediated apoptosis resistance associates with defective heat shock protein response in African-American men with prostate cancer. Br J Cancer. 2016;114(10):1090–100. https://doi.org/10.1038/bjc.2016.88.
38. Roh J-L, Park JY, Kim EH, Jang HJ, Kwon M. Activation of mitochondrial oxidation by PDK2 inhibition reverses cisplatin resistance in head and neck

cancer. Cancer Lett. 2016;371(1):20–9 [cited 2020 Jan 24] Available from: http://www.ncbi.nlm.nih.gov/pubmed/26607904.
39. Ruggieri V, Agriesti F, Scrima R, Laurenzana I, Perrone D, Tataranni T, et al. Dichloroacetate, a selective mitochondria-targeting drug for oral squamous cell carcinoma: a metabolic perspective of treatment. Oncotarget. 2015;6(2): 1217–30. https://doi.org/10.18632/oncotarget.2721.
40. Xuan Y, Hur H, Ham I-H, Yun J, Lee J-Y, Shim W, et al. Dichloroacetate attenuates hypoxia-induced resistance to 5-fluorouracil in gastric cancer through the regulation of glucose metabolism. Exp Cell Res. 2014;321(2): 219–30 [cited 2018 May 28] Available from: https://www.sciencedirect.com/science/article/pii/S0014482713005260?via%3Dihub.
41. Fang J, Xie J, Wang B-S, Wang B-S, Yu D-H, Yu D-H, et al. Dichloroacetate shifts the metabolism from glycolysis to glucose oxidation and exhibits synergistic growth inhibition with cisplatin in HeLa cells. Int J Oncol. 2011; 38(2):409–17 [cited 2018 May 28] Available from: http://www.spandidos-publications.com/ijo/38/2/409.
42. Yang Z, Tam KY. Anti-cancer synergy of dichloroacetate and EGFR tyrosine kinase inhibitors in NSCLC cell lines. Eur J Pharmacol. 2016;789:458–67 Available from: https://www.sciencedirect.com/science/article/pii/S0014299916305O9X?via%3Dihub.
43. Haugrud AB, Zhuang Y, Coppock JD, Miskimins WK. Dichloroacetate enhances apoptotic cell death via oxidative damage and attenuates lactate production in metformin-treated breast cancer cells. Breast Cancer Res Treat. 2014;147(3):539–50. https://doi.org/10.1007/s10549-014-3128-y.
44. Choi YW, Lim IK. Sensitization of metformin-cytotoxicity by dichloroacetate via reprogramming glucose metabolism in cancer cells. Cancer Lett. 2014; 346(2):300–8 [cited 2018 may 18] Available from: http://www.ncbi.nlm.nih.gov/pubmed/24480191.
45. Garon EB, Christofk HR, Hosmer W, Britten CD, Bahng A, Crabtree MJ, et al. Dichloroacetate should be considered with platinum-based chemotherapy in hypoxic tumors rather than as a single agent in advanced non-small cell lung cancer. J Cancer Res Clin Oncol. 2014;140(3):443–52. https://doi.org/10.1007/s00432-014-1583-9.
46. Ishiguro T, Ishiguro R, Ishiguro M, Iwai S. Co-treatment of dichloroacetate, omeprazole and tamoxifen exhibited synergistically antiproliferative effect on malignant tumors: in vivo experiments and a case report. Hepatogastroenterology. 2012;59(116):994–6 [cited 2016 Apr 12] Available from: http://www.ncbi.nlm.nih.gov/pubmed/22580646.
47. Shen YC, Ou DL, Hsu C, Lin KL, Chang CY, Lin CY, et al. Activating oxidative phosphorylation by a pyruvate dehydrogenase kinase inhibitor overcomes sorafenib resistance of hepatocellular carcinoma. Br J Cancer. 2013;108(1): 72–81. https://doi.org/10.1038/bjc.2012.559.
48. Liang Y, Hou L, Li L, Li L, Zhu L, Wang Y, et al. Dichloroacetate restores colorectal cancer chemosensitivity through the p53/miR-149-3p/PDK2-mediated glucose metabolic pathway. Oncogene. 2020;39(2):469–85 [cited 2020 Sep 25] Available from: http://www.nature.com/articles/s41388-019-1035-8.
49. Michelakis ED, Gurtu V, Webster L, Barnes G, Watson G, Howard L, et al. Inhibition of pyruvate dehydrogenase kinase improves pulmonary arterial hypertension in genetically susceptible patients. Sci Transl Med. 2017;9(413): eaao4583.
50. Shroads AL, Coats BS, McDonough CW, Langaee T, Stacpoole PW. Haplotype variations in glutathione transferase zeta 1 influence the kinetics and dynamics of chronic dichloroacetate in children. J Clin Pharmacol. 2015; 55(1):50–55. [cited 2018 Jun 14] Available from: http://doi.wiley.com/https://doi.org/10.1002/jcph.371
51. Dunbar EM, Coats BS, Shroads AL, Langaee T, Lew A, Forder JR, et al. Phase 1 trial of dichloroacetate (DCA) in adults with recurrent malignant brain tumors. Invest New Drugs. 2014;32(3):452–64 [cited 2018 Jun 14] Available from: http://www.ncbi.nlm.nih.gov/pubmed/24297161.
52. Chu QS, Sangha R, Spratlin J, Vos LJ, Mackey JR, Mcewan AJB, et al. A phase I open-labeled, single-arm, dose-escalation, study of dichloroacetate (DCA) in patients with advanced solid tumors. Invest New Drugs. 2015;1:603–10.
53. Tibes R, Falchook GS, Von Hoff DD, Weiss GJ, Iyengar T, Kurzrock R, et al. Results from a phase I, dose-escalation study of PX-478, an orally available inhibitor of HIF-1α. J Clin Oncol. 2010;28(15_suppl):3076–3076. [cited 2019 Jul 22] Available from: http://ascopubs.org/doi/https://doi.org/10.1200/jco.2010.28.15_suppl.3076.
54. Jewell UR, Kvietikova I, Scheid A, Bauer C, Wenger RH, Gassmann M. Induction of HIF-1α in response to hypoxia is instantaneous. FASEB J. 2001; 15(7):1312–4. https://doi.org/10.1096/fj.00-0732fje.
55. Abir R, Fisch B, Jessel S, Felz C, Ben-Haroush A, Orvieto R. Improving posttransplantation survival of human ovarian tissue by treating the host and graft. Fertil Steril 2011;95(4):1205–1210. Available from: http://dx.doi.org/https://doi.org/10.1016/j.fertnstert.2010.07.1082
56. Fernandes R, Hosoya K. Ichi, Pereira P. reactive oxygen species downregulate glucose transport system in retinal endothelial cells. Am J Physiol Cell Physiol. 2011;300(4):927–36.

Publisher's Note

9 Lebenslauf

Mein Lebenslauf wird aus datenschutzrechtlichen Gründen in der elektronischen Version meiner Arbeit nicht veröffentlicht.

10 Publikationsliste

Genome reorganization in different cancer types: detection of cancer specific breakpoint regions
Christoph Standfuß, Jonas Parczyk, Jérôme Ruhnau and Andreas Klein
Mol Cytogenet 12, 25 (2019). Molecular Cytogenetics volume 12, Article number: 25 (2019)
doi:10.1186/s13039-019-0435-3
Impact factor: 1.233 - 2-year Impact Factor 1.408 - 5-year Impact Factor

Synergisms of genome and metabolism stabilizing antitumor therapy (GMSAT) in human breast and colon cancer cell lines: a novel approach to screen for synergism
Jérôme Ruhnau*, Jonas Parczyk*, Kerstin Danker, Britta Eickholt, and Andreas Klein
*geteilte Erstautorenschaft
BMC Cancer. 2020; 20: 617. Published online 2020 Jul 2.
doi: 10.1186/s12885-020-07062-2 PMCID: PMC7331156 PMID: 32615946
Impact factor: 3.15 - 2-year Impact Factor 3.432 - 5-year Impact Factor

Dichloroacetate and PX-478 Exhibit Strong Synergistic Effects in a Various Number of Cancer Cell Lines.
Jonas Parczyk*, Jérôme Ruhnau*, Carsten Pelz, Max Schilling, Hao Wu, Nicole Nadine Piaskowski, Britta Eickholt, Hartmut Kühn, Kerstin Danker, Andreas Klein
*geteilte Erstautorenschaft
BMC Cancer. 2021
doi: 10.21203/rs.3.rs-88933/v1
Impact factor: 3.15 - 2-year Impact Factor 3.432 - 5-year Impact Factor

11 Danksagung

Mein Dank gilt in erster Linie meinem Betreuer Dr. Andreas Klein, ohne dessen unermüdlichen Einsatz und außergewöhnliche Präsenz als Mentor, Projektleiter und Freund das Promotionsvorhaben vor dem Hintergrund familiärer Ereignisse nicht hätte abgeschlossen werden können.

Das Gleiche gilt für meinen Kommilitonen, Kollegen und Freund Jonas Parczyk, der mit seiner Ausdauer, Genauigkeit und Präzision immer die richtigen Fragen gestellt hat, um unser jeweiliges wissenschaftliches Streben auf ein höheres Niveau zu heben.

Ganz besonders bedanken möchte ich mich bei meiner Lebensgefährtin, Pia Djermester, deren Liebe, Zuspruch und Unterstützung mir immer wieder die Kraft gegeben hat, weiterzumachen.

Für einen sehr lehrreichen und spannenden Ausflug in die Welt der Membranlipide und deren Oxidationsprodukte möchte ich mich herzlich
bei Prof. Dr. Hartmut Kühn bedanken.

Vielen Dank für die Unterstützung während des Projektes an:

Prof. Dr. Britta Eickholt

Karsten Parczyk

Max Schilling

Carsten Pelz

PD Dr. Kerstin Danker

PD Dr. rer. nat. Lothar Lucka

Marlon Tilgner

Vielen Dank an Sarra Amroune für Ihre Genauigkeit und selbstlose, interkontinentale Unterstützung in mehreren Phasen des Projektes.

Meinem Bruder Ansgar Ruhnau und meinem Vater Wolf-Henner Ruhnau gilt besonderer Dank für den starken familiären Rückhalt, der in den dunkelsten Zeiten und größten Herausforderungen stets ungebrochen blieb.

Vielen Dank an Dr. Jutta Hinke-Ruhnau für die Unterstützung des Projektes, auch wenn die Wissenschaft Sie nicht retten konnte.

Ruhe in Frieden.